Boundary integral equation methods for the calculation of complex eigenvalues for open spaces

Ryota Misawa

Acknowledgement

The author expresses his immeasurable gratitude to Professor Naoshi Nishimura at Graduate School of Informatics, Kyoto University, for his enthusiastic guidance and invaluable advice. Without his precious guidance, the author could not finish this thesis.

The author thanks Professor Yuusuke Iso, Professor Hitoshi Yoshikawa and Professor Mitsuaki Funakoshi for their reviews and criticisms.

The author also thanks Professor Kazuki Niino at Graduate School of Informatics, Kyoto University whose advice and works on boundary integral equation method made enormous contribution to the author's Ph.D. study.

The author thanks Professor Hitoshi Yoshikawa at Graduate School of Informatics, Kyoto University, again, and Professor Hiroshi Isakari at Graduate School of Engineering, Nagoya University for their advice and information.

The author also thanks the members of Computational Mechanics Laboratory for many valuable discussions.

The author is very grateful to Japan Society for the Promotion of Science for making his Ph.D. study possible by the financial support.

Finally, the author expresses his gratitude to his family for their supports in every way.

Contents

Chapter 1

Introduction

1.1 Introduction

Analyses of wave motions in open spaces such as infinite strips or parallel plate waveguides have various applications. For example, acoustic or elastic waves in waveguides are often used for non destructive evaluations (NDE), which detect cracks or defects inside strips without damaging the objects. These NDE problems are formulated as boundary value problems governed by Helmholtz' or the Navier-Cauchy equations. Waveguides are used also for carrying electromagnetic waves, and they are formulated as boundary value problems for Maxwell's equations.

It is known that open spaces have complex valued eigenvalues in contrast to compact domains which have real valued eigenvalues. In waveguide problems, for example, there exist anomalous frequencies near which the behavior of the solution changes suddenly. These anomalous frequencies can be classified into two types. One is the cutoff frequency (also called Rayleigh's anomaly or Wood's anomaly in periodic problems) at which the behavior of the far field changes. The values of cutoff frequencies are known. The other type of anomalies is the resonance anomaly which is related to the existence of resonance frequencies [1]. Mathematically, the resonance frequencies stand for complex eigenvalues (eigenfrequencies) at which there exist non-trivial solutions to the homogeneous boundary value problems (waveguide problems without incident wave). Particular eigensolutions corresponding to real-valued eigenvalues are called trapped modes which represent waves confined between nearby obstacles in the waveguide decaying exponentially towards the directions along the waveguide. Eigensolutions associated with complex eigenvalues with nonzero (negative) imaginary parts are called leaky modes. The leaky modes are also of interest because they are known to affect the behavior of the solutions considerably. Actually, numerical examples in this thesis will provide further evidence of the relevance of the leaky modes to physical phenomena. Determining the locations of resonance frequencies is of interest in various applications, since these frequencies are easily excited. It is therefore not surprising that there are many investigations devoted to both real and complex resonance frequencies. See [1, 2, 3, 4, 5], to mention just a few.

However, resonance frequencies (eigenvalues) in waveguides cannot be determined exactly except in simple cases, and efforts have been made to obtain them numerically. Such efforts include Linton and Evans [6], Hein et al. [7, 8], Duan et al. [9], Nannen and Schädle [10], which is by no means an exhaustive list. Many of these investigations truncate the original infinite waveguide to a finite domain with the help of certain absorbing boundary conditions such as PML (perfectly matched layer). However, one

has to be careful in applying truncation approaches in finding leaky modes because the corresponding eigenfunctions grow exponentially in the far fields.

Boundary integral equation method (BIEM) formulated with Green's function in waveguide problems is considered worth the investigation because it can deal with this exponential growth easily. Indeed, BIEM has the advantages that boundary and radiation conditions (i.e. exponential growth with complex frequency) are satisfied automatically. Thanks to this property, we do not have to truncate the original infinite domain or introduce additional tools such as PML, Hardy space method [10] with BIEM. As a matter of fact, BIEMs using Green's functions for waveguide problems have already been developed e.g. by Linton and Evans [6].

Application of BIEM to eigenvalue problems, however, is not without difficulty. Indeed, there are following three difficulties for solving eigenvalue problems with BIEM.

1. The computational cost of BIEM is as large as $O(N^2)$ (N: degrees of freedom (DOF)).

2. One has to solve non-linear eigenvalue problems.

3. One may obtain non-physical eigenvalues.

The primal purpose of this thesis is to resolve these difficulties for waveguide problems: namely, to develop fast solvers for waveguide problems for two dimensional Helmholtz' equation in an infinite strip with the homogeneous Neumann boundary condition on the sides and to apply it to eigenvalue problems to determine resonance frequencies correctly.

We alleviate the first difficulty with the fast methods for BIEMs. There are many efforts to reduce the computational cost of BIEMs, such as FMM (fast multipole method, [11]) and AIM (adaptive integral method, [12]) which reduce one matrix-vector multiplication to an $O(N(\log N)^\alpha)$ work ($\alpha \geq 0$). Some fast direct solvers, such as the method of Martinsson and Rokhlin [13] and methods based on the LU decomposition of $\mathcal{H}$-matrices [14], have also been investigated. Fast methods of evaluating Green's functions are also available, e.g., methods based on efficient integral expressions [15] or acceleration techniques such as Ewald's method [16, 17]. To the best of the author's knowledge, however, fast BIEMs for parallel plate waveguide problems have not been investigated so far.

It might be possible to combine these fast BIEMs with fast methods of evaluating Green's functions in our waveguide problem. However, an equally effective and simpler approach for this problem is to combine FMM with the method of images. This method makes use of a representation of Green's function in terms of series of fundamental solutions (free space Green's function) whose source points form images of the real source. This method is advantageous because we do not have to deal with Green's functions explicitly and because we can work with the standard FMM for the fundamental solution with minimum modifications. As a matter of fact, this method of images has been applied to periodic problems (Otani and Nishimura [18]) and to half space problems (Fukui and Kozuka [19], O'Neil et al. [20]). The original idea of using the method of images with FMM in periodic problems is found in the seminal paper by Greengard and Rokhlin [11]. Their idea is to regard the solution of the problem as the superposition of the contributions from an infinite number of images of the real source. In the periodic FMM, contributions from near images are evaluated with the help of the ordinary FMM and contributions from infinite number of far images are evaluated efficiently with a special M2L formula written in terms of lattice sums. These lattice

sums do not depend on the shape of the scatterer and can be precomputed once for all in the FMM algorithm. In this thesis, we shall see that the methodology developed for periodic FMMs can be utilized in waveguide problems as well with some modifications.

The second difficulty associated with this method has been the fact that it reduces the original linear problems to non-linear ones, which have typically been solved iteratively with zero-searches of related determinants, etc. Recent attempts of this type include Shipman and Venakides who solved a non-linear eigenvalue problem for integral equations to obtain the dispersion relation in periodic problems [21]. They solved the non-linear eigenvalue problems essentially by searching the zeros of the determinant by trial and error. Another attempt of this type is due to Cheng et al. [22] who solved the non-linear eigenvalue problem for the integral equation for photonic crystal fiber (PCF) waveguides in order to obtain propagating modes along the axial direction. They used Muller's method which finds complex roots of a certain scalar function iteratively.

However, this difficulty is now being resolved with the development of non-iterative solvers of non-linear eigenvalue problems such as the Sakurai-Sugiura projection method (SSM, [23, 24, 25]). The SSM determines eigenvalues inside a given contour γ in the complex plane using contour integrals defined on γ. The SSM with BIEM can find eigenvalues without truncating the domain or searching the zeros of the determinant of the matrix. Such attempts using standard BIEM can be found in Gao et al. [26] for 2D elasticity problems, and in Kleefeld [27] for interior transmission problems for Helmholtz' equation in 3D (using the method by Beyn [28] which is similar to the SSM). In this thesis, we propose a numerical method for finding resonance frequencies which uses the SSM and the fast BIEM (see Nose and Nishimura [29] for a related attempt in periodic problems, Zheng et al. [30] for 3D acoustic problems).

An advantage of this approach is that one can search eigenvalues within a particular domain in the complex domain. One can avoid inaccuracies caused by the branch cuts of Green's functions, or continuous spectra, by using γ's which do not cross them. Another advantage of this approach is that it can be used without much difficulty to find leaky modes because BIEM is not affected by the exponential growth of the related eigenfunctions, as we have already pointed out. In addition, the major part of SSM is the solution of forward problems, which can be accelerated with our FMM. In order to take these advantages, however, one needs solvers of waveguide problems for complex frequencies since SSM requires them even for determining real eigenvalues. We are thus led to a problem of finding the analytic continuation of our FMM-BIEM to complex frequencies. This problem is a delicate one since the standard series expression for Green's function for waveguide problems diverges exponentially for complex frequencies with negative imaginary parts.

The third difficulty is caused by the difference between the eigenvalues of the boundary value problem and those of the boundary integral equation (BIE) which may include eigenvalues irrelevant to the original boundary value problem. These spurious eigenvalues of the BIE are called "fictitious eigenvalues" while the resonance frequencies of the original boundary value problem are called "true eigenvalues". Many efforts have been devoted to the development of BIEs which are free from real valued fictitious eigenvalues such as combined integral equations [31], the Burton-Miller equation [32], the PMCHWT (Poggio-Miller-Chang-Harrington-Wu-Tsai) [33] and Müller [34] formulations. However, these BIEs for open spaces have complex fictitious eigenvalues (e.g. [30, 35] for the Burton-Miller and similar combined integral equation case). Few studies have focused on fictitious eigenvalue issues in complex eigenvalue problems.

This thesis also discusses a way of dealing with the third difficulty in transmission problems. We show that a small modification of the BIE enables us to clearly distinguish between the true eigenvalues and the fictitious ones. The modification can be applied to various integral equations, and we thus consider transmission problems for both waveguides for Helmholtz' equation in 2D and standard Maxwell's equations in 3D. As a matter of fact, related problems in the exterior Neumann problems for Helmholtz' equation in 3D have been discussed in [35] which uses the combined integral equations, etc. To the best of the author's knowledge, however, remedies for the transmission problems have not been developed yet. We also show, in particular, that eigenvalues of the Müller and PMCHWT formulations for Maxwell's equations are identical including fictitious ones.

Misawa and Nishimura have reported that even the Müller formulations without real fictitious eigenvalues may become inaccurate at certain conditions even in real frequency [36]. In this thesis, we also show numerically that this problem is caused by complex fictitious eigenvalues which are very close to real axis. We thus consider BIEs whose fictitious eigenvalues are so separated from real axis that they do not cause inaccuracies in the analysis with real frequencies. We investigate single integral equation (SIE) [37] in terms of the fictitious eigenvalues to see if it can resolve the inaccuracies. We consider the SIE for the following reasons: We can show that the fictitious eigenvalues of the SIE are either eigenvalues of exterior Dirichlet problem or interior impedance problem, and the latter ones can be controlled by adjusting weight coefficients so that the eigenvalues are separated far from real axis. On the other hand, the fictitious eigenvalues of the PMCHWT and Müller formulations are eigenvalues of certain transmission problems, which may have very small imaginary parts. We thus expect SIE to separate the fictitious eigenvalues far from real axis since its fictitious eigenvalues are not eigenvalues of transmission problems.

1.2 Organization of thesis

This thesis is organized as follows:

- In chapter 2, we discuss an FMM for solving waveguide problems and associated eigenvalue problems for Helmholtz' equation in a two dimensional infinite strip with the homogeneous Neumann boundary condition on the sides. Layer potentials with Green's function for this problem are evaluated efficiently with the help of the method of images and FMM. We apply FMM to solve some boundary value problems in waveguides and associated resonance frequency problems using the Sakurai-Sugiura projection method after discussing the required analytic continuation of the solutions to complex frequencies. Some numerical examples show the accuracy and the efficiency of the proposed method. We also present some results related to stopbands and the resonance frequencies.

  The material in this chapter is taken from Misawa et al. [38].

- In chapter 3, we propose new BIEs for transmission problems with which one can distinguish true and fictitious eigenvalues easily. Specifically, we consider waveguide problems for Helmholtz' equation in 2D and standard scattering problems for Maxwell's equations in 3D. We verify numerically that the proposed BIEs can separate the true eigenvalues (resonance frequencies) from the fictitious ones in these problems. We also show that the fictitious eigenvalues may affect the

accuracy of BIE solutions in standard boundary value problems even when the frequency is real.

The material in this chapter is taken from Misawa et al. [39] which is accepted for publication in SIAM Journal on Applied Mathematics.

- In chapter 4, we study the SIE to see if it can resolve the inaccuracy in analysis with real frequencies. We identify the fictitious eigenvalues of the SIE and investigate the behavior of the SIE from the viewpoint of the distribution of complex fictitious eigenvalues. Numerical examples suggest that a properly formulated SIE has complex fictitious eigenvalues with larger imaginary parts and is more accurate than the PMCHWT and Müller formulations in problems with real frequencies.

  The material in this chapter is taken from Misawa and Nishimura [40].

- In chapter 5, we summarize the thesis and note some issues which should be studied in future work.

Chapter 2

An FMM for waveguide problems of 2-D Helmholtz' equation and its application to eigenvalue problems

2.1 Introduction

This chapter discusses an FMM for solving waveguide problems and associated eigenvalue problems for Helmholtz' equation in a two dimensional infinite strip with the homogeneous Neumann boundary condition on the sides. Layer potentials with Green's function for this problem are evaluated efficiently with the help of the method of images and FMM. We apply FMM to solve some boundary value problems in waveguides and associated resonance frequency problems using the Sakurai-Sugiura projection method (SSM) after discussing the required analytic continuation of the solutions to complex frequencies.

This chapter is organized as follows. Section 2.2 shows the formulation of the BIEM and Green's function, followed by section 2.3 where we show the formulation and the outline of the FMM for waveguide problems. In section 2.4, we discuss a numerical method for finding resonance frequencies (eigenvalues) with the help of the SSM as well as analytic continuations of our FMM-BIEM to complex frequencies. Our numerical method is validated in section 2.5 with some numerical examples. Section 2.5 also presents results related to stopbands and the resonance frequencies.

The material in this chapter is taken from Misawa et al. [38].

2.2 Formulation

In this section, we formulate the waveguide problem considered in this chapter for Helmholtz' equation in 2-D and derive the boundary integral equations. We consider time-harmonic (with $e^{-i\omega t}$ time dependence) electromagnetic wave problems governed by two dimensional Helmholtz' equation.

2.2.1 Waveguide problems for Helmholtz' equation in 2-D

Let $P \subset \mathbb{R}^2$ be an infinite strip given by $P = [-1/2, 1/2] \times \mathbb{R}$. The sides of the strip P are denoted by $S_1^{\pm} = \{x = (x_1, x_2) \in \mathbb{R}^2 | x_1 = \pm 1/2\}$. We assume that P is divided

into a bounded domain $\Omega = \Omega_2$ and its complement $\Omega_1 = P \setminus \overline{\Omega_2}$, where Ω_2 indicates the scatterer. The boundary of the finite sized scatterer is $\partial\Omega = \partial\Omega_2$. We consider the problem of finding u which satisfies two dimensional Helmholtz' equation in Ω_1:

$$\Delta u + k_1^2 u = 0 \text{ in } \Omega_1 \tag{2.1}$$

and the homogeneous Neumann boundary condition on the sides of the strip $S_1^{\pm}$:

$$\frac{\partial u}{\partial x_1} = 0 \text{ on } S_1^{\pm} \tag{2.2}$$

where k_1 is the wave number in Ω_1 which is written as $k_1 = \omega\sqrt{\epsilon_1\mu}$ and ϵ_1 and μ are the permittivity in Ω_1 and the permeability in P (positive real), respectively. We assume that the permittivity ϵ_1 is constant in Ω_1 and the permeability μ is uniform in the strip P. We consider an incident wave u^{inc} in Ω_1 and impose the radiation condition which requires that the scattered wave $u^{\text{sca}} = u - u^{\text{inc}}$ is written as follows (e.g. [6]):

$$u^{\text{sca}}(x) \approx \sum_n C_n^{\pm} r_n^{\pm}(x) \text{ as } x_2 \to \pm\infty \tag{2.3}$$

where the function $r_n^{\pm}(x)$, called the n-th mode, is defined by

$$r_n^{\pm}(x) = \cos n\pi \left(x_1 + \frac{1}{2}\right) e^{\pm i\xi_n x_2} \tag{2.4}$$

and ξ_n in (2.4) stands for $\xi_n = i\sqrt{(n\pi)^2 - k_1^2}$, which is made single valued with the branch cuts given by $z = \pm(k_1 + it),\ t > 0$ for the square root

$$\sqrt{z^2 - k_1^2}. \tag{2.5}$$

These branch cuts are taken so that $\sqrt{z^2 - k_1^2} \to +\infty$ holds on the real axis as $z \to \pm\infty$. We use this definition of the square root unless specified otherwise. The summation in (2.3) is over such n that ξ_n is a real number.

Let $\boldsymbol{n}$ be the unit normal vector on $\partial\Omega$ directed towards Ω_1. The problems considered in this chapter are characterized by the following two types of boundary conditions on $\partial\Omega$:

- Transmission problem: find u which satisfies (2.1), (2.2), (2.3) and

$$\begin{aligned} &\Delta u + k_2^2 u = 0 \text{ in } \Omega_2 \\ &u^+ = u^-,\ \frac{1}{\epsilon_1}\frac{\partial u^+}{\partial n} = \frac{1}{\epsilon_2}\frac{\partial u^-}{\partial n} \text{ on } \partial\Omega \end{aligned}$$

  where the constant ϵ_2 stands for the permittivity in the scatter Ω_2, and k_2 is the wavenumber in Ω_2 which is written as $k_2 = \omega\sqrt{\epsilon_2\mu}$, and the superscript $+$ $(-)$ stands for the trace to $\partial\Omega$ from Ω_1 (Ω_2), $\partial/\partial n$ for the normal derivative, respectively.

- Neumann problem: find u which satisfies (2.1), (2.2), (2.3) and

$$\frac{\partial u}{\partial n} = 0 \text{ on } \partial\Omega$$

2.2.2 Green's function

We consider Green's function $\Gamma(x, y)$ which satisfies the following Helmholtz' equation in P:

$$\Delta_{\boldsymbol{x}}\Gamma(x, y) + k_1^2\Gamma(x, y) = -\delta(\boldsymbol{x} - \boldsymbol{y}),\ y \in P,$$

the homogeneous Neumann boundary condition on $S_1^{\pm}$:

$$\frac{\partial\Gamma(x, y)}{\partial x_1} = 0 \text{ on } S_1^{\pm},$$

and the radiation condition as $|x_2| \to \infty$ where δ is Dirac's delta function and bold letters $\boldsymbol{x}$, $\boldsymbol{y}$, etc. stand for the position vectors of the points x, y, etc.

It is known that Γ can be written as the following lattice-sum [17]:

$$\Gamma(x, y) = \sum_{l=-\infty}^{\infty} G(\boldsymbol{x} - \boldsymbol{y} - 2l\boldsymbol{e}_1) + \sum_{l=-\infty}^{\infty} G(\boldsymbol{x} - \boldsymbol{y}' - (2l + 1)\boldsymbol{e}_1) \tag{2.6}$$

where $\boldsymbol{y} = (y_1, y_2)$, $\boldsymbol{y}' = (-y_1, y_2)$, $\boldsymbol{e}_1 = (1, 0)$, $\boldsymbol{e}_2 = (0, 1)$ G is the fundamental solution of Helmholtz' equation in 2-D given by:

$$G(\boldsymbol{x} - \boldsymbol{y}) = \frac{i}{4}H_0^{(1)}(k_1|\boldsymbol{x} - \boldsymbol{y}|)$$

and $H_n^{(1)}$ stands for the Hankel function of the first kind and the n-th order, respectively.

We note that Γ can also be written as the following Fourier integral:

$$\begin{aligned}\Gamma(x, y) = {} & G(\boldsymbol{x} - \boldsymbol{y}' - \boldsymbol{e}_1) + G(\boldsymbol{x} - \boldsymbol{y}) + G(\boldsymbol{x} - \boldsymbol{y}' + \boldsymbol{e}_1) \\ & + \frac{1}{2\pi}\int_C \left(\frac{e^{q(x_1-y_1-2)+i\xi(x_2-y_2)}}{2q(1 - e^{-2q})} + \frac{e^{-q(x_1-y_1+2)+i\xi(x_2-y_2)}}{2q(1 - e^{-2q})}\right) d\xi \\ & + \frac{1}{2\pi}\int_C \left(\frac{e^{q(x_1+y_1-3)+i\xi(x_2-y_2)}}{2q(1 - e^{-2q})} + \frac{e^{-q(x_1+y_1+3)+i\xi(x_2-y_2)}}{2q(1 - e^{-2q})}\right) d\xi \end{aligned} \tag{2.7}$$

where $q = \sqrt{\xi^2 - k_1^2}$ and C denotes the path of integration from $-\infty + ik_1$ to $\infty - ik_1$ given by

$$\xi = \pm\sqrt{\tau^2 - 2ik_1\tau},\ \tau > 0$$

where the square root is taken such that $\operatorname{Im}\xi < 0$ holds ($k_1 > 0$). In (2.7), the original path of integration for the Fourier integral on the real axis has been changed to C given above. This change of the path can be justified since the path never crosses any of the poles or branch cuts of the integrand in the process of the path change when $\operatorname{Im} k_1 \geq 0$. As a matter of fact, this path of integration C is the steepest descent path for the case of $x_2 = y_2$.

The Green's function Γ can also be written as the following Poisson sum:

$$\Gamma(x, y) = \frac{e^{-p_0|x_2-y_2|}}{2p_0} + \sum_{l=1}^{\infty} \frac{e^{-p_l|x_2-y_2|}}{p_l} \cos\eta_l\left(x_1 + \frac{1}{2}\right)\cos\eta_l\left(y_1 + \frac{1}{2}\right) \tag{2.8}$$

where $\eta_l = l\pi$ and $p_l = \sqrt{\eta_l^2 - k_1^2}$. It is convenient to use (2.8) to evaluate $\Gamma(x, y)$ when $|x_2 - y_2|$ is large since the summand in (2.8) decays fast. We note that Γ diverges at specific wavenumbers given by $k_1 = p\pi, \forall p \in \mathbb{N}$, which are called cutoff frequencies. Numerical methods which use Green's function obviously fail right at cutoff frequencies. Our present method could deal with this problem with techniques similar to those proposed in [41] in related periodic problems. However, we do not get into further details of this issue by assuming $k_1 \neq p\pi$ in this thesis. This is because our method is observed to work even near (but not right at) cutoff frequencies and because the solutions do not change much there compared to dramatic changes near resonance frequencies.

2.2.3 Boundary integral equations

We obtain the boundary integral equations defined on the boundary of the scatterer as follows:

- Transmission problems

$$\begin{pmatrix} -(\mathcal{D}_1 + \mathcal{D}_2) & \epsilon_1 \mathcal{S}_1 + \epsilon_2 \mathcal{S}_2 \\ -(\frac{\mathcal{N}_1}{\epsilon_1} + \frac{\mathcal{N}_2}{\epsilon_2}) & \mathcal{D}'_1 + \mathcal{D}'_2 \end{pmatrix} \begin{pmatrix} u \\ q \end{pmatrix} = \begin{pmatrix} u^{\text{inc}} \\ \frac{1}{\epsilon_1} \frac{\partial u^{\text{inc}}}{\partial n} \end{pmatrix} \tag{2.9}$$

- Neumann boundary value problems

$$\frac{1}{2} u - (\mathcal{D}_1 + \alpha \mathcal{N}_1)\, u = u^{\text{inc}} + \alpha \frac{\partial u^{\text{inc}}}{\partial n_x} \tag{2.10}$$

where α is an arbitrary complex number with non-zero imaginary part which we set to be $\alpha = -i/k_1$ in the sequel. In (2.9) and (2.10), $\mathcal{S}_i$ and $\mathcal{D}_i$ are single and double layer potentials and $\mathcal{D}'_i$, and $\mathcal{N}_i$ are their normal derivatives defined as follows:

$$\mathcal{S}_i q(x) = \int_{\partial\Omega} G^i(x, y) q(y)\, ds_y \qquad \mathcal{D}_i u(x) = \int_{\partial\Omega} \frac{\partial G^i(x, y)}{\partial n_y} u(y)\, ds_y$$
$$\mathcal{D}'_i q(x) = \int_{\partial\Omega} \frac{\partial G^i(x, y)}{\partial n_x} q(y)\, ds_y \quad \mathcal{N}_i u(x) = \fint_{\partial\Omega} \frac{\partial^2 G^i(x, y)}{\partial n_x \partial n_y} u(y)\, ds_y$$

where $\fint$ stands for finite part of a divergent integral, G^1 is defined by $G^1(x, y) = \Gamma(x, y)$ and G^2 is the fundamental solution of Helmholtz' equation in 2-D with the wavenumber of k_2. Eq.(2.9) is well known as the PMCHWT formulation for transmission problems. We note that the PMCHWT formulation does not suffer from the fictitious eigenvalue problems for real ω (which is not necessarily true for complex ω. We will discuss this problem in detail in chapter 3 and do not elaborate in this chapter. However, we have checked that numerical examples to follow in this chapter do not include fictitious ones.). We also note that the discretized equations in (2.9) are ordered so that they guarantee fast convergence of the solution with GMRES (generalized minimal residual method, [42]) [43, 44].

Eq.(2.10) is the well-known Burton-Miller equation which does not suffer from the fictitious eigenvalue problems. This property remains true even with complex ω if $\operatorname{Im} \alpha < 0$ holds (see [35] for a similar result for a related integral equation). We solve the discretized versions of equations (2.9) and (2.10) to obtain numerical solutions for the above boundary value problems.

2.2.4 Far fields

The solution of the waveguide problem can be written as follows in the limit of $x_2 \to \pm\infty$ with the help of the radiation condition in (2.3):

$$u(x) = \delta_\pm u^{\mathrm{inc}} + \sum_n A_n^\pm r_n^\pm(x)$$

where $\delta_+ = 0,\ \delta_- = 1$, and we have assumed that the incident wave u^{inc} propagates toward $x_2 \to +\infty$. The coefficients $A_n^\pm$ are computed as follows:

$$A_n^\pm = \delta_{n0}^\pm + \frac{i}{2\xi_n f_n} \int_{\partial\Omega} \left(r_n^\mp(x) \frac{\partial u}{\partial n_x}(x) - \frac{\partial r_n^\mp(x)}{\partial n_x} u(x) \right) ds_x,$$

once one obtains u and $\partial u/\partial n$ on $\partial\Omega$, where $f_n = 1$ $(n = 0)$ or $f_n = 1/2$ (otherwise) and $\delta_{n0}^\pm$ is 1 if $n = 0$ and the superscript is plus, and 0 otherwise. We then have the energy conservation law [6] given by:

$$E := \sum_n f_n \xi_n (|A_n^-|^2 + |A_n^+|^2) = 1 \tag{2.11}$$

when $u^{\mathrm{inc}} = r_0^+$. The terms $f_n \xi_n |A_n^-|^2$ and $f_n \xi_n |A_n^+|^2$ are the energy reflectance and transmittance normalized by the incident energy, respectively. The following difference can therefore be used as an error indicator of numerical results:

$$|E - 1.0|. \tag{2.12}$$

2.3 Fast multipole method for waveguide problems

2.3.1 Method of images

We now proceed to the formulation of an FMM for waveguide problems with the homogeneous Neumann conditions on the sides of the strip. Our objective is to compute the potentials which appear in (2.9) and (2.10), namely, $\mathcal{S}_1, \mathcal{D}_1, \mathcal{D}'_1$ and $\mathcal{N}_1$, efficiently. With the lattice-sum expression in (2.6), we can regard Green's function Γ as a superposition of the effects from an infinite number of the mirror images of the source $\boldsymbol{y}$, i.e., $\boldsymbol{y} \pm 2l\boldsymbol{e}_1$ $(l = 1, 2, \cdots)$ and $\boldsymbol{y}' \pm (2l+1)\boldsymbol{e}_1$ $(l = 0, 1, \cdots)$. This fact allows us to view potentials in (2.9) and (2.10) as a superposition of potentials of mirror images of the scatterer as shown in Fig.2.1, thus making it possible to extend the ordinary FMM to waveguide problems.

2.3.2 Formulation of the FMM

We now outline the FMM based on the method of images, which is related to the FMM for periodic problems proposed by Otani and Nishimura [18]. We consider the low-frequency FMM, because most of applications of the present formulation belong to this category. We first prepare some formulae used in our FMM.

Let $V^{\mathrm{Far}}(x)$ be the potential function defined in terms of the fundamental solution G by

$$V^{\mathrm{Far}}(x) = \int_{\partial\Omega_F} \left(G(\boldsymbol{x} - \boldsymbol{y}) \frac{\partial \phi}{\partial n_y}(y) - \frac{\partial G}{\partial n_y}(\boldsymbol{x} - \boldsymbol{y}) \phi(y) \right) ds_y,$$

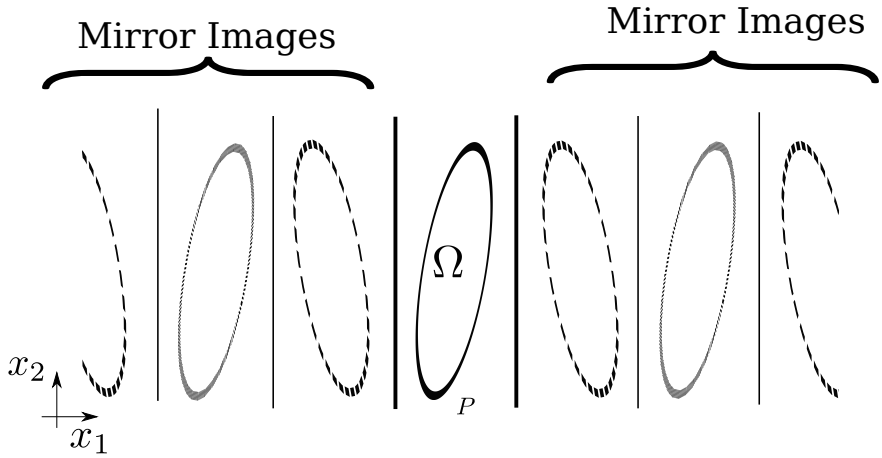

Figure 2.1: Method of images. The normal image is shown with solid line.

where $\partial\Omega_F$ is a subset of $\partial\Omega$ which is far from x. The well-known multipole expansion of $V^{\text{Far}}(x)$ is given by:

$$\begin{aligned} V^{\text{Far}}(x) &= \frac{i}{4}\sum_{n=-\infty}^{\infty} I_n(\overrightarrow{Xx})\sum_{m=-\infty}^{\infty} O_{-n-m}(\overrightarrow{YX})M_m(Y) \\ &= \frac{i}{4}\sum_{n=-\infty}^{\infty} I_n(\overrightarrow{Xx})L_{-n}(X), \end{aligned} \tag{2.13}$$

where X is a point near x and Y is a point near $\partial\Omega_F$ such that $|\overrightarrow{Yy}+\overrightarrow{Xx}| < |\overrightarrow{XY}|$ holds for $\forall y \in \partial\Omega_F$, respectively. The functions I_n and O_n are the inner and outer solutions of Helmholtz' equation defined, respectively, as follows:

$$I_n(\overrightarrow{Ox}) = i^n J_n(k_1 r)e^{in\theta},\ O_n(\overrightarrow{Ox}) = i^n H_n^{(1)}(k_1 r)e^{in\theta},$$

where (r,θ) is the polar coordinate of (x_1,x_2) and J_n is the Bessel function of the n-th order. The number $M_n(Y)$ is the multipole moment around Y defined as follows:

$$M_n(Y) = (-1)^n \int_{\partial\Omega_F}\left(I_n(\overrightarrow{Yy})\frac{\partial\phi}{\partial n_y}(y) - \frac{\partial I_n(\overrightarrow{Yy})}{\partial n_y}\phi(y)\right)ds_y,$$

and $L_n(X)$ is the local coefficient, which is related to M_n by the M2L formula given by:

$$L_n(X) = \sum_{m=-\infty}^{\infty} O_{n-m}(\overrightarrow{YX})M_m(Y). \tag{2.14}$$

We follow Rokhlin [45] to truncate the series in (2.13) and (2.14) at p terms given by:

$$p = \max(k_1 d + 6\log(k_1 d + \pi), 40)$$

where d is the diagonal length of the relevant FMM cell.

We now divide the part of P which includes the scatterers into square cells whose side lengths are equal to the width of the strip as shown in Fig.2.2. They are called

the (original) level 0 FMM cells. We stack sufficient numbers of level 0 cells along x_2 axis to cover the scatterers if they cannot be covered by a single level 0 cell (we take 3 cells in the strip P in the case of Fig.2.2). We note that there exist an infinite number of mirror images of the original level 0 cells. Multipole moments in the mirror images are exactly the same as those in the original level 0 cells except possibly for signs since the mirror images are given as one shifts and possibly flips ($x_1 \to -x_1$) the original level 0 cells. Indeed, the following relation holds:

$$M_n(\overline{Y}) = \begin{cases} M_n(Y), \text{ (for normal images)} \\ (-1)^n M_{-n}(Y), \text{ (for flipped images)} \end{cases} \tag{2.15}$$

where Y and $\overline{Y}$ are the centers of the original level 0 cell and its corresponding mirror image, respectively. We now focus on the target cell in Fig.2.2 painted in black where we compute the potentials, and set the center of the target cell to be $O = (0, 0)$. We then consider the contributions from other cells including mirror images to the target cell. It is clear that contributions from sources in the white cells around the target cell can be evaluated with the help of the ordinary FMM and (2.15). As regards the contributions from other cells, we apply (2.13) to cells filled with checker and stripe patterns in Fig.2.2 to see that these cells give rise to the following contributions:

$$V_s^{\text{Far}}(x) = \frac{i}{4} \sum_{n=-\infty}^{\infty} I_n(\overrightarrow{Ox}) \sum_{m=-\infty}^{\infty} \left(O_{-n-m}^{\text{even}}(s) + (-1)^m O_{-n+m}^{\text{odd}}(s) \right) M_m(Y). \tag{2.16}$$

where V_s^{Far} is the sum of contributions from far cells which are s units away (s may be negative) in x_2 direction from the target cell. The symbols O_n^{even} and O_n^{odd} stand for the following lattice sums:

$$O_n^{\text{even}}(s) = \begin{cases} \displaystyle\sum_{l=-\infty}^{\infty} O_n(-(2l\boldsymbol{e}_1 + s\boldsymbol{e}_2)), \ |s| \geq 2 \\ \displaystyle\left(\sum_{l=-\infty}^{-1} + \sum_{l=1}^{\infty} \right) O_n(-(2l\boldsymbol{e}_1 + s\boldsymbol{e}_2)), \ |s| \leq 1 \end{cases} \tag{2.17}$$

$$O_n^{\text{odd}}(s) = \begin{cases} \displaystyle\sum_{l=-\infty}^{\infty} O_n(-((2l+1)\boldsymbol{e}_1 + s\boldsymbol{e}_2)), \ |s| \geq 2 \\ \displaystyle\left(\sum_{l=-\infty}^{-2} + \sum_{l=1}^{\infty} \right) O_n(-((2l+1)\boldsymbol{e}_1 + s\boldsymbol{e}_2)), \ |s| \leq 1. \end{cases} \tag{2.18}$$

and the expression in (2.16) is summed over a finite interval of s (from 0 to 2 in the case of Fig.2.2). We note that lattice sums in (2.17) and (2.18) are used to evaluate the contributions from cells filled with checker and stripe patterns which are $|s|$ units away from the target cell along the x_2 direction, respectively (see Fig.2.2).

2.3.3 Computation of lattice sums

We compute the lattice sums by using the Fourier integral and the Poisson summation formula since the series expressions for O_n^{even} and O_n^{odd} in (2.17) and (2.18) converge very slowly. If $|s| < 2$, we compute O_n^{even} and O_n^{odd} by using the Fourier integrals as

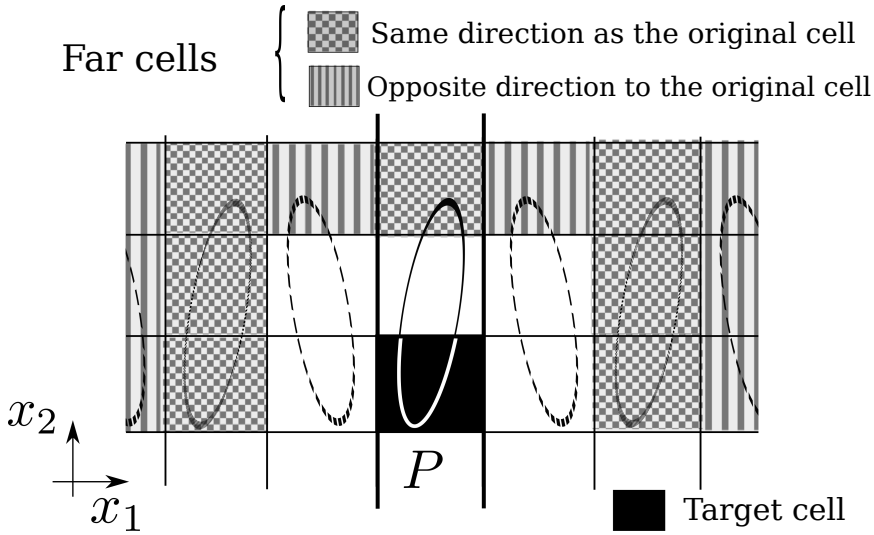

Figure 2.2: Normal and flipped mirror images of level 0 FMM cells

follows:

$$O_n^{\text{even}}(s) = \left(\sum_{l=-a+1}^{-1} + \sum_{l=1}^{a-1}\right) O_n(-(2l\boldsymbol{e}_1 + s\boldsymbol{e}_2)) + \frac{2}{\pi i}\int_C \frac{e^{-is\xi-2aq}\left(\left(-\frac{\xi-q}{ik_1}\right)^n + \left(-\frac{\xi+q}{ik_1}\right)^n\right)}{2q(1-e^{-2q})} d\xi \tag{2.19}$$

$$O_n^{\text{odd}}(s) = \left(\sum_{l=-a}^{-2} + \sum_{l=1}^{a-1}\right) O_n(-((2l+1)\boldsymbol{e}_1 + s\boldsymbol{e}_2)) + \frac{2}{\pi i}\int_C \frac{e^{-is\xi-(2a+1)q}\left(\left(-\frac{\xi-q}{ik_1}\right)^n + \left(-\frac{\xi+q}{ik_1}\right)^n\right)}{2q(1-e^{-2q})} d\xi, \tag{2.20}$$

where a is a natural number which controls the convergence rate of the integrals in (2.19) and (2.20). These formulae are obtained as one differentiates (2.7) (see Otani and Nishimura [18] for the derivation of similar results in periodic problems). As in the case of Green's function, the path of integration for the Fourier integral on the real axis is changed into the path C given by $\xi = \pm\sqrt{\tau^2 - 2ik_1\tau}$ in (2.19) and (2.20). We then take $a = 3$ and compute these integrals numerically in this thesis. If $|s| \geq 2$, we use the Poisson summation formula to compute O_n^{even} and O_n^{odd}:

$$O_n^{\text{even}}(s) = \sum_{l=-\infty}^{\infty} \frac{e^{-|s|p_l}}{4p_l}\left(\frac{\eta_l + \text{sgn}(s)p_l}{k_1}\right)^n \tag{2.21}$$

$$O_n^{\text{odd}}(s) = \sum_{l=-\infty}^{\infty} (-1)^l \frac{e^{-|s|p_l}}{4p_l}\left(\frac{\eta_l + \text{sgn}(s)p_l}{k_1}\right)^n \tag{2.22}$$

where we have used the same notation as in 2.2.2. These formulae are obtained as one differentiates (2.8).

Since O_n^{even} and O_n^{odd} depend only on the wavenumber k_1, they can be precomputed once for all in the FMM algorithm, and the computational cost for evaluating O_n^{even}

and O_n^{odd} does not depend on the DOF N for the problem and the shape of the scatterer. Therefore, the computational cost for our FMM is $O(N)$ as in the ordinary low frequency FMM.

Note that the difference between FMMs for waveguide problems and periodic problems in [18] is found in the M2L formula in (2.16) where 2 lattice sums are involved, while the periodic M2L formula includes one lattice sum. Also, the contributions from the near replicas of the original level 0 cells (white cells in Fig. 2.2) are evaluated after flipping scatterers in these replicas. Another difference is found in the use of Poisson's formula in (2.21) and (2.22) in the waveguide case, which could also be useful in periodic cases, but are more important in waveguides with many or long scatterers. Further addition to results in [18] will be made in the next section where the analytic continuation of the BIEM to complex ω is discussed in connection with SSM.

2.4 Numerical method of calculating resonance frequencies

This section discusses a numerical method of finding resonance frequencies. Mathematically, the resonance frequencies correspond to complex ω's at which the uniqueness of the solution of the problem does not hold. To determine them numerically, we write the discretized version of the integral equation in (2.9) or (2.10) as follows:

$$A(\omega)\mathsf{x} = \mathsf{b}. \tag{2.23}$$

The matrix $A(\omega)$ stands for the discretization of (2.9) or (2.10) which depends on ω in a non-linear manner, and is analytic in the complex plane cut along certain lines which we shall determine later. We reduce the problem of finding resonance frequencies to the non-linear eigenvalue problems of finding ω's such that the homogeneous equation $A(\omega)\mathsf{x} = 0$ has non-trivial solutions.

As a matter of fact, similar non-linear eigenvalue problems for the integral equations appear in periodic problems which have been addressed in Nose and Nishimura [29]. They successfully solved an eigenvalue problem for the Floquet wavenumber in periodic boundary value problems for Helmholtz' equation using the Sakurai-Sugiura projection method (SSM, [23, 24, 25]). We thus solve our eigenvalue problem for waveguide problems by using SSM, which we explain briefly in the next section.

2.4.1 Sakurai-Sugiura projection method

The SSM is an algorithm which finds non-linear eigenvalues of a matrix $A(z) \in \mathbb{C}^{N\times N}$ (i.e., the values of z for which the equation $A(z)\mathsf{x} = 0$ has non-trivial solutions) in the interior of γ where $A(z)$ is analytic, where γ is a certain closed contour in the complex plane. The SSM introduces two Hankel matrices $H_{mL} = [M_{i+j-2}]_{i,j=1}^{m} \in \mathbb{C}^{mL\times mL}$ and $H_{mL}^{<} = [M_{i+j-1}]_{i,j=1}^{m} \in \mathbb{C}^{mL\times mL}$ where M_k is a matrix defined as follows:

$$M_k = P^H \frac{1}{2\pi i}\int_\gamma z^k A^{-1}(z) Q dz,\ k = 0, \cdots, 2m-1, \tag{2.24}$$

and P and Q are arbitrary $N \times L$ matrices, respectively. The non-linear eigenvalues for the original problem are then obtained as solutions of the generalized eigenvalue problem given by $H_{mL}^{<}\mathsf{x} = zH_{mL}\mathsf{x}$. The corresponding eigenvectors for the original non-linear eigenvalue problem can also be obtained.

We set γ to be an ellipse which is parametrized by θ as $(\mathrm{Re}\,\gamma_0 + r_1 \cos\theta, \mathrm{Im}\,\gamma_0 + r_2 \sin\theta)$ where γ_0 is the center and r_1 and r_2 are the lengths of the major and minor axes of the ellipse, respectively. Also, the matrices M_k's in (2.24) are evaluated numerically with the N_{SS}-point trapezoidal rule. The number of eigenvalues within γ, denoted by K, is unknown which is determined as the number of singular values of H_{mL} larger than a given threshold δ. We thus see that one has to set parameters γ_0, r_1, r_2, m, L, N_{SS} and δ in order to use the SSM. We note that the costly inversion of $A(z)$ in (2.24) can be accelerated with FMM.

A few comments on the choice of the parameters of the SSM are in order. In all computations in this chapter, we set the parameters and γ so that we obtain up to about ten eigenvalues within a single contour. One can determine δ by checking the behavior of the singular values of H_{mL}. For example, the largest singular value of H_{mL} in the first problem in 2.5.2 for the γ centered at $5.2 + 0i$, was 3.36 and the second largest one was as small as 7.5×10^{-8}. We can obviously choose a proper threshold δ so that irrelevant small singular values are omitted. If the choice of δ is not clear, it means either that there are too many eigenvalues inside the contour, or that a spectrum outside the contour is too close to γ. One can deal with the former case by choosing larger values for m or L, or by using a smaller γ. The latter case is considered to be due to the numerical error of the integral in (2.24) [24]. This case usually results in inaccuracy of the obtained eigenvalues or even spurious eigenvalues. One may also deal with the latter problem by adjusting the contour γ, or by improving the accuracy of the integrals M_k with increased N_{SS}, L or the DOF of BIEM. An easier way to deal with the latter problem, however, is to test eigenvalues with the "reliability index" r_i proposed in [24]. The reliability index is defined based on an observation that spurious eigenvalues usually correspond to inferior singular values of H_{mL}. The larger the r_i is, the more reliable the corresponding eigenvalue is. See 2.5.2 for examples of the use of r_i. As regards the choice of P and Q we use random numbers. The case with $L \geq 2$ is called the block-SSM [24] while the original SSM in [23] uses vectors for P and Q (i.e., $L = 1$). We use the block-SSM because of the better accuracy [24]. Large L makes the calculation costly, however, it is required when one calculates eigenvalues with large multiplicities.

We remark that the approach in [22] and the SSM are related in that they search zeros or poles of similar functions. An advantage of SSM, however, is that it is not iterative while Muller's method used in [22] is iterative.

2.4.2 Analytic continuation of O_n^{even} and O_n^{odd} to complex ω

The variable z in the SSM is actually the frequency ω in our problem, which is a real number physically. In order to use the SSM, however, we need to evaluate $A(z)$ for complex z. Hence, we have to consider the analytic continuation of the Green's function to complex ω and hence to complex wavenumber k_1. This continuation must be interpreted carefully. In fact, if the wavenumber k_1 has a negative imaginary part, the lattice-sum expression of Green's function in (2.6) and O_n^{even} and O_n^{odd} in (2.17) and (2.18) diverge since the Hankel functions of the first kind $H_n^{(1)}(z)$ blow up as $|z| \to \infty$ when $\mathrm{Im}\, z < 0$.

One shows, however, that the Green's function computed as the Fourier integrals in (2.7) takes a finite value even if k_1 has a negative imaginary part unless k_1 is at a cutoff frequency. The same conclusion holds true with the Poisson summation formulae in (2.8) when we have $x_2 \neq y_2$ and with the lattice sums O_n^{even} (O_n^{odd}) computed with (2.19) and (2.21) ((2.20) and (2.22)), respectively. Hence, the Fourier integrals and the

Poisson sum representations give the desired analytic continuation of Green's function and the lattice sums.

We now determine the branch cuts of the above analytic continuations of Green's function and lattice sums given as the Fourier integrals and the Poisson sums. We first consider the integral on C in (2.7). Similar integrals in (2.19) and (2.20) can be treated analogously. Assume that $\operatorname{Re} k_1 > 0$. We note that the integral in (2.7) can be rewritten into the following form with the path of integration on the positive real axis:

$$\int_0^\infty \frac{f(\tau)}{2\sqrt{\tau^2 - 2ik_1\tau}\left(1 - e^{-2(\tau - ik_1)}\right)} d\tau. \tag{2.25}$$

where $f(\tau)$ is a function which stands for the numerator of the integrand in (2.7). The function $f(\tau)$ is analytic near the path of integration excluding the origin. One shows that the integral in (2.25) converges unless $k_1 = p\pi$ ($p \in \mathbb{N}$) (cutoff frequency) as one checks the behavior of the numerator as $\tau \to +\infty$ and the singularity of the integrands. One also shows that (2.25) diverges at the cutoff frequency. The poles of the integrand in (2.25) can be written as

$$z_p = -\operatorname{Im} k_1 + i(\operatorname{Re} k_1 - p\pi),\ p = 0, 1, 2, \cdots. \tag{2.26}$$

If $\operatorname{Im} k_1 < 0$, we see that the pole z_p may cross the positive real axis (i.e., the path of integration), and the integral in (2.25) changes discontinuously as $\operatorname{Re} k_1$ varies near $p\pi$. If $\operatorname{Im} k_1 > 0$, however, the pole z_p never crosses the path of integration and the integral in (2.25) remains continuous. We therefore see that the following lines are the branch cuts of the integral in (2.25), and, hence, of Green's function Γ in (2.7):

$$k_1 = p\pi - i\kappa,\ p \in \mathbb{N}, \kappa \geq 0 \tag{2.27}$$

Obviously, the choice of the branch cuts of the Green's function given as the Poisson sum (2.8) has to be consistent with (2.27). As a matter of fact, one shows that the branch cuts for the square root in (2.5) are the right choice. Indeed, as we consider the behavior of the Poisson sum in (2.8) when k_1 is around $p\pi$, we see that

$$\lim_{\delta \to +0} \sqrt{(p\pi)^2 - (p\pi + \delta - it)^2} = -\lim_{\delta \to +0} \sqrt{(p\pi)^2 - (p\pi - \delta - it)^2}, \tag{2.28}$$

holds for $t > 0$ by considering the definition of the square root in (2.5). Eq.(2.28) shows that the p-th summand in the Poisson sum in (2.8) changes discontinuously when k_1 crosses the lines in (2.27). Therefore, the lines in (2.27) are also branch cuts of the Poisson sum in (2.8), and hence of (2.21) and (2.22), as well.

We thus see that the analytic continuation of the Green's function for a complex ω is obtained just by setting a complex ω in (2.7) and (2.8) unless (2.27) holds. We can therefore apply the SSM to our integral equations by taking a contour γ in (2.24) so that it does not touch (2.27).

We note, however, that Green's function and related lattice sums blow up as $\operatorname{Im} k_1 \to -\infty$ and the computation of these functions becomes difficult.

2.5 Numerical examples

In this section, we solve some boundary value problems (transmission and Neumann problems) and the associated eigenvalue problems in order to test the performance of

the proposed method. We use piecewise constant boundary elements and the collocation method in the following examples. The required integrals are computed after splitting the kernel functions into the singular part and the remainder. The former part is integrated analytically, while the remainder is computed with the Gaussian quadrature. We solve the discretized integral equations iteratively with GMRES. In the following examples we set the tolerance (relative error) for GMRES to be 10^{-8}. Also, we set $\epsilon_1 = 1$ and $\mu = 1$, i.e., $\omega = k_1$. The incident wave is $u^{\text{inc}} = r_0^+(x) = e^{ik_1x_2}$ unless stated otherwise. The following computations were carried out with rather fine meshes in order to improve the accuracy near resonance frequencies although we consider only low-frequency cases. We used a cluster of Appro GreenBlade 8000 (Intel Xeon core) at the Academic Center for Computing and Media Studies of Kyoto University for the computation.

2.5.1 Accuracy and computational time

To test the accuracy of the proposed method, we first consider cases in which we can obtain exact solutions. We introduce the error indicators of the numerical solution u and q relative to the exact solutions defined as follows:

$$\text{error}_u = \frac{\sqrt{\sum_{i=1}^N |u(i) - u^{\text{exact}}(i)|^2}}{\sqrt{\sum_{i=1}^N |u^{\text{exact}}(i)|^2}}, \ \text{error}_q = \frac{\sqrt{\sum_{i=1}^N |q(i) - q^{\text{exact}}(i)|^2}}{\sqrt{\sum_{i=1}^N |q^{\text{exact}}(i)|^2}} \tag{2.29}$$

where $u(i)$ and $q(i)$ are the numerical solutions for u and q on the i-th element and $u^{\text{exact}}(i)$ and $q^{\text{exact}}(i)$ are the corresponding exact solutions, respectively.

We solve a transmission problem for M circular scatterers each having a radius of 0.3 and whose centers are $(0,0)$, $(0,-1), \cdots$ and $(0,-M+1)$ (Fig.2.3). We consider the case of $M = 4$ and set $\epsilon_2 = 1$ in each of the circles, $\epsilon_1 = 1$ in the outside, and $\omega = 10$ $(= 3.18 \times \pi)$. Obviously, the incident wave gives the exact solution in this case. We vary the DOF to test the accuracy and the computational time. Fig.2.4 shows the computational time needed to obtain the numerical solution (including the computational time for the lattice sums O_n^{even} and O_n^{odd}, and the code is parallelized with OpenMP and the number of CPU is 16.) and the relative error of u defined in (2.29). We found that GMRES converges within 7 iterations at the most in this example. Fig.2.4 shows that the computational time and the error are approximately $O(N)$ and $O(1/N)$, respectively. Also, we see that the solution is accurate to within about a relative error of 1.2% even with the coarsest mesh. We thus verify the accuracy and the efficiency of our method.

2.5.2 Neumann problems

Half elliptic notch

We next consider the scattering by a half elliptic notch shown in Fig.2.5(a) with the homogeneous Neumann condition. The center of the notch is $(-0.5, 0)$ and the major and minor axes of the notch are 1.5 and 0.75, respectively. We vary ω within the interval of $(0, 2\pi)$ to compute the reflectance and the transmittance defined in 2.2.4. The number of elements on each ellipse is 1000. Fig.2.5(b) and (c) show the reflectances and transmittances obtained by our method and the results by Linton and Evans [6], respectively. We see that the results in Fig.2.5(b) agree well with those in Fig.2.5(c) except for some spikes in Fig.2.5(c). These spikes are due to the fictitious eigenvalues,

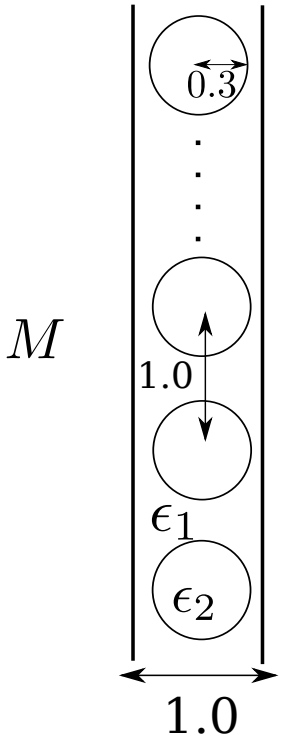

Figure 2.3: Multiple circular scatterers

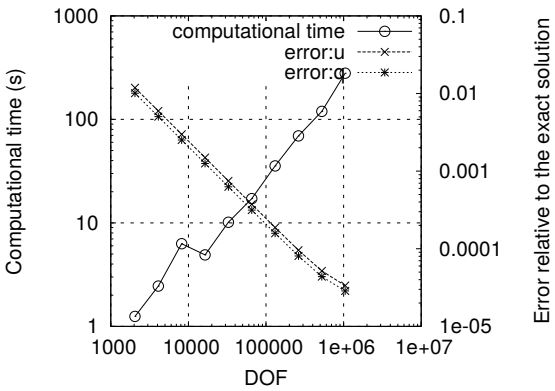

Figure 2.4: Total computational time and error relative to the exact solution (4 circular scatterers)

as Linton and Evans point out [6]. These spikes do not appear in Fig.2.5(b) because we use the Burton-Miller equation. Note that the conservation law (2.11) holds to within 0.2% in our method for all the ω's tested.

Half elliptic notch: eigenvalues

We next validate our implementation of SSM by considering the fictitious eigenvalues in Fig.2.5(c). Namely, we check if we can find all the eigenvalues corresponding to the locations of the spikes in Fig.2.5(c) when we set $\alpha = 0$ and none of them if we set $\alpha = -i/k_1$ in (2.10). In the numerical calculation, we set the contours of the SSM γ to be 2 ellipses with major and minor axes of 0.5 and 0.2 and centers of $5.2 + i0$ and $5.7 + i0$, respectively. Other parameters for the SSM are $N_{SS} = 64,\ m = 8,\ \delta = 0.1$ and $L = 6$.

With $\alpha = 0$ we have obtained two eigenvalues with very small imaginary parts given by $\omega/\pi = 1.637 - 4.485 \times 10^{-7}i$ and $\omega/\pi = 1.938 - 4.788 \times 10^{-7}i$, which agree well with the spikes in Fig.2.5(c). When we set $\alpha = -i/k_1$, however, we did not find any eigenvalues. This result suggests the validity of our implementation of the SSM. The computational times for obtaining eigenvalues inside each γ were about 77s for $\alpha = 0$ and 203s for $\alpha = -i/k_1$, respectively (the code is parallelized with OpenMP-MPI $8 \times 8 = 64$ CPU cores).

Elliptic scatterer: eigenvalues near a branch cut

We next consider eigenvalues near a branch cut since other numerical approaches using PML are known to suffer from spurious eigenvalues caused by continuous spectrum [9]. We follow Duan et al. [9] to consider a Neumann problem for rotated single

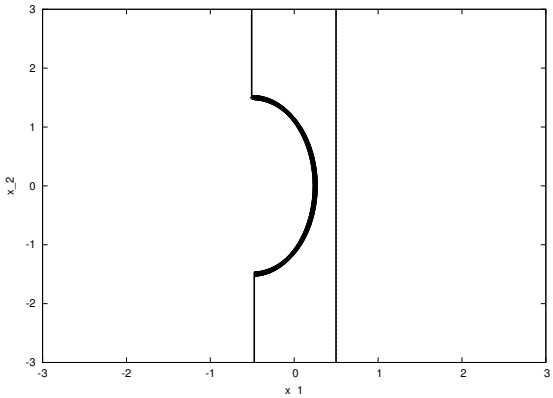

(a) Half elliptic notch

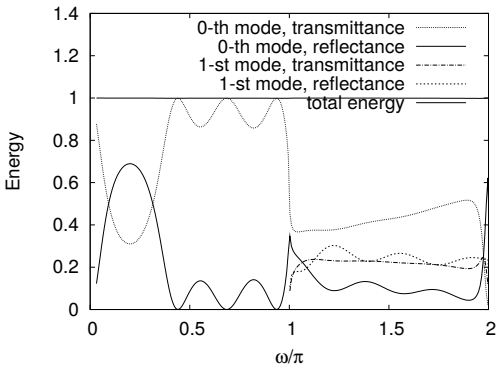

(b) Transmittances and reflectances obtained by our FMM

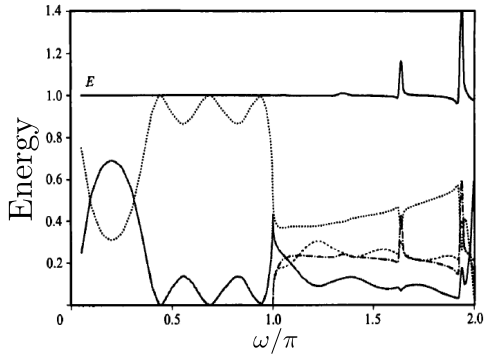

(c) Figure.4 of Linton and Evans [6] (Reproduced with permission. Axis labels are modified to be consistent with our notations)

Figure 2.5: Transmittance and the Reflectance

elliptic scatterer in order to investigate this issue. The center of the scatterer is on the centerline of the waveguide, the major and minor axis lengths are 0.5 and 0.2 and the angle of rotation of the major axis is ϕ from the centerline $x_2 = 0$. In our computation, we take the major axis length to be 0.4999 in order to avoid the contact of the scatterer with the waveguide wall. We vary ϕ from $0°$ to $90°$ to obtain the eigenvalues of this problem near the branch cut $\omega = \pi - it$ $(t \geq 0)$. As the contours of the SSM, we use 6 ellipses whose axis lengths are 1.0 (0.5) along the real (imaginary) axis and whose centers are $\{2.14, 4.143\} - 0.25i \times p$ $(p = 0, 1, 2)$. The distance between these contours and the branch cut is about 0.05% of π, which is the real part of the relevant cutoff frequency. The number of elements on the elliptic scatterer is 100. We tested three values $N_{SS} = 64, 128, 256$, and the other parameters of the SSM are the same as in the previous examples. Figs.2.6(a) and (b) show the eigenvalues and the contours of the SSM, and the results obtained by Duan et al. [9] (Figure.9(a) in [9]), respectively. Note that the axes are scaled with 2π in Figs.2.6. The eigenvalues for different ϕ's (every 2 degrees between $0°$ to $90°$ in Fig.2.6(a)) are plotted together in these graphs.

In Figs.2.6, eigenvalues which compose a smooth curve to the left of $\mathrm{Re}\,\omega/2\pi \approx 0.49$ are considered to be true resonance frequencies, while those scattered near $\mathrm{Re}\,\omega/2\pi \approx 0.5$ in Fig.2.6(b) are spurious ones, respectively. We see that the true resonance frequencies are obtained robustly with different parameters of SSM, in contrast to the results by Duan et al. [9] obtained with PML, where even the numerical results for these true resonance frequencies seem to depend on the choice of PML parameters. As

a matter of fact, SSM also does obtain spurious eigenvalues near the branch cut, as one can see in Fig.2.6(c) which is a blow-up of Fig.2.6(a) near $\mathrm{Re}\,\omega/2\pi = 0.5$. The color in this figure indicates the value of the reliability index r_i discussed in 2.4.1. Those eigenvalues with smaller values of r_i (blue symbols) are considered spurious not only because of their small r_i but also because they disappear as one increases N_{SS}. This figure also shows that the spread of spurious eigenvalues with SSM are more confined near the branch point than the results in Fig.2.6(b). In addition, we see that some of almost real eigenvalues with larger r_i in the interval of $0.49 < \mathrm{Re}\,\omega/2\pi < 0.5$ are quite likely to be true ones. We thus plot those eigenvalues with $r_i > 20\delta$ in Fig.2.6(d). We believe that this figure includes true ones. We note that there exists an eigenvalue with very small imaginary part at $\omega/2\pi \approx 0.492$. This eigenvalue is obtained for the $\phi = 90°$ case where the waveguide is approximately equivalent to a semi-infinite waveguide which is terminated by a semi-elliptic arc. For comparison we calculated eigenvalues for this semi-infinite waveguide by using the SSM with a finer mesh to obtain $\omega/2\pi = 0.4921 - 4.408 \times 10^{-5}i$ which is close to the eigenvalue in Fig.2.6(d). We emphasize that we did not set the contours of the SSM so as to avoid the spurious eigenvalues with $\mathrm{Re}\,\omega/2\pi > 0.5$ found in Fig.2.6(b) (for example, the ones near $0.52 - 0.07i$ are obviously enclosed by the contours of the SSM in Fig.2.6(a)).

We thus conclude that the SSM is quite reliable even near branch cuts. This observation suggests that the present approach is of interest particularly when the reliability is more important than the computational cost.

2.5.3 Transmission problems

We next test the performances of our methods in transmission problems.

Transmittances

We first show the results of far field analysis for transmission problems with $M = 1, 4, 16$ circles shown in Fig.2.3. We set $\epsilon_2 = 10$ and vary ω within the interval of $(0, 2\pi)$ in these examples. The number of elements on each circle is 1000.

Fig.2.7(a) shows the total transmittance $\sum_n \xi_n f_n |A_n^+|^2$. The convergence of GMRES was achieved within 400 iterations even in the worst case. We see that the energy transmittance for a single scatterer ($M = 1$) varies smoothly with ω. In the multiple scatterers cases with $M = 4, 16$, on the other hand, there exist sudden changes of the energy, and also stopbands between $\omega \approx 2.75$ and 4.0, and between $\omega \approx 4.7$ and 5.2. We can find stopbands even in the $M = 4$ scatterers case although the change of the energy transmittance in the $M = 16$ case seems to be sharper. We also see that there exists a very sharp passband near $\omega \approx 3.75$. Fig.2.7(b) shows the transmittances near $\omega \approx 3.75$ plotted in the logarithmic scale. We notice that the passband shown in Fig.2.7(a) near $\omega \approx 3.75$ actually consists of many very sharp passbands. This cluster of stopbands exists only in the cases of multiple scatterers $M = 4, 16$. The number of passbands for the case $M = 16$ is much larger than that of the case of $M = 4$. Fig.2.7(c) shows the error of the energy conservation law in (2.12), which holds to within 3.1%. The frequencies with large error correspond to the very sharp passbands at $\omega \approx 3.75$ and very sharp spikes at $\omega \approx 5.85$, and the energy conservation law holds more accurately elsewhere.

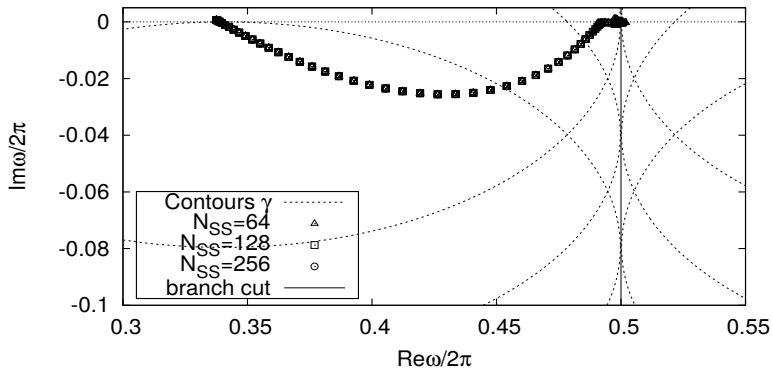

(a) Eigenvalues for various angles of rotation ϕ.

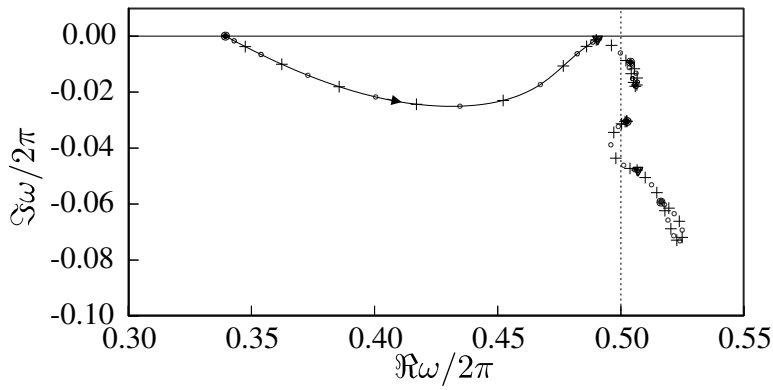

(b) Figure.9(a) of Duan et al. [9](Reproduced with permission. Axis labels are modified to be consistent with our notations, and figure number is removed from the original figure.)

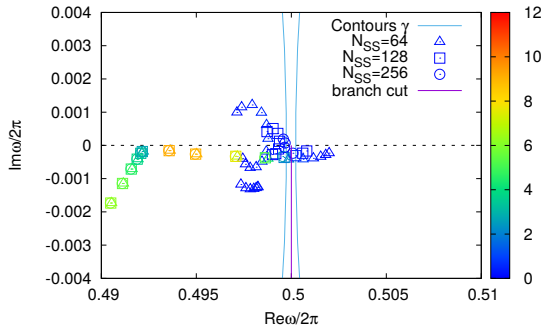

(c) Eigenvalues and reliability indices for various angles of rotation ϕ near $\mathrm{Re}\,\omega/2\pi = 0.5$

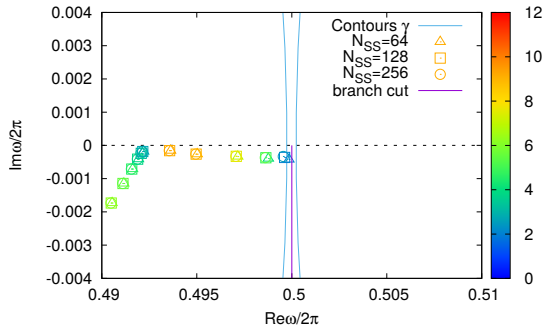

(d) Eigenvalues with $r_i > 20\delta$

Figure 2.6: Eigenvalues for various rotated single elliptic scatterers

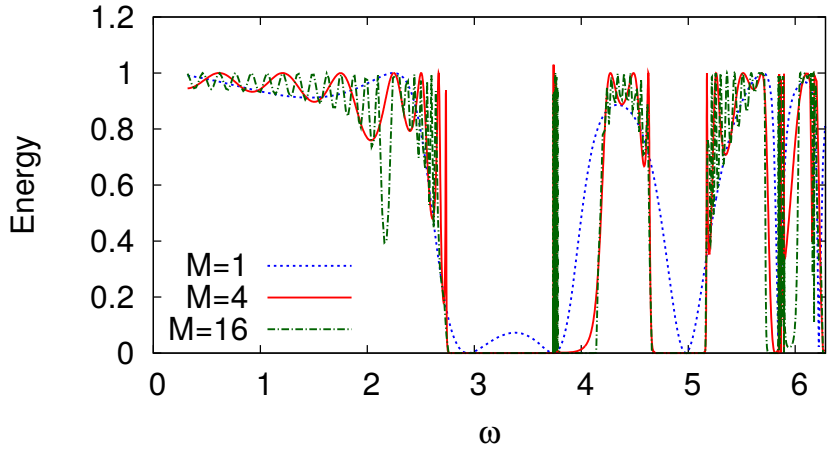

(a) Transmittance, $\omega \in (0, 2\pi)$

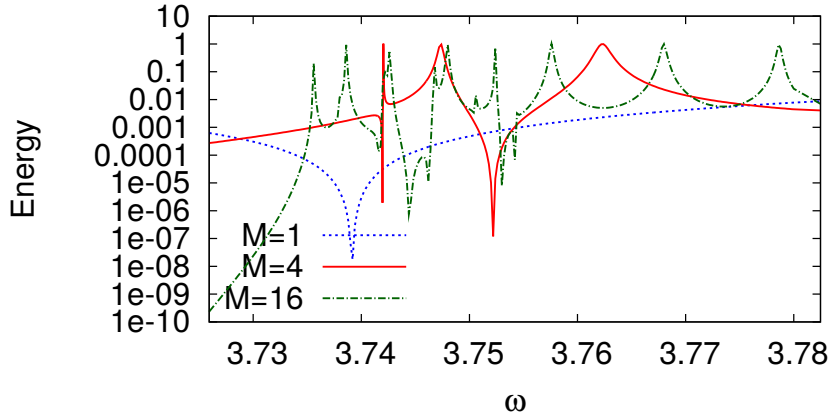

(b) Transmittance, $\omega \in (3.73, 3.78)$, logarithmic scale

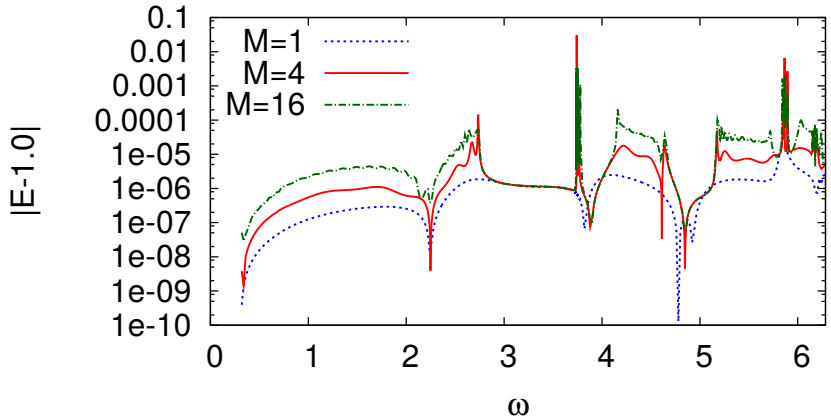

(c) error $|E - 1.0|$, $\omega \in (0, 2\pi)$

Figure 2.7: Transmittance and the energy conservation law

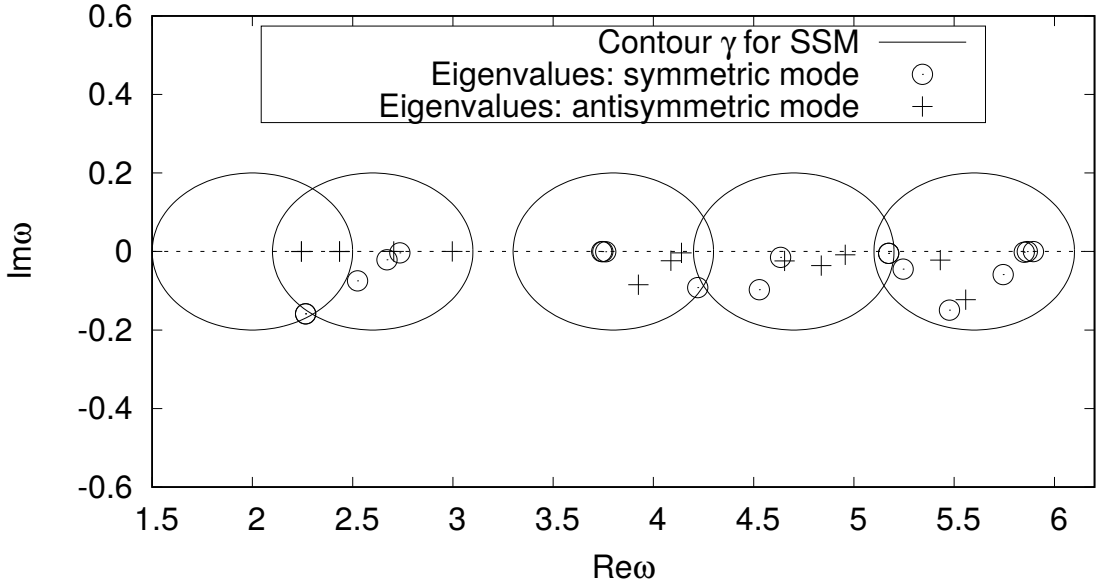

Figure 2.8: Eigenvalues and the contour for the SSM. ○: eigenvalues with symmetric eigenmodes about the centerline, +: eigenvalues with antisymmetric modes about the centerline.

Eigenvalues

The above phenomena of the sudden changes of the transmittance are similar to those in periodic transmission problems [16, 21] or in Neumann problems for waveguides [8], and are considered to be related to the existence of the resonance frequencies. To see this, we apply the SSM to determine the eigenvalues ω of the integral operator in (2.9) for the case of $M = 4$ scatterers.

We set the contours of the SSM to be ellipses whose major and minor axes are 0.5 and 0.2, and other parameters for the SSM are set to be $N_{SS} = 128,\ m = 12,\ L = 6$ and $\delta = 0.01$.

We plot the obtained eigenvalues and the contours used in the SSM in Fig.2.8. Almost all of these eigenvalues have expected non-positive imaginary parts except for some eigenvalues having positive imaginary parts smaller than 10^{-6} in magnitude. The minuscule positive imaginary parts of some eigenvalues are quite likely to be due to the numerical error and these eigenvalues are possibly real numbers in reality. Although it is difficult to conclude that they are in fact real eigenvalues or not, it is enough for us to know the magnitude of the imaginary part in order to tell how seriously the eigenvalue affects the behavior of the solution.

Due to the geometric symmetry about the centerline $x_1 = 0$, the eigenmodes (non-trivial solutions for corresponding eigenvalues) are divided into symmetric and anti-symmetric modes about the centerline. The eigenvalues with symmetric modes are plotted with circles and those with antisymmetric modes are plotted with plus signs in Fig.2.8.

The computational time for obtaining eigenvalues inside each γ was about 91.5 and 25.9 minutes on average with OpenMP parallelized with 16 CPU cores and OpenMP-MPI parallerized with $8 \times 8 = 64$ CPU cores, respectively. Note that the needed number of inversion $A^{-1}(\omega_j)Q$ is $128(= N_{SS}) \times 6(= L) = 768$.

Resonance frequencies

We examine if all the eigenvalues in Fig.2.8 actually have some relevance to resonance phenomena. Fig.2.9 shows the eigenvalues and solutions ($||u||$ and transmittances) against ω, where $||u||$ stands for the L^2 norm of u on $\partial\Omega$. The upper and the lower graphs of Fig.2.9(a) show the eigenvalues with symmetric eigenmodes about the centerline and the transmittances produced by an incident r_0^+ wave which is symmetric about the centerline, respectively. This figure shows that each eigenvalue corresponds to a peak in the transmittances.

We also consider the case of incident antisymmetric wave about the centerline, in which antisymmetric eigenmodes may be excited. Fig.2.9(b) and (c) show the eigenvalues whose eigenmodes are antisymmetric about the centerline (the upper graphs) and $||u||$'s and transmittances against ω (the lower graphs), respectively. Note that the incident wave r_1^+ and the scattered waves are evanescent (hence no transmittance) for $\omega < \pi$ (Fig.2.9(b)) and the solution for this problem does not exist at the eigenvalues, which is in contrast to the incident plane wave case where the solution exists (this can be proved with a small modification to the proof for a related result in periodic problems shown in [46]). In Fig.2.9(b), we can see sudden changes and blow up of the solutions at eigenvalues: $\mathrm{Re}\,\omega = 2.244,\ 2.434,\ 2.704$ and 2.996, which are almost real numbers. We can also find a peak in the transmittances in Fig.2.9(c) for each of the eigenvalues as in the symmetric case.

We thus conclude that eigenvalues in Fig.2.8 are actually resonance frequencies. In addition, the smaller the imaginary part of the eigenvalue is, the more suddenly the solution changes near these eigenvalues.

Finally, we note that stopbands appear to exist between two consecutive eigenvalues having relatively small imaginary parts.

Non-symmetric scatterers

We also show numerical results for a perturbed case in which the centers of the scatterers considered in the previous section are shifted from $x_1 = 0$ to $x_1 = 0.1$. In this case, the scatterers and the eigenmodes are no longer symmetric about the centerline of the waveguide. We consider the $M = 4$ case as an example. Fig.2.10 shows the eigenvalues between $\omega = 2.0$ and $\omega = 6.0$ obtained with SSM (Parameters for the SSM are the same as in the previous examples) and the transmittances with incident r_0^+ and r_1^+ waves. In the upper figure, we have indicated by colors those eigenvalues branched from ones having symmetric (red) or antisymmetric (green) eigenmodes in the configuration without shift. With a slight abuse of words, we call those eigenvalues symmetric or antisymmetric according to their colors in this figure.

Once again, we see that eigenvalues with smaller imaginary parts cause sharper peaks. We also note that the response to the symmetric (antisymmetric) incident r_0^+ (r_1^+) wave is strongly affected by symmetric (antisymmetric) eigenvalues, but is influenced by antisymmetric (symmetric) ones as well. For example, the stopbands in the r_0^+ wave response appear to exist basically between consecutive symmetric eigenvalues having small imaginary parts, with some passbands corresponding to antisymmetric eigenvalues.

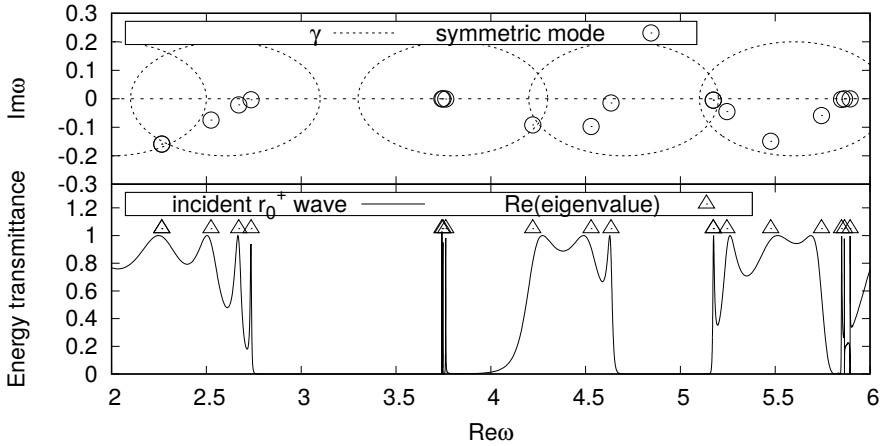

(a) Transmittances for incident r_0^+

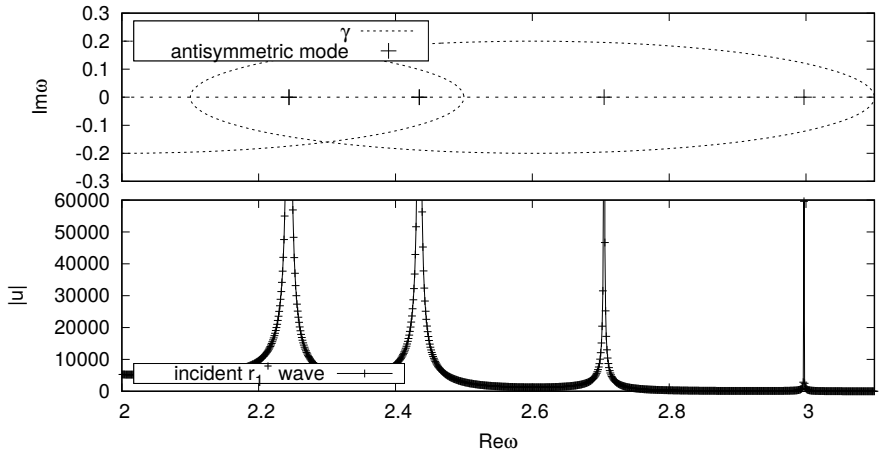

(b) $||u||$'s for incident r_1^+

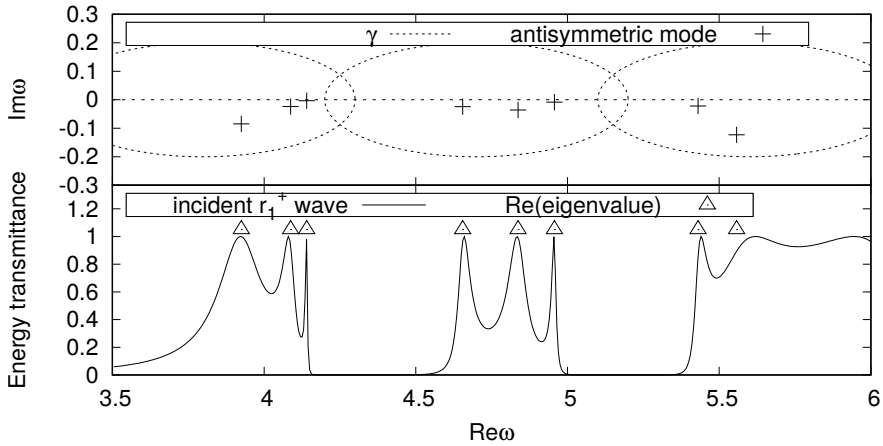

(c) Transmittances for incident r_1^+

Figure 2.9: Eigenvalues and solutions

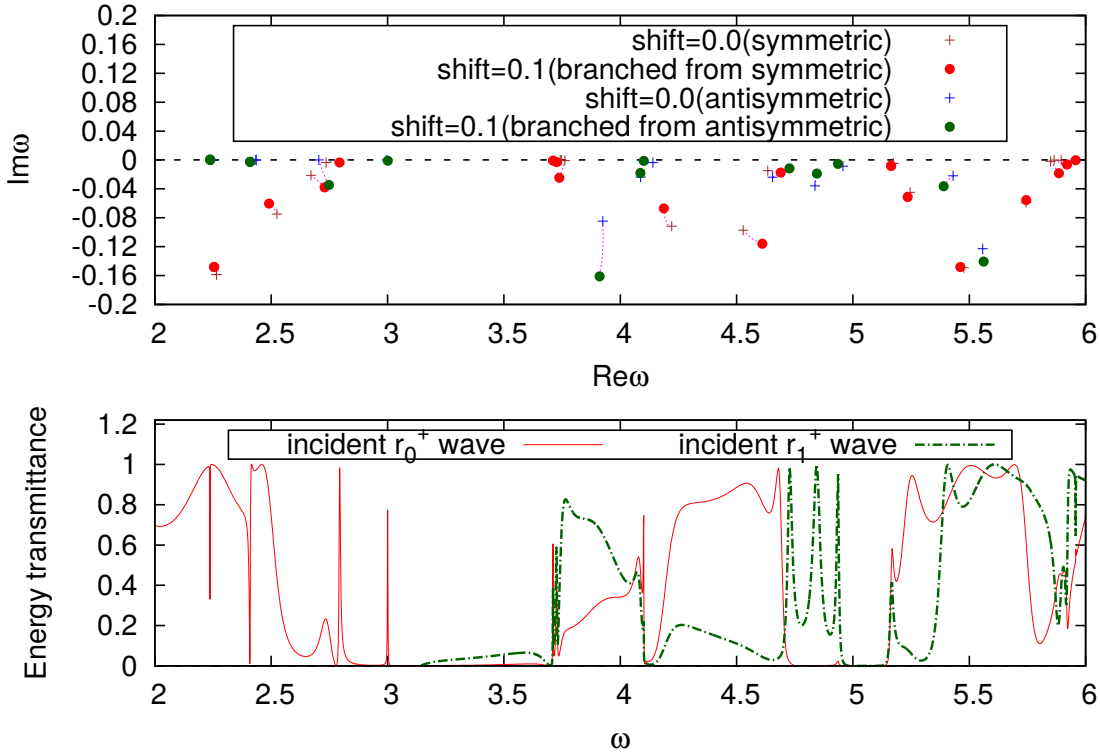

Figure 2.10: Eigenvalues and transmittances for 4 circular scatterers perturbed from the centerline.

2.6 Concluding remarks

- We have proposed an FMM for solving scattering problems for a two dimensional infinite strip with the homogeneous Neumann boundary condition on the sides, with the help of the method of images. We have also combined our method with the Sakurai-Sugiura projection method to find resonance frequencies for the waveguide problems after considering the analytic continuation of the formulation into a complex ω. The proposed methods are shown to be useful through numerical examples.

- As we have mentioned in chapter 2.2.3, the PMCHWT formulation presented in this chapter is not without fictitious eigenvalue problems if one considers leaky modes. Indeed, the fictitious eigenvalues of our formulation are the complex eigenvalues of an infinite domain having the original scatterer with the material constants of the interior and exterior interchanged. Fortunately, this problem is resolved as one replaces G^2 in (2.9) by the "incoming" fundamental solution $(-i/4)H_0^{(2)}(k_2|\boldsymbol{x}|)$. The fictitious eigenvalues can then easily be distinguished from the true ones since the former are with positive imaginary parts, while the latter are with non-positive imaginary parts. The current formulation, however, is still useful in many practical applications since the fictitious eigenvalues are often very far from true ones of interest. Indeed, we have checked that all the eigenvalues for transmission problems presented in this chapter are true ones by using the modified formulation. Further details of this issue is discussed in the next chapter.

Chapter 3

Boundary integral equations for calculating complex eigenvalues of transmission problems

3.1 Introduction

In chapter 2, we have shown that the resonance frequency problems can be solved efficiently with the boundary integral equation method (BIEM) and Sakurai-Sugiura projection method (SSM). However, BIEM may have fictitious eigenvalues even when one uses the PMCHWT or Müller formulations which are known to be resonance free when the frequency is real valued. In this chapter, we propose new BIEs for transmission problems with which one can distinguish true and fictitious eigenvalues easily.

This chapter is organized as follows: In section 3.2, we formulate the transmission resonance problems and the corresponding coupled BIEs for the waveguide problems for Helmholtz' equation in 2D and the standard scattering problems for Maxwell's equations in 3D. We consider both Müller's and PMCHWT formulations for these 2 cases. We then identify fictitious eigenvalues for the integral equations considered and propose BIEs which can distinguish true and fictitious eigenvalues clearly. We show, in particular, that eigenvalues of the Müller and PMCHWT formulations for Maxwell's equations are identical including fictitious ones. In section 3.3, we present some numerical examples which prove the effectiveness of the proposed method. We also show that true complex eigenvalues affect the behavior of the solution and that fictitious complex eigenvalues may deteriorate the accuracy of the solutions for the ordinary boundary value problems with real frequencies.

The material in this chapter is taken from Misawa et al. [39] which is accepted for publication in SIAM Journal on Applied Mathematics.

3.2 Formulation

In this section, we formulate transmission resonance problems and derive BIEs discussed in this study. We consider one single scatterer for simplicity, although the results in the following discussions hold for multiple scatterers cases as well.

3.2.1 Transmission resonance problems for waveguides for Helmholtz' equation

We first consider elastic waves governed by Helmholtz' equation in 2D. Let P be an infinite strip given by $P = [-1/2, 1/2] \times \mathbb{R}$. Also, let $\Omega = \Omega_2 \subset P$ be a finite sized scatterer, $\partial\Omega = \partial\Omega_2$ be its boundary and $\Omega_1 = P \setminus \overline{\Omega_2}$. We consider the following homogeneous transmission problem: find u which satisfies Helmholtz' equation

$$\Delta u + k_\nu^2 u = 0 \quad \text{in } \Omega_\nu \ (\nu = 1, 2),$$

boundary conditions

$$u^+ = u^- \ (= u), \quad s_1 \frac{\partial u^+}{\partial n} = s_2 \frac{\partial u^-}{\partial n} \ (= q) \quad \text{on } \partial\Omega, \tag{3.1}$$

and the homogeneous Neumann boundary condition on the sides of the strip:

$$\frac{\partial u}{\partial x_1} = 0 \quad \text{on } x_1 = \pm\frac{1}{2}.$$

We impose the radiation condition which requires that u is written as follows:

$$u(x) \approx \sum_{l \geq 0} C_l^{\pm} \cos l\pi \left(x_1 + \frac{1}{2} \right) e^{-\sqrt{(l\pi)^2 - k_1^2}|x_2|} \text{ as } x_2 \to \pm\infty, \tag{3.2}$$

where ρ_ν, s_ν and $k_\nu = \omega\sqrt{\rho_\nu / s_\nu}$ are the density, shear modulus (real numbers) and the wavenumber in Ω_ν $(\nu = 1, 2)$, respectively. The frequency ω is allowed to take a complex value. Also, the superscript $+$ $(-)$ in (3.1) stands for the trace to $\partial\Omega$ from Ω_1 (Ω_2), $\partial/\partial n$ for the normal derivative and $\boldsymbol{n}$ for the unit normal vector on $\partial\Omega$ directed towards Ω_1, respectively. We make the square root $\sqrt{(l\pi)^2 - k_1^2}$ in (3.2) single valued as a function of k_1 by taking the branch which is analytic in the complex plane cut along $(-l\pi, -l\pi - i\infty)$ and $(l\pi, l\pi - i\infty)$ and approaches $-ik_1$ in the upper plane as $|k_1| \to \infty$. This definition of the square root ensures that the summands in (3.2) decay as $l \to \infty$ and allows the analytic continuation of the radiation condition to a complex ω.

In the following, we call the above homogeneous problem the "waveguide problem" or the "original BVP" (original boundary value problem). The transmission resonance problem determines resonance frequencies at which the waveguide problem has non-trivial solutions. We call resonance frequencies "true eigenvalues" in order to distinguish without ambiguity from the "fictitious eigenvalues" which we shall describe in 3.2.3. We note that the true eigenvalues of the waveguide problem have non-positive imaginary parts.

3.2.2 BIEs for Helmholtz' equation

We now formulate BIEs for the transmission resonance problem. We define U^ν as follows:

$$U^\nu(x) = (-1)^\nu \left(\frac{1}{s_\nu} \int_{\partial\Omega} G^\nu(x, y) q(y) ds_y - \int_{\partial\Omega} \frac{\partial G^\nu(x, y)}{\partial n_y} u(y) ds_y \right), \ \nu = 1, 2 \tag{3.3}$$

where G^1 stands for Green's function for the waveguide with the wavenumber k_1 and G^2 for the fundamental solution with the wavenumber k_2, respectively:

$$G^1(x,y) = \sum_{l=0}^{\infty} \frac{e^{-\sqrt{(l\pi)^2-k_1^2}|x_2-y_2|}}{2f_l\sqrt{(l\pi)^2-k_1^2}} \cos l\pi\left(x_1+\frac{1}{2}\right)\cos l\pi\left(y_1+\frac{1}{2}\right) \tag{3.4}$$

$$G^2(x,y) = \frac{i}{4}H_0^{(1)}(k_2|\boldsymbol{x}-\boldsymbol{y}|). \tag{3.5}$$

In (3.4), f_l is 1 for $l=0$ and $1/2$ for $l \neq 0$ and $H_n^{(\iota)}$ stands for the Hankel function of the ι-th kind and n-th order, respectively. Also, bold letters $\boldsymbol{x}$, $\boldsymbol{y}$, etc. stand for the position vectors of the points x, y, etc.

It is well-known that U^ν $(\nu = 1,2)$ give potential representations of the solution u of the transmission problem in 3.2.1 in Ω_ν with the boundary traces of the solution as the layer-potential densities, iff U^1 (U^2) vanishes in Ω_2 $(\mathbb{R}^2 \setminus \overline{\Omega_2})$. This condition gives

$$U^{1-} = U^{2+} = \frac{\partial U^{1-}}{\partial n} = \frac{\partial U^{2+}}{\partial n} = 0 \text{ on } \partial\Omega. \tag{3.6}$$

The Müller formulation of BIE for Helmholtz' equation in 2D given by

$$\begin{aligned}
&\frac{s_1+s_2}{2}u - \int_{\partial\Omega}\left(s_1\frac{\partial G^1}{\partial n_y} - s_2\frac{\partial G^2}{\partial n_y}\right)u\,ds_y + \int_{\partial\Omega}\left(G^1-G^2\right)q\,ds_y = 0\\
&\frac{s_1+s_2}{2s_1s_2}q - \int_{\partial\Omega}\left(\frac{\partial^2 G^1}{\partial n_x\partial n_y} - \frac{\partial^2 G^2}{\partial n_x\partial n_y}\right)u\,ds_y + \int_{\partial\Omega}\left(\frac{1}{s_1}\frac{\partial G^1}{\partial n_x} - \frac{1}{s_2}\frac{\partial G^2}{\partial n_x}\right)q\,ds_y = 0
\end{aligned} \tag{3.7}$$

is derived from (3.6) with the help of the conditions

$$-s_1U^{1-} = s_2U^{2+},\ -\frac{\partial U^{1-}}{\partial n} = \frac{\partial U^{2+}}{\partial n} \quad \text{on } \partial\Omega. \tag{3.8}$$

We also consider the following PMCHWT formulation:

$$\begin{aligned}
&\int_{\partial\Omega}\left(\frac{\partial G^1}{\partial n_y} + \frac{\partial G^2}{\partial n_y}\right)u\,ds_y - \int_{\partial\Omega}\left(\frac{1}{s_1}G^1 + \frac{1}{s_2}G^2\right)q\,ds_y = 0\\
&\fint_{\partial\Omega}\left(s_1\frac{\partial^2 G^1}{\partial n_x\partial n_y} + s_2\frac{\partial^2 G^2}{\partial n_x\partial n_y}\right)u\,ds_y - \int_{\partial\Omega}\left(\frac{\partial G^1}{\partial n_x} + \frac{\partial G^2}{\partial n_x}\right)q\,ds_y = 0
\end{aligned} \tag{3.9}$$

obtained similarly from the conditions

$$U^{1-} = U^{2+},\ s_1\frac{\partial U^{1-}}{\partial n} = s_2\frac{\partial U^{2+}}{\partial n} \quad \text{on } \partial\Omega. \tag{3.10}$$

One may want to solve the transmission resonance problems by finding complex ω's such that these integral equations have non-trivial solutions, i.e., the non-linear eigenvalues for BIEs in (3.7) or (3.9). This issue is further discussed in the next section.

3.2.3 Fictitious eigenvalues

We have reduced the transmission resonance problem to a non-linear eigenvalue problem for BIEs in (3.7) or (3.9). However, as we shall see, these equations may pick up fictitious eigenvalues which we now characterize.

We discuss in detail the Müller formulation because the PMCHWT case can be treated in a similar manner. We note that the following statement holds (a similar statement is given in [21]): A frequency ω at which the BIEs in (3.7) have non-trivial solutions corresponds either to the eigenvalue of the original waveguide problem or that of the following transmission resonance problem for v in the free space $\mathbb{R}^2$ in which the governing equations in Ω_1 and Ω_2 are interchanged; we refer to [47] for the (3-D) explicit form of the radiation condition for a complex wavenumber:

$$\Delta v + k_2^2 v = 0 \text{ in } \mathbb{R}^2 \setminus \overline{\Omega_2}, \quad \Delta v + k_1^2 v = 0 \text{ in } \Omega_2, \tag{3.11}$$

$$v^- = v^+, \quad s_2 \frac{\partial v^-}{\partial n} = s_1 \frac{\partial v^+}{\partial n} \quad \text{on } \partial\Omega \tag{3.12}$$

$$\text{outgoing radiation condition with } k_2 \text{ in } \mathbb{R}^2 \setminus \overline{\Omega_2}. \tag{3.13}$$

To see this, we define a function v using a set of non-trivial solutions (u, q) of the BIEs in (3.7) as:

$$v(x) = \begin{cases} -\frac{1}{s_1} U^2(x) & x \in \mathbb{R}^2 \setminus \overline{\Omega_2} \\ \frac{1}{s_2} U^1(x) & x \in \Omega_2 \end{cases} . \tag{3.14}$$

If $v \equiv 0$ in $\mathbb{R}^2 \setminus \partial\Omega$, the function w defined by:

$$w(x) = \begin{cases} U^1(x) & x \in \Omega_1 \\ U^2(x) & x \in \Omega_2 \end{cases} . \tag{3.15}$$

gives a non-trivial solution of the waveguide problem, as we have noted. We thus see that the ω is an eigenvalue of the waveguide problem. If $v \not\equiv 0$ identically in $\mathbb{R}^2 \setminus \partial\Omega$, v is a non-trivial solution of the BVP in (3.11)-(3.13) as we can see from (3.8). We call this BVP the "fictitious BVP".

A similar discussion shows that the PMCHWT formulation given in (3.9) may have, in addition to true eigenvalues, fictitious eigenvalues which correspond to eigenvalues of the following free space transmission problem:

$$\Delta v + k_2^2 v = 0 \text{ in } \mathbb{R}^2 \setminus \overline{\Omega_2}, \quad \Delta v + k_1^2 v = 0 \text{ in } \Omega_2, \tag{3.16}$$

$$v^- = v^+, \quad s_1 \frac{\partial v^-}{\partial n} = s_2 \frac{\partial v^+}{\partial n} \text{ on } \partial\Omega \tag{3.17}$$

$$\text{outgoing radiation condition with } k_2 \text{ in } \mathbb{R}^2 \setminus \overline{\Omega_2}. \tag{3.18}$$

One may say that fictitious eigenvalues exist because the BIEs in (3.7) and (3.9) cannot distinguish the original BVP and the fictitious BVP since these BIEs lose the information of the domains while we take their limits to the boundary.

We thus see that an eigenvalue obtained with the BIEM with (3.7) may be an eigenvalue of the free space transmission problem in (3.11)-(3.13), which has nothing to do with the original BVP and, hence, is fictitious. These fictitious eigenvalues have negative imaginary parts because the homogeneous transmission problem has only the trivial solution when $\operatorname{Im}\omega \geq 0$ [48]. Hence, the BIE in (3.7) is free from fictitious eigenvalues as long as one considers real frequencies. When one deals with leaky modes, however, it is hard to tell whether an eigenvalue obtained with the BIEMs in (3.7) is a true eigenvalue or not, because both true and fictitious eigenvalues appear in the lower complex plane. Similar conclusions apply to (3.9) as well.

3.2.4 New BIEs

One can resolve the above problem simply by using the incoming fundamental solution given by:

$$-\frac{i}{4}H_0^{(2)}(k_2|\boldsymbol{x}-\boldsymbol{y}|) \tag{3.19}$$

for G^2 in (3.7), instead of the outgoing one in (3.5). This remedy keeps the true eigenvalues unchanged, while the corresponding fictitious transmission problem (3.11)-(3.13) is now replaced by the one with (3.11), (3.12) and the incoming radiation condition with k_2 in $\mathbb{R}^2 \setminus \overline{\Omega_2}$. The corresponding (fictitious) eigenvalues have positive imaginary parts because of the incoming radiation condition. In fact, we see that $(\overline{v}, \overline{\omega})$ is an eigenpair of the problem defined by (3.11), (3.12) and the incoming radiation condition if (v, ω) is an eigenpair of (3.11)-(3.13). Therefore, we can distinguish the fictitious eigenvalues from the true eigenvalues with this change of the formulation. The same method can be applied to (3.9) as well.

3.2.5 Transmission resonance problems for Maxwell's equations

We next consider transmission problems for Maxwell's equations in 3D free space. Let Ω_2 be a finite scatterer, $S = \partial\Omega_2$ be its boundary and $\Omega_1 = \mathbb{R}^3 \setminus \overline{\Omega_2}$. The transmission resonance problem for Maxwell's equations is stated as follows: find $\boldsymbol{E}$ which satisfies Maxwell's equations:

$$\nabla \times (\nabla \times \boldsymbol{E}) - k_\nu^2 \boldsymbol{E} = 0 \quad \text{in } \Omega_\nu \ (\nu = 1, 2)$$

boundary conditions

$$\begin{aligned} &\boldsymbol{E}^+ \times \boldsymbol{n} = \boldsymbol{E}^- \times \boldsymbol{n} \ (= \boldsymbol{m}), \\ &\boldsymbol{n} \times \frac{1}{i\omega}\left(\frac{1}{\mu_1}\nabla \times \boldsymbol{E}^+\right) = \boldsymbol{n} \times \frac{1}{i\omega}\left(\frac{1}{\mu_2}\nabla \times \boldsymbol{E}^-\right) \ (= \boldsymbol{j}) \quad \text{on } S \end{aligned} \tag{3.20}$$

and the outgoing radiation condition with k_1 in Ω_1 given by:

$$\boldsymbol{E} = \sum_{n=1}^{\infty}\sum_{m=-n}^{n} \alpha_n^m \boldsymbol{\Phi}_n^m(x) + \beta_n^m \nabla \times \boldsymbol{\Phi}_n^m(x), \ \boldsymbol{\Phi}_n^m(x) = \nabla \times \left\{\boldsymbol{x} h_n^{(1)}(k_1 r) Y_n^m(\theta, \phi)\right\} \quad \text{for } |\boldsymbol{x}| > R \tag{3.21}$$

where superscript $+$ $(-)$ stands for the trace to S from Ω_1 (Ω_2), ϵ_ν, μ_ν are the permitivity and permeability (real numbers) and $k_\nu = \omega\sqrt{\epsilon_\nu \mu_\nu}$ in Ω_ν, respectively. Also, α_n^m and β_n^m are numbers, (r, θ, ϕ) is the spherical coordinate of $\boldsymbol{x}$, $h_n^{(1)}$ is the spherical Hankel function of the 1st kind, Y_n^m is the spherical harmonics and $R > 0$ is a constant such that $|\boldsymbol{x}| < R$ holds for $\forall \boldsymbol{x} \in \overline{\Omega_2}$. The above expression in (3.21) allows the analytic continuation of the Silver–Müller radiation condition to a complex k_1.

3.2.6 BIEs for Maxwell's equations

We next consider the BIEs for Maxwell's equations. We introduce the following potential representation of $\boldsymbol{E}$ via the surface magnetic current $\boldsymbol{m}$ and the electronic current

$\boldsymbol{j}$ (see (3.20)):

$$\begin{aligned}
&\tilde{E}_i^\nu(x) \\
&= (-1)^\nu \int_S \left\{ e_{ijk} \frac{\partial \Gamma^\nu(x,y)}{\partial x_j} m_k(y) - i\omega\mu_\nu \left(\delta_{ip} + \frac{1}{k_\nu^2} \frac{\partial}{\partial y_i} \frac{\partial}{\partial y_p} \right) \Gamma^\nu(x,y) j_p(y) \right\} dS_y
\end{aligned} \tag{3.22}$$

where $\Gamma^\nu(x,y)$ stands for the fundamental solution of Helmholtz' equation in 3D:

$$\Gamma^\nu(x,y) = \frac{e^{ik_\nu|\boldsymbol{x}-\boldsymbol{y}|}}{4\pi|\boldsymbol{x}-\boldsymbol{y}|}. \tag{3.23}$$

These representations give the solution of the original BVP with the boundary traces of the solution as the densities $\boldsymbol{m}$ and $\boldsymbol{j}$ iff the following equations hold:

$$\tilde{\boldsymbol{E}}^1 = 0 \quad \text{in } \Omega_2, \ \tilde{\boldsymbol{E}}^2 = 0 \quad \text{in } \Omega_1. \tag{3.24}$$

The integral equations for the Müller formulation can be written as follows [34]:

$$\begin{aligned}
&\frac{\epsilon_1+\epsilon_2}{2}\boldsymbol{m} - \boldsymbol{n} \times \int_S \left(\epsilon_1 \nabla_x \Gamma^1 - \epsilon_2 \nabla_x \Gamma^2\right) \times \boldsymbol{m}\, dS_y \\
&+ \frac{i}{\omega}\boldsymbol{n} \times \int_S \left(k_1^2 \Gamma^1 - k_2^2 \Gamma^2\right) \boldsymbol{j}\, dS_y + \frac{i}{\omega}\boldsymbol{n} \times \int_S \left(\nabla_x\nabla_x \Gamma^1 - \nabla_x\nabla_x \Gamma^2\right) \cdot \boldsymbol{j}\, dS_y = 0, \\
&\frac{\mu_1+\mu_2}{2}\boldsymbol{j} - \boldsymbol{n} \times \int_S \left(\mu_1 \nabla_x \Gamma^1 - \mu_2 \nabla_x \Gamma^2\right) \times \boldsymbol{j}\, dS_y \\
&- \frac{i}{\omega}\boldsymbol{n} \times \int_S \left(k_1^2 \Gamma^1 - k_2^2 \Gamma^2\right) \boldsymbol{m}\, dS_y - \frac{i}{\omega}\boldsymbol{n} \times \int_S \left(\nabla_x\nabla_x \Gamma^1 - \nabla_x\nabla_x \Gamma^2\right) \cdot \boldsymbol{m}\, dS_y = 0.
\end{aligned} \tag{3.25}$$

The above Müller formulation for the Maxwell's equations is derived from (3.24) via the potential in (3.22) as follows:

$$\begin{aligned}
-\epsilon_1 \tilde{\boldsymbol{E}}^{1-} \times \boldsymbol{n} &= \epsilon_2 \tilde{\boldsymbol{E}}^{2+} \times \boldsymbol{n} \\
-\tfrac{1}{i\omega}\boldsymbol{n} \times \left(\nabla \times \tilde{\boldsymbol{E}}^{1-}\right) &= \tfrac{1}{i\omega}\boldsymbol{n} \times \left(\nabla \times \tilde{\boldsymbol{E}}^{2+}\right)
\end{aligned} \quad \text{on } S. \tag{3.26}$$

The PMCHWT formulation for the Maxwell equations can be written as follows [33]:

$$\begin{aligned}
&- \boldsymbol{n} \times \int_S \left(\nabla_x \Gamma^1 + \nabla_x \Gamma^2\right) \times \boldsymbol{m}\, dS_y + i\omega\boldsymbol{n} \times \int_S \left(\mu_1 \Gamma^1 + \mu_2 \Gamma^2\right) \boldsymbol{j}\, dS_y \\
&+ \frac{i}{\omega}\boldsymbol{n} \times \fint_S \left(\frac{1}{\epsilon_1}\nabla_x\nabla_x \Gamma^1 + \frac{1}{\epsilon_2}\nabla_x\nabla_x \Gamma^2\right) \cdot \boldsymbol{j}\, dS_y = 0, \\
&- \boldsymbol{n} \times \int_S \left(\nabla_x \Gamma^1 + \nabla_x \Gamma^2\right) \times \boldsymbol{j}\, dS_y - i\omega\boldsymbol{n} \times \int_S \left(\epsilon_1 \Gamma^1 + \epsilon_2 \Gamma^2\right) \boldsymbol{m}\, dS_y \\
&- \frac{i}{\omega}\boldsymbol{n} \times \fint_S \left(\frac{1}{\mu_1}\nabla_x\nabla_x \Gamma^1 + \frac{1}{\mu_2}\nabla_x\nabla_x \Gamma^2\right) \cdot \boldsymbol{m}\, dS_y = 0,
\end{aligned} \tag{3.27}$$

which we obtain from (3.22) and (3.24) using

$$\begin{aligned}
\tilde{\boldsymbol{E}}^{1-} \times \boldsymbol{n} &= \tilde{\boldsymbol{E}}^{2+} \times \boldsymbol{n} \\
\tfrac{1}{i\omega}\boldsymbol{n} \times \left(\tfrac{1}{\mu_1}\nabla \times \tilde{\boldsymbol{E}}^{1-}\right) &= \tfrac{1}{i\omega}\boldsymbol{n} \times \left(\tfrac{1}{\mu_2}\nabla \times \tilde{\boldsymbol{E}}^{2+}\right)
\end{aligned} \quad \text{on } S. \tag{3.28}$$

The above homogeneous BIEs in (3.25) and (3.27) have both true eigenvalues and fictitious ones as in Helmholtz' case. The fictitious eigenvalues for the Müller formulation are the eigenvalues ω of the following BVP for $\boldsymbol{H}$:

$$\nabla \times (\nabla \times \boldsymbol{H}) - k_\nu^2 \boldsymbol{H} = 0 \quad \text{in} \quad \Omega_{\nu'} \ (\nu \neq \nu',\ \nu = 1, 2) \tag{3.29}$$

$$\boldsymbol{H}^- \times \boldsymbol{n} = \boldsymbol{H}^+ \times \boldsymbol{n}, \quad \boldsymbol{n} \times \left(\frac{1}{\epsilon_1} \nabla \times \boldsymbol{H}^- \right) = \boldsymbol{n} \times \left(\frac{1}{\epsilon_2} \nabla \times \boldsymbol{H}^+ \right) \quad \text{on } S \tag{3.30}$$

$$\text{outgoing radiation condition for } \boldsymbol{H} \text{ with } k_2 \text{ in } \Omega_1 \tag{3.31}$$

where $\boldsymbol{H}$ is related to $\tilde{\boldsymbol{E}}$ in (3.26) via

$$\boldsymbol{H} = \begin{cases} -\epsilon_1 \tilde{\boldsymbol{E}}^1 \text{ in } \Omega_2 \\ \epsilon_2 \tilde{\boldsymbol{E}}^2 \text{ in } \Omega_1 \end{cases} . \tag{3.32}$$

The fictitious boundary value problem for the PMCHWT formulation is given by

$$\nabla \times (\nabla \times \boldsymbol{E}) - k_\nu^2 \boldsymbol{E} = 0 \quad \text{in} \quad \Omega_{\nu'} \ (\nu \neq \nu',\ \nu = 1, 2) \tag{3.33}$$

$$\boldsymbol{E}^- \times \boldsymbol{n} = \boldsymbol{E}^+ \times \boldsymbol{n}, \ \boldsymbol{n} \times \left(\frac{1}{\mu_1} \nabla \times \boldsymbol{E}^- \right) = \boldsymbol{n} \times \left(\frac{1}{\mu_2} \nabla \times \boldsymbol{E}^+ \right) \text{ on } S \tag{3.34}$$

$$\text{outgoing radiation condition for } \boldsymbol{E} \text{ with } k_2 \text{ in } \Omega_1. \tag{3.35}$$

where $\boldsymbol{E} = \tilde{\boldsymbol{E}}^\nu$ in $\Omega_{\nu'}$. As a matter of fact, the fictitious eigenvalues for the Müller and PMCHWT formulations are the same. Indeed, the fictitious BVPs for the Müller and PMCHWT formulations transform to each other by the following "changes of variables":

$$\boldsymbol{H} = \frac{\nabla \times \boldsymbol{E}}{i\omega\mu_\nu} \text{ in } \Omega_{\nu'} \tag{3.36}$$

$$\boldsymbol{E} = -\frac{\nabla \times \boldsymbol{H}}{i\omega\epsilon_\nu} \text{ in } \Omega_{\nu'} \tag{3.37}$$

Namely, one obtains (3.34) by rewriting (3.30) with (3.37). Also, one obtains (3.30) by using (3.36) in (3.34). These changes of variables also keep Maxwell's equations and the radiation conditions unchanged. Hence the eigenvalues of the Müller and PMCHWT formulations are identical including fictitious ones. Incidentally, this conclusion is quite obvious from a physical point of view since the problems defined by (3.29)-(3.31) and (3.33)-(3.35) are the same transmission problem formulated in terms of either the magnetic or electric field.

Also in Maxwell's equations with (3.25) or (3.27), we can distinguish true and fictitious eigenvalues by replacing Γ^2 with the incoming fundamental solution given by:

$$\frac{e^{-ik_2|\boldsymbol{x}-\boldsymbol{y}|}}{4\pi|\boldsymbol{x}-\boldsymbol{y}|}.$$

A fictitious eigenpair $(\boldsymbol{H}, \omega)$ of (3.29)-(3.31) are changed to $(\bar{\boldsymbol{H}}, \bar{\omega})$ with this new formulation.

3.3 Numerical examples

In this section, we present some numerical examples to test the performances of the proposed method. We used Appro GreenBlade 8000 (with Intel Xeon cores) at the

Academic Center for Computing and Media Studies of Kyoto University, and FX10 Supercomputer System (with SPARC64^{TM}IXfx cores) at the Information Technology Center of the University of Tokyo for the computation. The codes are parallelized with OpenMP and MPI.

3.3.1 Discretization of BIEs

We use both Müller and PMCHWT formulations (in (3.7) and (3.9), respectively) for solving the waveguide problems for Helmholtz' equation. The BIEs in (3.7) and (3.9) are discretized with piecewise constant boundary elements and the collocation method (the singular parts of the integrals are evaluated analytically, and the remainders are computed with the Gaussian quadrature). The discretized BIE for (3.7) converges fast in GMRES since the operator is a compact perturbation of a constant. The PMCHWT formulation in (3.9) discretized with collocation is also known to converge fast in GMRES if the unknowns are ordered in a proper manner ([43], [44]). The matrix-vector product operation is accelerated with the FMM for waveguide problems proposed in chapter 2.

For Maxwell's equations, we use only the Müller formulation in (3.25) because eigenvalues of the Müller and PMCHWT formulations are identical as we have noted in 3.2.6. The BIE in (3.25) is discretized with triangular boundary elements and Nyström's method discussed in [49] using the three point Gaussian quadrature rule on a triangle. For the local correction, the contributions of the static parts of the fundamental solution are calculated analytically after interpolating the densities linearly, and those of the remainder are integrated numerically with the Gaussian quadrature. The discretized BIE converges fast with GMRES [49]. The matrix-vector product operation is accelerated with the low frequency FMM following [49].

3.3.2 Sakurai-Sugiura projection method (SSM)

We use SSM described in 2.4.1 to calculate eigenvalues. In this chapter, we set the contour γ of the SSM to be a rectangle in the following numerical examples. We compute the contour integral in (2.24) numerically with the standard Gaussian quadrature applied to 4 integrals on each side of the rectangle. We set m in (2.24) to be $m = 12$ or $m = 24$. The inverse of the matrix in (2.24) is computed approximately with the FMM and GMRES. We set the tolerance (relative error) for GMRES to be 10^{-8} in the examples to follow.

3.3.3 Resonances in 2D Helmholtz waveguides

We first discuss waveguide problems for Helmholtz' equation in 2D defined in 3.2.1. We consider 4 circular scatterers with the radii of $r_0 = 0.4$ whose centers are $(0, 0)$, $(0, -1)$, $(0, -2)$ and $(0, -3)$, respectively. In this case, we can check if the proposed approach is able to separate fictitious eigenvalues from the true ones since the fictitious eigenvalues can be determined semi-analytically. In fact, the fictitious eigenvalues ω for Müller's integral equation in (3.7), are zeros of the following expression

$$-s_2 H_n^{(\iota)}(k_2 r_0)\frac{d}{dr}J_n(k_1 r_0) + s_1 \frac{d}{dr}H_n^{(\iota)}(k_2 r_0)J_n(k_1 r_0) \tag{3.38}$$

where $\iota = 1$ for the ordinary method (outgoing) and $\iota = 2$ for the proposed method (incoming), respectively. The fictitious eigenvalues for the PMCHWT case are calculated similarly.

Table 3.1: BIEs

Method No.	kernel function G^2 in (3.3)	formulation
1	$(-i/4)H_0^{(2)}(k_2\lvert\boldsymbol{x}-\boldsymbol{y}\rvert)$	Müller
2	$(i/4)H_0^{(1)}(k_2\lvert\boldsymbol{x}-\boldsymbol{y}\rvert)$	Müller
3	$(-i/4)H_0^{(2)}(k_2\lvert\boldsymbol{x}-\boldsymbol{y}\rvert)$	PMCHWT
4	$(i/4)H_0^{(1)}(k_2\lvert\boldsymbol{x}-\boldsymbol{y}\rvert)$	PMCHWT

The following material constants are used in waveguide problems: $\rho_1 = 1$, $s_1 = 1$, $\rho_2 = 0.37$ and $s_2 = 0.2$. They are supposed to model flint glass inclusions within an iron plate with an appropriate normalization. We discretized each circular boundary with 4000 elements (the DOF is 32000), used 32 (64) integration points on each side of γ to approximate the integrals in (2.24) for $\mathrm{Re}\,\omega < \pi$ ($\mathrm{Re}\,\omega > \pi$) and set $L = 10$ (L: number of random vectors used in SSM. See 2.4.1.). The number of integration points on γ is chosen so that we can calculate eigenvalues close to the branch cuts accurately. We tested 4 methods shown in Table 3.1. The methods 1 and 3 are the proposed methods while methods 2 and 4 are standard ones.

Fig. 3.1 shows all eigenvalues obtained with the 4 methods, where open (solid) symbols stand for the true (fictitious) eigenvalues. The paths of integration γ in (2.24) are also shown in Fig. 3.1. This figure shows that the true eigenvalues obtained with the proposed integral equations (methods 1 and 3) agree well with those obtained with the standard approaches (methods 2 and 4) whose accuracy has been examined extensively in chapter 2. This figure further shows that one can clearly distinguish true and fictitious eigenvalues with the proposed methods, in which fictitious ones have positive imaginary parts, while this is not the case with the standard methods (see, for example, the fictitious eigenvalues whose real parts are close to 6). We note that one of true eigenvalues is very close to the branch point π, whose real part, actually, is slightly smaller than π. We have checked that this eigenvalue has a sufficiently large reliability index proposed in [24]. For validation, we also plot the exact fictitious eigenvalues obtained as the zeros of (3.38) in Fig. 3.1, which agree with numerical fictitious eigenvalues. In the upper graph of Fig. 3.2, we plot only those true eigenvalues from Fig. 3.1 obtained with method 1 which have symmetric (with respect to x_1) eigenmodes. The lower graph of Fig. 3.2 shows the energy transmittance produced by the symmetric incident wave given by $e^{ik_1x_2}$ for real ω. Fig. 3.3 is a blow-up of Fig. 3.2 for $\omega \in (5, 6.3)$. We see that the true eigenvalues with small non-positive imaginary parts are close to the peaks or dips of the energy transmittance for real frequencies. We observe similar behaviors with eigenvalues having antisymmetric eigenmodes, but we omit the details here.

Fig. 3.4 shows the number of iterations needed in GMRES at the integration points on the lower (magenta) paths of integration in Fig. 3.1 (Note that the upper paths are used just for obtaining the fictitious eigenvalues of the proposed method, which are not needed in practice). Figs. 3.4(a) and (b) show the Müller and PMCHWT cases, while Figs. 3.4(c) and (d) give the side views ($\mathrm{Im}\,\omega$ v.s. number of iterations) of Figs. 3.4(a) and (b), respectively. We observe that the numbers of iterations needed in the proposed methods (methods 1 and 3) are smaller than those of the standard ones when $|\,\mathrm{Im}\,\omega|$ is large.

We also consider the case in which more fictitious eigenvalues appear and the

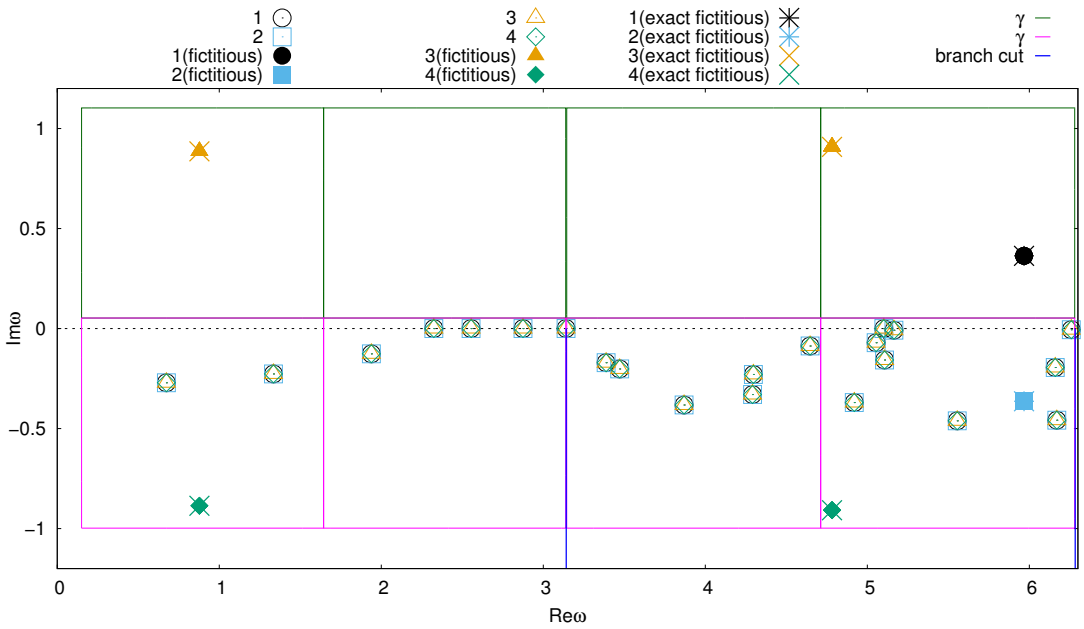

Figure 3.1: Eigenvalues obtained with each method. Solid symbols stand for fictitious eigenvalues. The paths γ's are taken to be close to the branch cuts in (2.27) but not to touch them.

proposed method is more important. We consider 3 circular scatterers having different physical quantities with the radii of $r_0 = 0.4$ whose centers and physical quantities are $\{(0,0), \rho_2 = 0.4, s_2 = 0.2\}$, $\{(0,-1), \rho_3 = 1, s_3 = 5\}$, and $\{(0,-2), \rho_4 = 1, s_4 = 10\}$, respectively. Fig. 3.5(a) and (b) show eigenvalues of the standard (outgoing) and proposed (incoming) BIEs, respectively (The same paths as in Fig. 3.1 and 64 integration points on the sides are used. Other parameters are the same as those used for obtaining Fig. 3.1.). We see that the proposed BIEs can separate true eigenvalues (blue symbols) from the fictitious ones (red symbols) while the standard BIEs obtain all eigenvalues in the lower complex plane, in this case also.

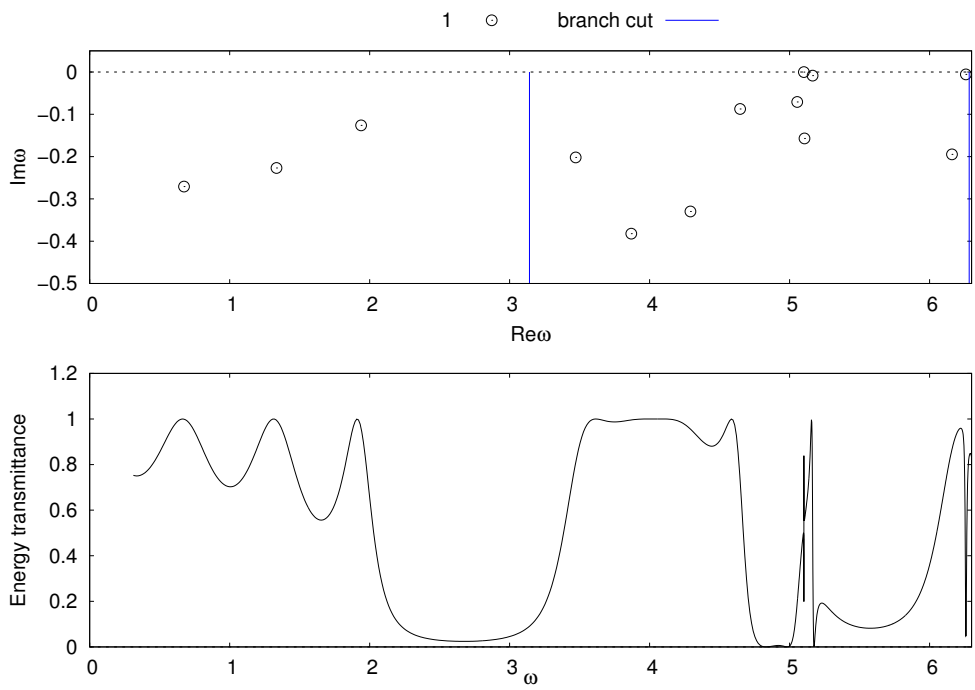

Figure 3.2: Eigenvalues with symmetric modes (upper) and energy transmittance for incident plane wave $e^{ik_1x_2}$ (lower).

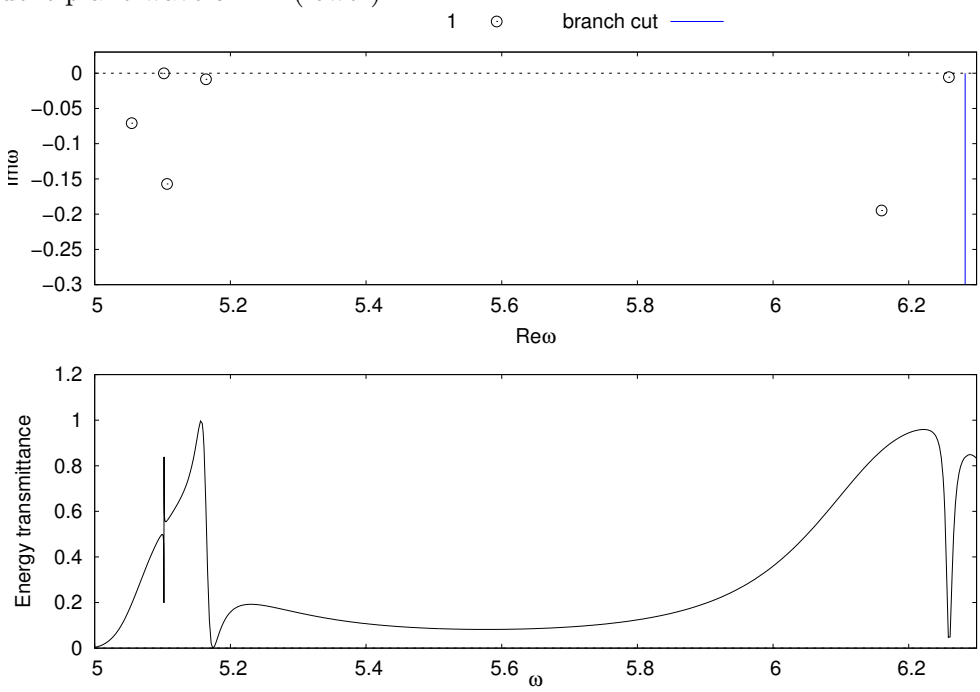

Figure 3.3: Eigenvalues with symmetric modes (upper) and energy transmittance for incident $e^{ik_1x_2}$ (lower) for $\omega \in (5, 6.3)$. (Blowup of Fig. 3.2.)

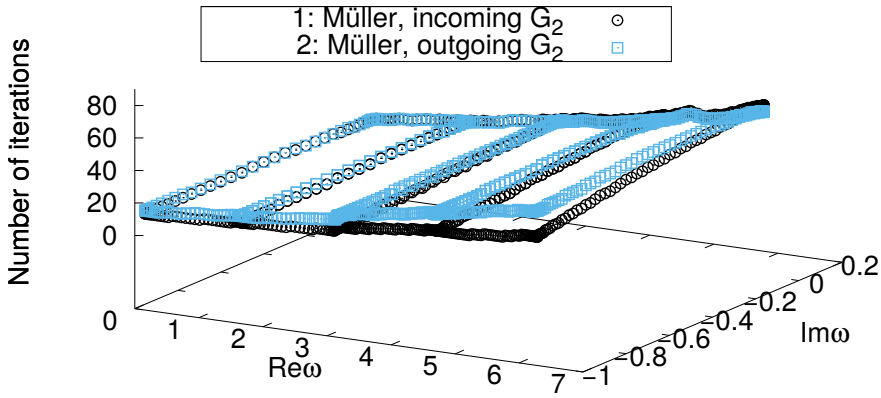

(a) Müller

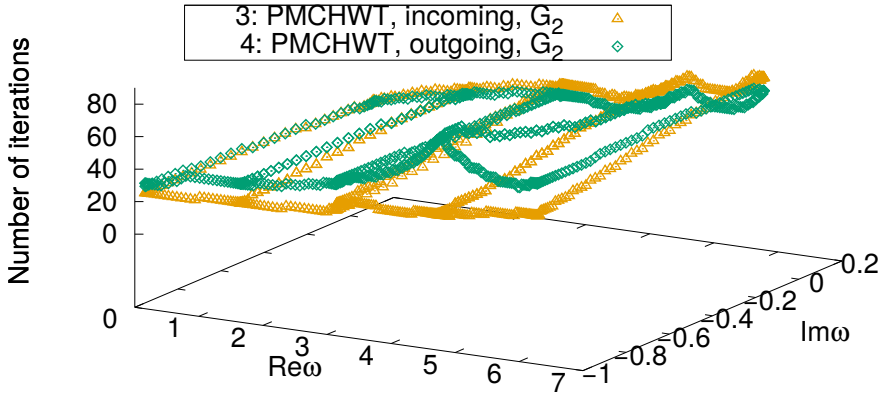

(b) PMCHWT

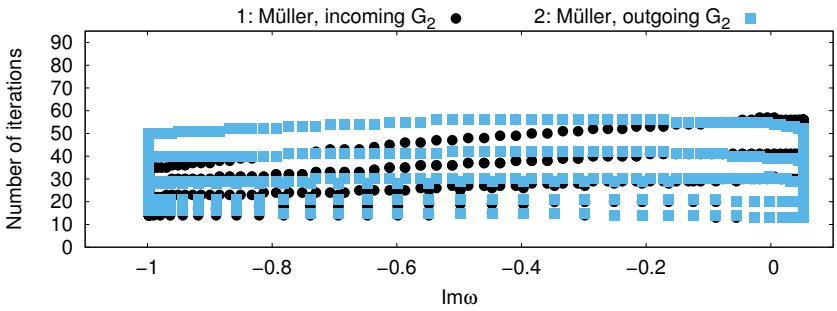

(c) Müller, $\mathrm{Im}\,\omega$ v.s. number of iterations

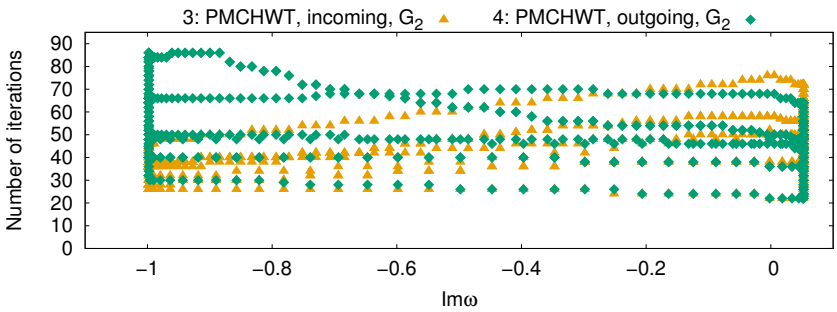

(d) PMCHWT, $\mathrm{Im}\,\omega$ v.s. number of iterations

Figure 3.4: Number of iterations needed at integration points on the contour γ.

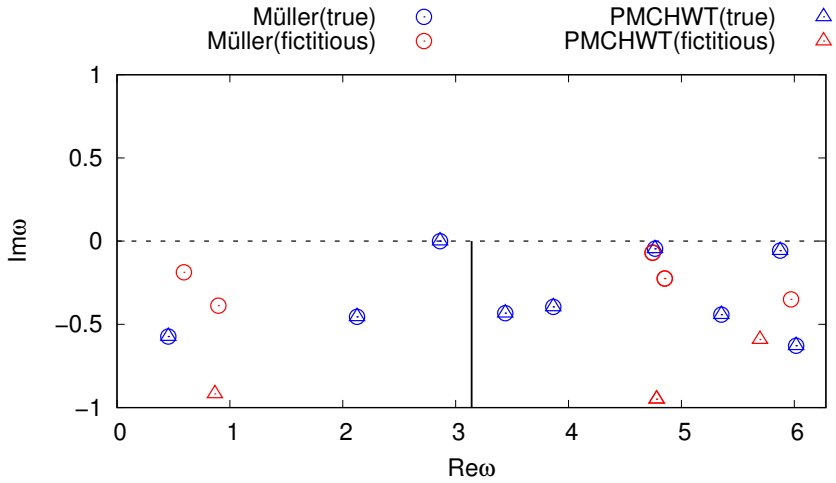

(a) Standard BIEs

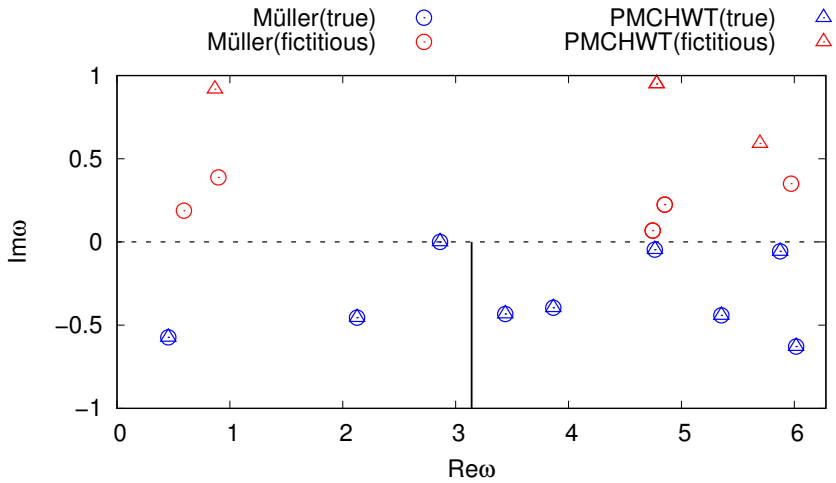

(b) Proposed BIEs

Figure 3.5: Eigenvalues of BIEs for 3 circular scatterers having different physical quantities. The branch cut extending from π is shown.

3.3.4 Complex resonances for Maxwell's equations in 3D free space

We next consider the transmission resonance problem in 3 dimensional free space for Maxwell's equations. Note that all eigenvalues for the free space transmission problems are leaky and no real eigenvalues exist. However, these problems may have eigenvalues with small imaginary parts, which cause anomalous phenomena as we shall see.

In the first example, we consider a single spherical shell

$$\Omega_2 = \left\{ (x_1, x_2, x_3) \in \mathbb{R}^3 \mid 0.8 < \sqrt{x_1^2 + x_2^2 + x_3^2} < 1 \right\}$$

which encloses $\Omega_3 = \left\{ (x_1, x_2, x_3) \in \mathbb{R}^3 \mid \sqrt{x_1^2 + x_2^2 + x_3^2} < 0.8 \right\}$ and is surrounded by $\Omega_1 = \mathbb{R}^3 \setminus \overline{\Omega_2 \cup \Omega_3}$. We set $\epsilon_1 = 1,\ \epsilon_2 = 5,\ \epsilon_3 = 1$ in $\Omega_1,\ \Omega_2,\ \Omega_3$, respectively, and $\mu = 1$ everywhere. Many true and fictitious eigenvalues appear in this problem, as we shall see.

We now consider the transmission problem for this system. Fictitious eigenvalues for this problem are the eigenvalues for:

- a single spherical scatterer Ω_3 having the permitivity $\epsilon = 5$ with radius $= 0.8$ in the free space having the permitivity $\epsilon = 1$
- a single spherical scatterer $\Omega_2 \cup \Omega_3$ having the permitivity $\epsilon = 1$ with radius $= 1.0$ in the free space having permitivity $\epsilon = 5$.

Of course, these fictitious BVPs are with appropriate radiation conditions.

The upper figure of Fig. 3.6 shows all eigenvalues obtained with the proposed and standard methods. Here, we used the paths γ shown in Fig. 3.6 and discretized the shell surface with 7300 triangular elements (3920 (3380) elements for $\partial\Omega_1$ ($\partial\Omega_3$) and the total DOF is 87600). We set the number of integration points on each side of γ to be 16, and the number of random vectors L for SSM to be 20 except for the most left rectangle in the upper figure where $L = 10$, respectively. We set larger L and smaller γ's for calculating higher eigenvalues which have larger multiplicities due to geometric symmetry of the problem. One may set a smaller L for geometrically less symmetric scatterers. Note that some eigenvalues outside γ are obtained, which happens occasionally in SSM [24]

To validate our results, we note that both true and fictitious eigenvalues for this problem can be determined easily by means of the Mie-series [50]. These exact eigenvalues, both true ones and fictitious ones for the proposed and standard methods, are plotted with triangular symbols in the upper figure of Fig. 3.6. We see that numerical eigenvalues are obtained correctly and the proposed method has no fictitious ones in the lower complex plane.

The connection between physical phenomena and true eigenvalues is examined next. We consider the transmission problem for the same scatterer as above with the incident electric field of $\boldsymbol{E}^{\text{inc}} = (e^{ik_1 x_3}, 0, 0)$ with real ω and plot the scattered energy defined by

$$E^{\text{sca}} = \int_{\partial\Omega_1} \text{Re}\left(\boldsymbol{E}^{\text{sca}} \times \boldsymbol{n} \cdot \overline{\boldsymbol{H}^{\text{sca}}}\right) dS = \int_{\partial\Omega_1} \text{Re}\left(\boldsymbol{m}^{\text{sca}} \cdot \overline{\boldsymbol{j}^{\text{sca}}} \times \boldsymbol{n}\right) dS \tag{3.39}$$

in the lower figure of Fig. 3.6 where the superscript "sca" stands for the scattered field (i.e., $\boldsymbol{E}^{\text{sca}} = \boldsymbol{E} - \boldsymbol{E}^{\text{inc}}$). We see that true eigenvalues with imaginary parts smaller than about 0.2 correspond to peaks of the energy.

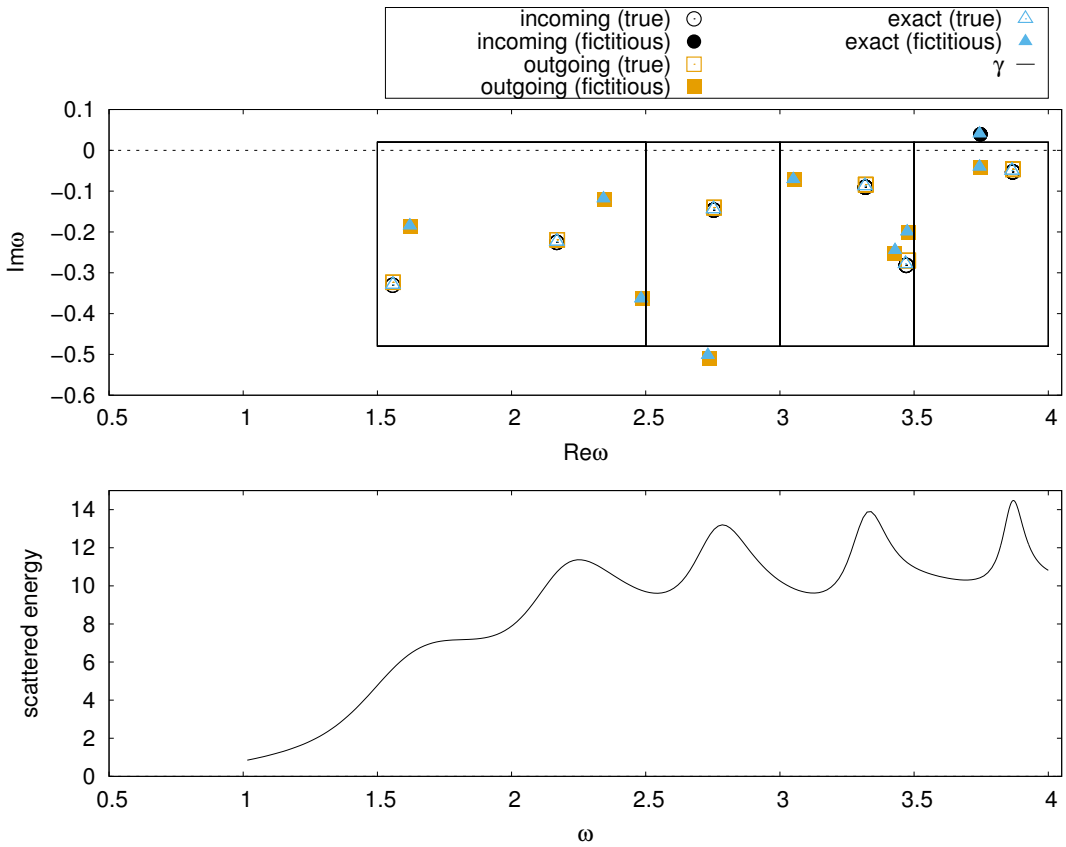

Figure 3.6: Upper: eigenvalues, Lower: scattered energy defined in (3.39) for incident electric field: $(e^{ik_1x_3}, 0, 0)$. Solid symbols stand for fictitious eigenvalues.

Fig. 3.7(a) shows the number of iterations needed in GMRES at the integration points on the paths of integration and Fig. 3.7(b) gives the side view of Fig. 3.7(a). As with Helmholtz' case, we see that the number of iterations needed in the proposed (incoming) method are smaller than those of the standard (outgoing) method when $|\operatorname{Im}\omega|$ is large. However, this is not necessarily the case when $|\operatorname{Im}\omega|$ is small.

The second example is related to eigenvalues for multiple scatterers. We consider two spherical scatterers Ω_2 and Ω_3 ($\Omega_2 \cap \Omega_3 = \phi$) in the free space $\Omega_1 = \mathbb{R}^3 \setminus \overline{\Omega_2 \cup \Omega_3}$, whose radii are 0.8, 0.4 and centers are $(0, 0, 0)$, $(1.4, 0, 0)$, respectively. We set $\epsilon_1 = 4$, $\epsilon_2 = 1$ and $\epsilon_3 = 20$ in Ω_1, Ω_2 and Ω_3, respectively. The fictitious eigenvalues for this problem can be obtained easily by means of the Mie-series although the true ones are not very easy to determine.

The upper figure of Fig. 3.8 shows eigenvalues obtained with the proposed (incoming) method. Here, we discretized the surfaces of Ω_2 and Ω_3 with 2880 and 4500 triangular elements, respectively (note that the wavenumber in Ω_3 is higher than that of Ω_2) and the total DOF is 88560. We used 16 (32) integration points on each side of γ for the left (right) paths in Fig. 3.8 and set $L = 20$. The solid rectangles indicate the (exact) fictitious eigenvalues for this problem which one would obtain with the standard (outgoing) method. This figure clearly shows the usefulness of our method

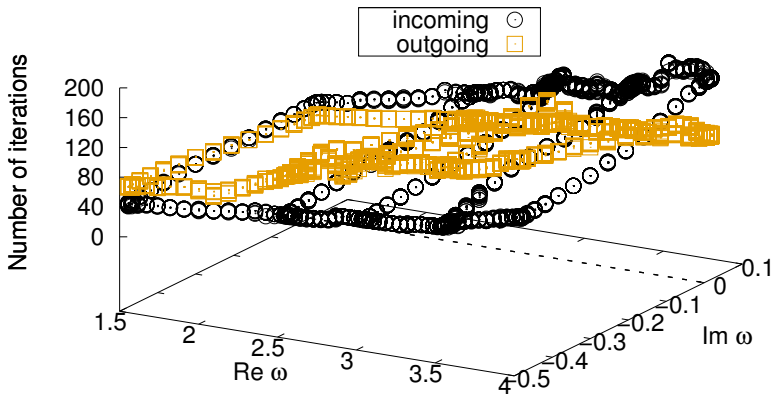

(a)

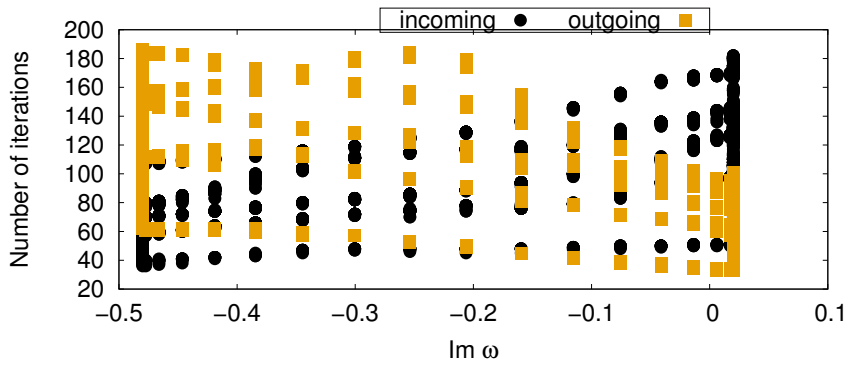

(b)

Figure 3.7: Number of iterations needed at integration points on the contour. (spherical shell)

without which it would be very cumbersome, if not impossible, to separate true eigenvalues from so many fictitious ones. Also plotted in the upper figure of Fig. 3.8 are the exact true eigenvalues for the single scatterer problem for Ω_3 (i.e., the case with $\epsilon_1 = \epsilon_2 = 4,\ \epsilon_3 = 20$). (True eigenvalues for the single scatterer Ω_2 (the case with $\epsilon_1 = \epsilon_3 = 4,\ \epsilon_2 = 1$) do not exist in the frequency range considered in this figure). We see that true eigenvalues near the real axis for the two spherical scatterer problem are very close to certain eigenvalues for the single scatterer problem, thus indicating that these two scatterer eigenvalues can be interpreted as perturbations of single scatterer eigenvalues.

The lower figure of Fig. 3.8 shows the scattered energy in (3.39) for the incident electric field given by $\boldsymbol{E}^{\mathrm{inc}} = (e^{ik_1x_3}, 0, 0)$ with real ω. Also in this case, we see that the scattered energy and the eigenvalues with small imaginary parts are related, the latter being close to the peaks of the scattered energy.

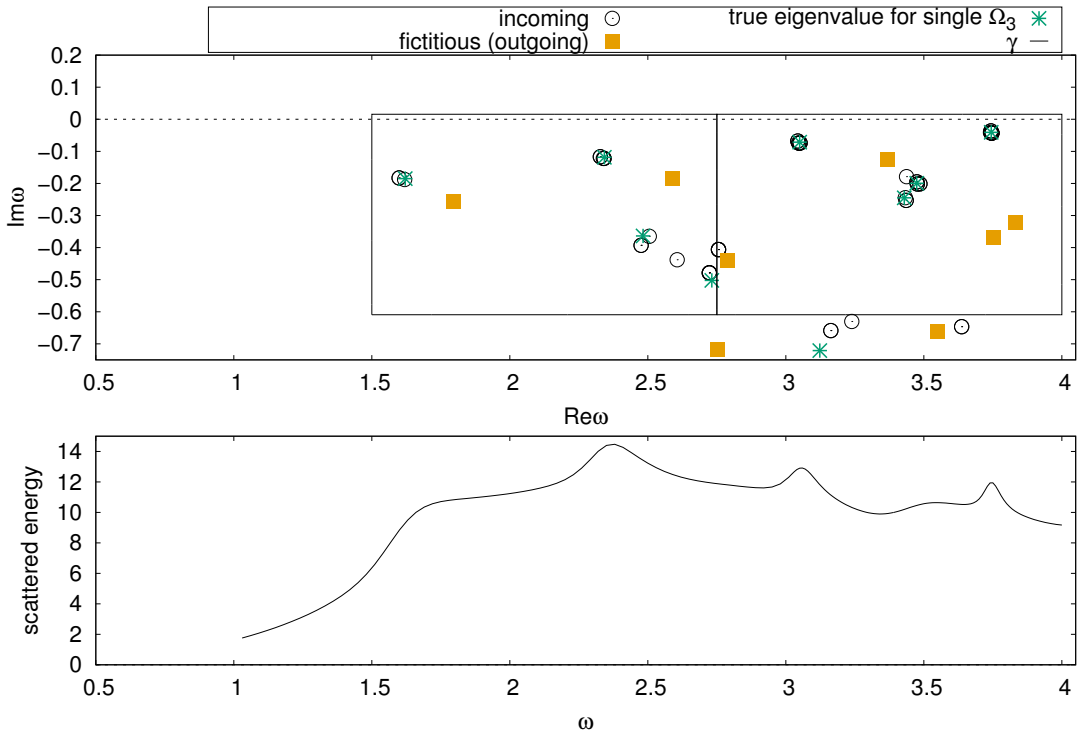

Figure 3.8: Upper: eigenvalues, Lower: scattered energy defined in (3.39) for incident electric field: $(e^{ik_1x_3}, 0, 0)$. Note that the asterisks stand for true eigenvalues for one single scatterer Ω_3.

Finally, we show a result which implies that the fictitious eigenvalues may affect the accuracy of BIE solutions in ordinary problems even when the frequency is real. We consider a single spherical scatterer Ω_2 whose radius is 1.0 and set $\Omega_1 = \mathbb{R}^3 \setminus \overline{\Omega_2}$. The permitivities in Ω_1 and Ω_2 are $\epsilon_1 = 6$ and $\epsilon_2 = 1$, respectively. We computed the eigenvalues for this single scatterer problem with the proposed (incoming) and standard (outgoing) methods using 5120 triangular elements (61440 DOF) to approximate the surface of the spherical scatterer. Also, the paths of integration γ for SSM are taken so that they include fictitious eigenvalues with positive imaginary parts just for the purpose of checking. We set the parameter L (see sec. 2.4.1) large ($L = 32$) because all

eigenvalues for this problem have large multiplicities. For example, the right rectangle in the upper figure of Fig. 3.9 contains as many as 50 eigenvalues. The number of integration points on each side of γ is 16.

The upper figure of Fig. 3.9 shows all the computed eigenvalues, of which the one at $\omega = 2.785 - 0.574i$ (surrounded by a circle) is a true one and others are fictitious. This figure also includes exact eigenvalues obtained with the Mie-series thus showing that we can determine both true and fictitious eigenvalues accurately. Note that there exist a few fictitious eigenvalues with very small imaginary parts. We next solved a transmission problem for the same scatterer with the incident electric field given by $\boldsymbol{E}^{\mathrm{inc}} = (e^{ik_1x_3}, 0, 0)$ with real ω and plotted the error relative to the exact solution in the lower figure of Fig. 3.9, where we defined the error as:

$$\text{error} = \frac{1}{2}\left(\frac{\|\boldsymbol{m} - \boldsymbol{m}^{\mathrm{Mie}}\|}{\|\boldsymbol{m}^{\mathrm{Mie}}\|} + \frac{\|\boldsymbol{j} - \boldsymbol{j}^{\mathrm{Mie}}\|}{\|\boldsymbol{j}^{\mathrm{Mie}}\|}\right). \tag{3.40}$$

In (3.40), $\boldsymbol{m}^{\mathrm{Mie}}$ and $\boldsymbol{j}^{\mathrm{Mie}}$ represent the Mie-series solutions, and the norm is the $\mathcal{L}^2$ norm on the boundary. We see that the error is large near fictitious eigenvalues with small imaginary parts regardless of whether we use the proposed integral equation or the standard one. This result implies that even the Müller formulation, which is free of real fictitious eigenvalues, may possibly be inaccurate near complex fictitious eigenvalues with small imaginary parts. Similar observation has been reported by Misawa and Nishimura in [36]. The same conclusion is quite likely to be true with the PMCHWT formulation which has the same eigenvalues as the Müller formulation.

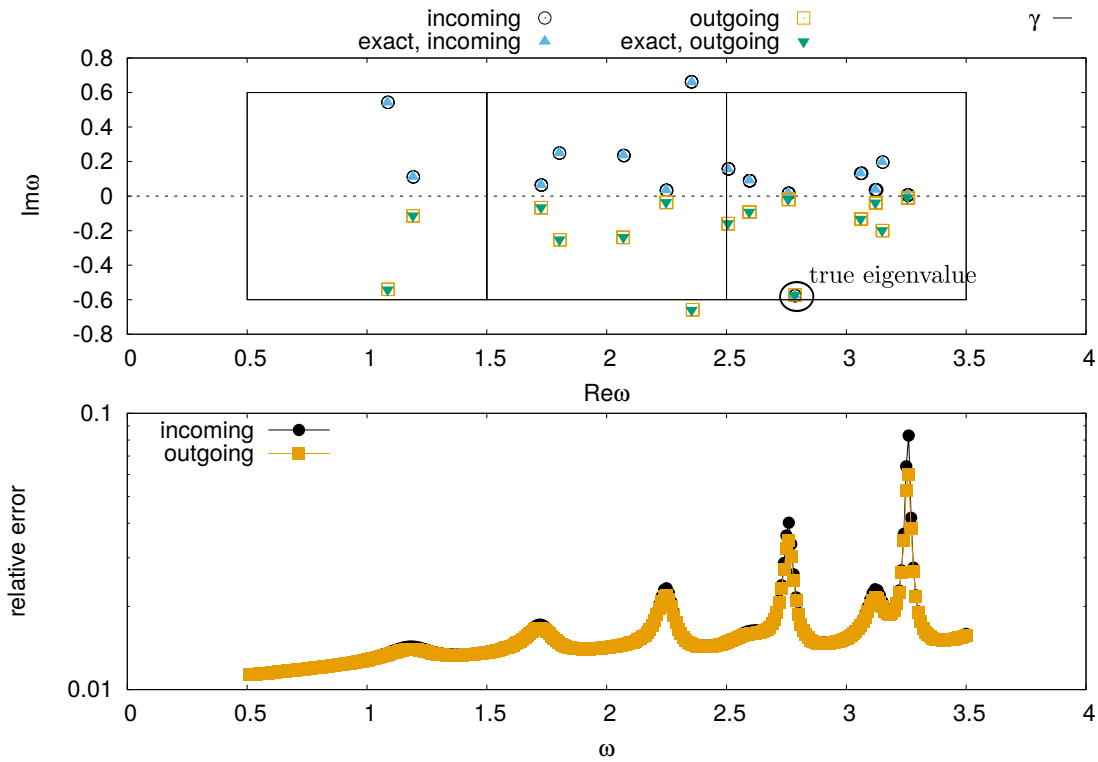

Figure 3.9: Upper: eigenvalues, Lower: error defined in (3.40) of the solution of the transmission problem with incident electric field $(e^{ik_1x_3}, 0, 0)$.

3.4 Conclusions

The results presented in this chapter can be summarized as follows:

- We have proposed new boundary integral equations for determining complex eigenvalues of the transmission problems with which one can distinguish true and fictitious eigenvalues easily. We verified that the proposed method could separate the true eigenvalues from the fictitious ones in two dimensional waveguide problems for Helmholtz' equation and three dimensional transmission problems for Maxwell's equations.

- The number of iterations needed in the proposed method for solving BIEs is smaller than that for the standard method when $|\operatorname{Im}\omega|$ is large. However, the situation may be reversed if $|\operatorname{Im}\omega|$ is small.

- Even the proposed formulation cannot resolve the inaccuracy caused by the fictitious eigenvalues in the ordinary BVPs because it cannot avoid the presence of fictitious eigenvalues close to the real axis.

Chapter 4

A study on the single integral equation method for transmission problems based on the distribution of complex fictitious eigenvalues

4.1 Introduction

As we have seen in chapter 3, boundary integral equations (BIEs) for wave problems may suffer from inaccuracies caused by the presence of fictitious eigenvalues. Even BIEs without real fictitious eigenvalues may have complex fictitious eigenvalues with very small imaginary parts, and these eigenvalues may cause inaccuracies when one solves problems with real frequencies.

In this chapter, we consider transmission problems for Helmholtz' equation in 2D and study the single integral equation (SIE) to see if it can resolve the problem of inaccuracies. We investigate the behavior of SIE from the viewpoint of the distribution of complex fictitious eigenvalues.

This chapter is organized as follows: In section 4.2, we show the formulation of transmission problems and BIEs considered in this study. We identify the fictitious eigenvalues of the SIE in 4.2.3. We show some numerical examples in section 4.3, which suggest that a properly formulated SIE has complex fictitious eigenvalues with larger imaginary parts and is more accurate than the PMCHWT and Müller formulations in problems with real frequencies.

The material in this chapter is taken from Misawa and Nishimura [40].

4.2 Formulation

4.2.1 Transmission problems

In this chapter, we consider the following transmission problem in free space for electromagnetic waves governed by Helmholtz' equation in 2D. Let $\Omega = \Omega_2$ be a finite sized scatterer with the boundary denoted by $\partial\Omega$, and $\Omega_1 = \mathbb{R}^2 \setminus \overline{\Omega_2}$. Our transmission

problem is to find u which satisfies

$$\Delta u + k_i^2 u = 0 \text{ in } \Omega_i \ (i = 1, 2) \tag{4.1}$$

$$u^+ = u^- \ (= u), \ \frac{1}{\epsilon_1}\frac{\partial u^+}{\partial n} = \frac{1}{\epsilon_2}\frac{\partial u^-}{\partial n} \ (= q) \text{ on } \partial\Omega \tag{4.2}$$

$$u^{\mathrm{sca}} = u - u^{\mathrm{inc}} \text{ satisfies the outgoing radiation condition in the free space} \tag{4.3}$$

where ϵ_i is the permitivity (positive real constant) in Ω_i, k_i is the wavenumber given by $k_i = \omega\sqrt{\epsilon_i}$ (the permeability is uniformly equal to 1), superscript $+(-)$ stands for boundary trace from $\Omega_1(\Omega_2)$, $\partial/\partial n$ for the normal derivative and $\boldsymbol{n}$ for the unit normal vector on $\partial\Omega$ directed towards Ω_1, respectively, and u^{inc} is incident wave. Eigenvalues of the transmission problem are complex frequencies $\omega \in \mathbb{C}$ at which the homogeneous transmission problem with $u^{\mathrm{inc}} = 0$ has non-trivial solutions. The radiation condition in (4.3) with complex frequencies is given by a superposition of outgoing waves [47]. It is known that eigenvalues in the free space have negative imaginary parts.

4.2.2 Single integral equation (SIE)

We first show the SIE for transmission problems, following basically section 5 in Kleinman and Martin [37]. We assume that the solution of the transmission problem in the exterior domain Ω_1 is given by the following integral representation with a density function ψ on $\partial\Omega$:

$$U = u^{\mathrm{inc}} + a\int_{\partial\Omega} G^1(x,y)\psi(y)\,ds_y + b\int_{\partial\Omega}\frac{\partial G^1(x,y)}{\partial n_y}\psi(y)\,ds_y \tag{4.4}$$

where G^1 is the outgoing fundamental solution given by $G^1(x,y) = (i/4)H_0^{(1)}(k_1|\boldsymbol{x}-\boldsymbol{y}|)$ and a, b are constants which we will determine later. We substitute the boundary values obtained with $u = U^+$ and $q = (1/\epsilon_1)\partial U^+/\partial n$ into the Green identity with G^2 and use (4.2) to obtain

$$0 = \epsilon_2\int_{\partial\Omega} G^2(x,y)q(y)\,ds_y - \int_{\partial\Omega}\frac{\partial G^2(x,y)}{\partial n_y}u(y)\,ds_y, \ x \in \Omega_1 \tag{4.5}$$

where G^2 is the incoming fundamental solution given by $G^2(x,y) = (-i/4)H_0^{(2)}(k_2|\boldsymbol{x}-\boldsymbol{y}|)$ (we use the incoming fundamental solution for G^2 in order to separate true and fictitious eigenvalues).

One obtains the following boundary integral equation with respect to ψ by taking outer trace of (4.5) to $\partial\Omega$:

$$\epsilon_2\mathcal{S}_2\left(\frac{1}{\epsilon_1}\mathcal{M}_1\psi\right) - \left(\frac{\mathcal{I}}{2} + \mathcal{D}_2\right)\mathcal{L}_1\psi = \frac{1}{2}u^{\mathrm{inc}} + \mathcal{D}_2 u^{\mathrm{inc}} - \epsilon_2\mathcal{S}_2\left(\frac{1}{\epsilon_1}\frac{\partial u^{\mathrm{inc}}}{\partial n}\right). \tag{4.6}$$

where $\mathcal{I}$ is the identity, $\mathcal{S}_i$, $\mathcal{D}_i$, $\mathcal{D}'_i$, $\mathcal{N}_i$ $(i = 1, 2)$ are layer potentials defined by

$$\mathcal{S}_i q(x) = \int_{\partial\Omega} G^i(x,y)q(y)\ ds_y \qquad \mathcal{D}_i u(x) = \int_{\partial\Omega}\frac{\partial G^i(x,y)}{\partial n_y}u(y)\ ds_y$$

$$\mathcal{D}'_i q(x) = \int_{\partial\Omega}\frac{\partial G^i(x,y)}{\partial n_x}q(y)\ ds_y \quad \mathcal{N}_i u(x) = \fint_{\partial\Omega}\frac{\partial^2 G^i(x,y)}{\partial n_x \partial n_y}u(y)\ ds_y.$$

Also, $\mathcal{L}_1$ and $\mathcal{M}_1$ give the outer traces of integral terms in (4.4) and their normal derivatives to the boundary, respectively, which can be written as follows:

$$\mathcal{L}_1\psi = a\mathcal{S}_1\psi + b\left(\frac{\mathcal{I}}{2} + \mathcal{D}_1\right)\psi$$
$$\mathcal{M}_1\psi = a\left(-\frac{\mathcal{I}}{2} + \mathcal{D}_1'\right)\psi + b\mathcal{N}_1\psi.$$

We call (4.6) the single integral equation (SIE) since the unknown function is only ψ on $\partial\Omega$. One obtains the solutions of transmission problem by substituting ψ to Green's identities after solving (4.6). For example, one can obtain boundary values u, q by using :

$$u = u^{\text{inc}} + \mathcal{L}_1\psi,\ q = \frac{1}{\epsilon_1}\left(\frac{\partial u^{\text{inc}}}{\partial n} + \mathcal{M}_1\psi\right) \text{ on } \partial\Omega.$$

We note that the SIE in (4.6) is the Fredholm equation of the second kind and the operator is a compact perturbation of a constant [37] and the accumulation point of the eigenvalues of the operator on the LHS in (4.6) is the constant, and we thus expect that the discretized equation leads to the convergence with a small number of iterations in GMRES. Indeed, fast convergence of SIE in GMRES is reported in [51] (the SIE used in [51] is slight different from ours.).

4.2.3 Fictitious eigenvalues of the SIE

The fictitious eigenvalues of the SIE in (4.6) are the eigenvalues of either of the following problems:

- exterior Dirichlet problem

$$\begin{aligned}&\Delta v + k_2^2 v = 0 \text{ in } \Omega_1, \quad v^+ = 0 \text{ on } \partial\Omega\\ &v \text{ satisfies the incoming radiation condition in the free space}\end{aligned} \tag{4.7}$$

- interior impedance problem

$$\Delta v + k_1^2 v = 0 \text{ in } \Omega_2, \quad av^- + b\frac{\partial v^-}{\partial n} = 0 \text{ on } \partial\Omega \tag{4.8}$$

To see this, suppose $u^{\text{inc}} \equiv 0$ and define U and V as follows:

$$U(x) = \begin{cases} W(x) \text{ in } \Omega_1 \\ \epsilon_2 \displaystyle\int_{\partial\Omega} G^2(x,y)\frac{1}{\epsilon_1}\frac{\partial W^+(y)}{\partial n_y}\,ds_y - \int_{\partial\Omega}\frac{\partial G^2(x,y)}{\partial n_y}W^+(y)\,ds_y \text{ in } \Omega_2 \end{cases}$$
$$V(x) = \begin{cases} -\epsilon_2 \displaystyle\int_{\partial\Omega} G^2(x,y)\frac{1}{\epsilon_1}\frac{\partial W^+(y)}{\partial n_y}\,ds_y + \int_{\partial\Omega}\frac{\partial G^2(x,y)}{\partial n_y}W^+(y)\,ds_y \text{ in } \Omega_1 \\ W(x) \text{ in } \Omega_2 \end{cases}$$

where

$$W(x) = a\int_{\partial\Omega} G^1(x,y)\psi(y)\,ds_y + b\int_{\partial\Omega}\frac{\partial G^1(x,y)}{\partial n_y}\psi(y)\,ds_y$$

We now assume that $\psi \not\equiv 0$ is a non-trivial solution of the SIE with ω. If $U \equiv 0$ in $\mathbb{R}^2 \setminus \partial\Omega$ holds, $V \not\equiv 0$ in Ω_2, since $\psi = 0$ otherwise. Thus, $V \not\equiv 0$ in Ω_2 gives the solution of the interior impedance problem in (4.8). If $U \not\equiv 0$ in $\mathbb{R}^2 \setminus \partial\Omega$ and $V \equiv 0$ in Ω_1 hold, U solves the original transmission problem. If $U \not\equiv 0$ in $\mathbb{R}^2 \setminus \partial\Omega$ and $V \not\equiv 0$ in Ω_1 hold, V solves the exterior Dirichlet problem in (4.7). This concludes the proof.

We now discuss our choice of the constants a, b. We first remember that our objective is to study the SIE from the view point of the fictitious eigenvalues. To this end, we have to separate the true eigenvalues from fictitious ones. We have already done this with the fictitious eigenvalues derived from the exterior Dirichlet problem in (4.7) since we use the incoming solution for G^2 so that the radiation condition in (4.7) is incoming. As regards the fictitious eigenvalues derived from the interior impedance problem in (4.8), we can distinguish them from true ones if we choose a, b in a way that $\mathrm{Im}(a/b) > 0$ holds. This can be checked as follows: the solution v of (4.8) satisfies

$$-\mathrm{Im}\left(\frac{a}{b}\right)\int_{\partial\Omega}|v|^2\,ds + 2\,\mathrm{Re}\,k_1\,\mathrm{Im}\,k_1\int_{\Omega_2}|v|^2\,dV = 0, \tag{4.9}$$

and the only v which satisfies (4.9) is zero if $\mathrm{Im}(a/b)$ and $\mathrm{Re}\,k_1\,\mathrm{Im}\,k_1$ have different signs. We thus see that the fictitious eigenvalues derived from (4.8) are separated from the true ones since we have $\mathrm{Im}(a/b) > 0$ by assumption, and $\mathrm{Re}\,k_1 > 0$ and $\mathrm{Im}\,k_1 < 0$ with the true eigenvalues. We also note that the fictitious eigenvalues derived from (4.8) are the same as those of the Burton-Miller equation. It is observed that the fictitious eigenvalues of the Burton-Miller equation are most separated from the real axis if one chooses

$$a = 1,\ b = -\frac{i}{k_1} \tag{4.10}$$

[30]. Actually, this choice has long been known to be good also in minimizing the condition numbers of the Burton-Miller equation and similar combined integral equation [52, 53]. We thus use (4.10) in the following formulations. We also note that the eigenvalues of (4.8) become real if one chooses $a = 0$ or $b = 0$ since (4.8) becomes the interior Neumann or Dirichlet problem, respectively.

4.2.4 The PMCHWT and Müller formulations

We show the PMCHWT and Müller formulations considered in this study for the reference. The PMCHWT and Müller formulations are given in the following form in a unified manner by using coefficients c_1, c_2, d_1, d_2 [36]:

$$\begin{pmatrix} \frac{c_1-c_2}{2}\mathcal{I} - (c_1\mathcal{D}_1 + c_2\mathcal{D}_2) & (c_1\epsilon_1\mathcal{S}_1 + c_2\epsilon_2\mathcal{S}_2) \\ -(d_1\mathcal{N}_1 + d_2\mathcal{N}_2) & \frac{d_1\epsilon_1-d_2\epsilon_2}{2}\mathcal{I} + (d_1\epsilon_1\mathcal{D}'_1 + d_2\epsilon_2\mathcal{D}'_2) \end{pmatrix}\begin{pmatrix} u \\ q \end{pmatrix} = \begin{pmatrix} c_1 u^{\mathrm{inc}} \\ d_1\frac{\partial u^{\mathrm{inc}}}{\partial n} \end{pmatrix} \tag{4.11}$$

The PMCHWT formulation is obtained as one sets $(c_1, c_2, d_1, d_2) = (1, 1, 1/\epsilon_1, 1/\epsilon_2)$. The Müller formulations are obtained so that the hypersingular terms of the kernels $\mathcal{N}_1$ and $\mathcal{N}_2$ are canceled. This can be archived with any choice of c_1, c_2 since $\mathcal{S}_i$ and $\mathcal{D}_i$ have at most weakly singular kernels. We thus consider the following two choices here: Müller 1: $(c_1, c_2, d_1, d_2) = (1/\epsilon_1 - 1/\epsilon_2, 1, -1)$ and Müller 2: $(c_1, c_2, d_1, d_2) = (\epsilon_1, -\epsilon_2, 1, -1)$, respectively. The coefficients in Müller 1 are chosen so that the weak singularity of the kernel of $\mathcal{S}_i$ cancels (the Müller 1 is the same as (3.7) although the physical target is different). The coefficients of the Müller 2 are chosen so that the eigenvalues of the BIE are identical to those of the PMCHWT just as in the case for Maxwell's equations.

4.3 Numerical examples

We show some numerical examples, in which we mainly focus on the case when the wave velocity in Ω_2 is larger than that of Ω_1. In this case, the fictitious eigenvalues of the PMCHWT and Müller formulations in (4.11) correspond to eigenvalues of the transmission problems in which the wave velocity in Ω_2 is smaller than that of Ω_1, and more likely to have eigenvalues with small imaginary parts as we have seen in the last numerical example of chapter 3 (see Fig. 3.9).

4.3.1 Circular scatterer in the free space

We first consider the single circular scatterer case with the radius of r_0. In this case, the eigenvalues of the transmission problem and the fictitious eigenvalues of the BIEs can be obtained analytically. For example, true eigenvalues of the transmission problem and fictitious ones for the BIEs are given as zeros of the following functions:

- transmission eigenvalues

$$-H_n^{(1)}(k_1 r_0)\frac{1}{\epsilon_2}\frac{d}{dr}J_n(k_2 r_0) + J_n(k_2 r_0)\frac{1}{\epsilon_1}\frac{d}{dr}H_n^{(1)}(k_1 r_0) \tag{4.12}$$

- fictitious eigenvalues of the SIE

$$H_n^{(2)}(k_2 r_0)\left(aJ_n(k_1 r_0) + b\frac{d}{dr}J_n(k_1 r_0)\right) \tag{4.13}$$

- fictitious eigenvalues of the PMCHWT and Müller formulations in (4.11)

$$c_2 H_n^{(2)}(k_2 r_0) d_1 \frac{d}{dr}J_n(k_1 r_0) - c_1 J_n(k_1 r_0) d_2 \frac{d}{dr}H_n^{(2)}(k_2 r_0) \tag{4.14}$$

We calculate the eigenvalues semi-analytically by calculating the zeros of these functions with SSM (we vary n in (4.12), (4.13) and (4.14) from 0 to 40).

We set parameters to be $(\epsilon_1, \epsilon_2) = (4, 1)$ and $r_0 = 1$. Fig. 4.1 shows the (analytical) eigenvalues of the boundary integral equations. The rectangle with a fine border line represents the domain within which we searched the eigenvalues. We used six paths to obtain Fig. 4.1, although only the periphery is shown for the visibility. Note that the eigenvalues in the upper complex plane are the fictitious eigenvalues for each BIE while the ones in the lower complex plane are the true eigenvalues of the transmission problem. We see that the PMCHWT and Müller formulations have fictitious eigenvalues which are very close to real axis as $\mathrm{Re}\,\omega$ increases while those of the SIE are more separated from real axis. Figs 4.2 show the blow up of Fig. 4.1 in $\mathrm{Im}\,\omega \in (-0.1, 0.1)$ (the upper figure), average of the $\mathcal{L}^2$ error of the solutions u, q relative to the exact solution for incident plane wave $u^{\mathrm{inc}} = e^{ik_1 x_2}$ with real frequencies (the middle three figures), and the numbers of iterations needed in GMRES to obtain the solutions (the lower figure). Here, we discretized the circle with 1000 piecewise constant elements and the tolerance for the GMRES was set to be 10^{-8}. We used the standard BIEs (namely, outgoing solution for G^2) for solving ordinary problems with real frequencies since calculation of eigenvalues are not required although we have shown BIEs formulated with the incoming fundamental solution for G^2. We see that the PMCHWT and Müller formulations become inaccurate near frequencies close to fictitious eigenvalues with very small imaginary parts. On the other hand, the SIE which does not

have fictitious eigenvalues with small imaginary parts computes the solution more accurately than the PMCHWT and Müller formulations. We also see that the Müller formulations are more inaccurate than the PMCHWT, even though the Müller 2 and PMCHWT formulations have exactly the same eigenvalues. This phenomenon can be explained to some extent and reported by Misawa and Nishimura in [36]. However, a complete explanation and error estimates of BIEM solutions in relation to distance between a frequency and eigenvalues still remain future subjects. Fig 4.3(a) shows the imaginary part of the solution $\mathrm{Im}\, u$ at $\omega \approx 7.76$ where the Müller 1 is inaccurate (peak indicated by arrow in the middle figure of Fig. 4.2) obtained with each BIE. The solution obtained with the Müller 1 formulation has spurious oscillation while the ones obtained with the other BIEs agree well with the exact solution. Fig. 4.3(b) shows the error of the Müller 1 solution defined by $\mathrm{Im}(u - u^{\mathrm{exa}})$ (where u^{exa} stands for the exact solution) on the boundary of the scatterer. We see that the error has 13 waves on the boundary. This is quite plausible because we have checked that the fictitious eigenvalue which cause the inaccuracy near $\omega \approx 7.76$ (point indicated by arrow in the upper figure of Fig. 4.2) is one of zeros of (4.14) with $n = 13$, and the eigenmode oscillates with $\exp(13i\theta)$(θ: polar coordinate) on the circular boundary. This indicates that inaccuracies near the eigenvalues are caused by the contamination due to fictitious modes of the BIEM solutions. We also see that the SIE converges with the smallest number of iterations among BIEs tested (see the lower figure of Fig. 4.2). We have SIE, Müller 1, Müller 2 and PMCHWT in the increasing order of number of iterations. The numbers of iterations of the PMCHWT and Müller formulations increase suddenly near the eigenvalues while that of the SIE does not.

Fig. 4.4 shows the similar numerical results as in Fig. 4.2 for the case $(\epsilon_1, \epsilon_2) = (1, 4)$ in which the material constants are interchanged. In this case, all the BIEs can fairly separate their fictitious eigenvalues from real axis, but those of the SIE are the most separated (see the upper figure of Figs. 4.4). On the other hand, there are many true eigenvalues with very small imaginary parts, and all BIEs shown here become inaccurate near these eigenvalues (middle figure). However, the SIE seems to be less affected by the eigenvalues than the other BIEs. The number of iterations of the SIE is small in this case also (the lower figure).

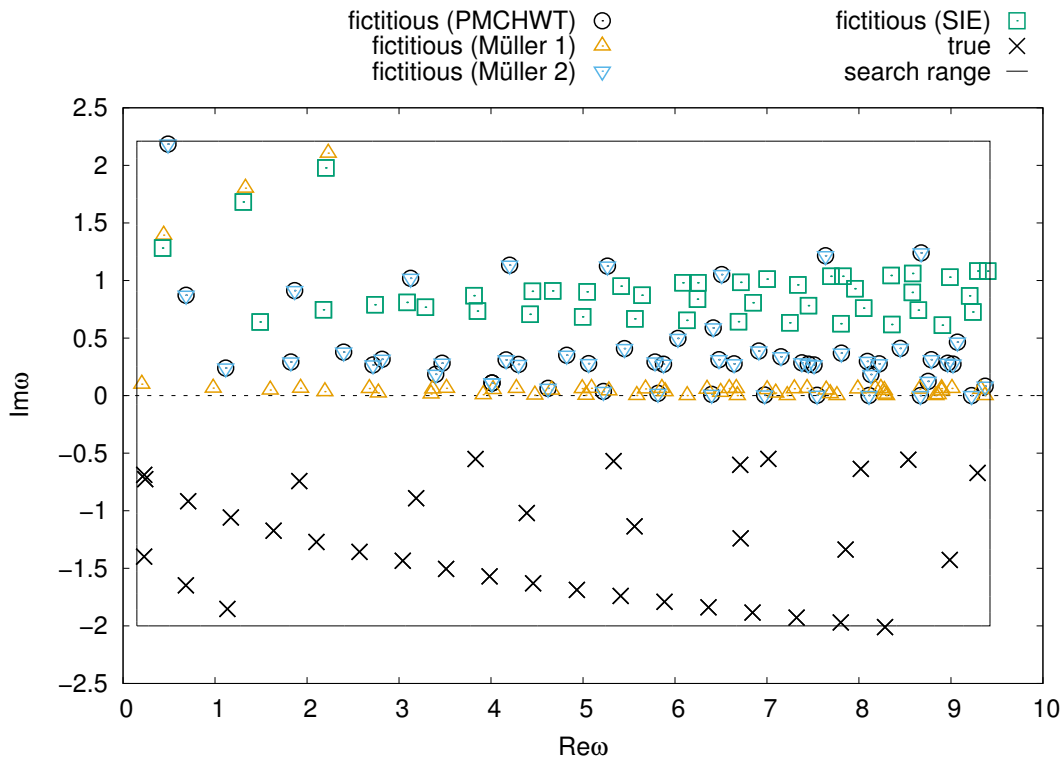

Figure 4.1: Analytical eigenvalues for various BIEs for single circular scatterer ($\epsilon_1 = 4, \epsilon_2 = 1$).

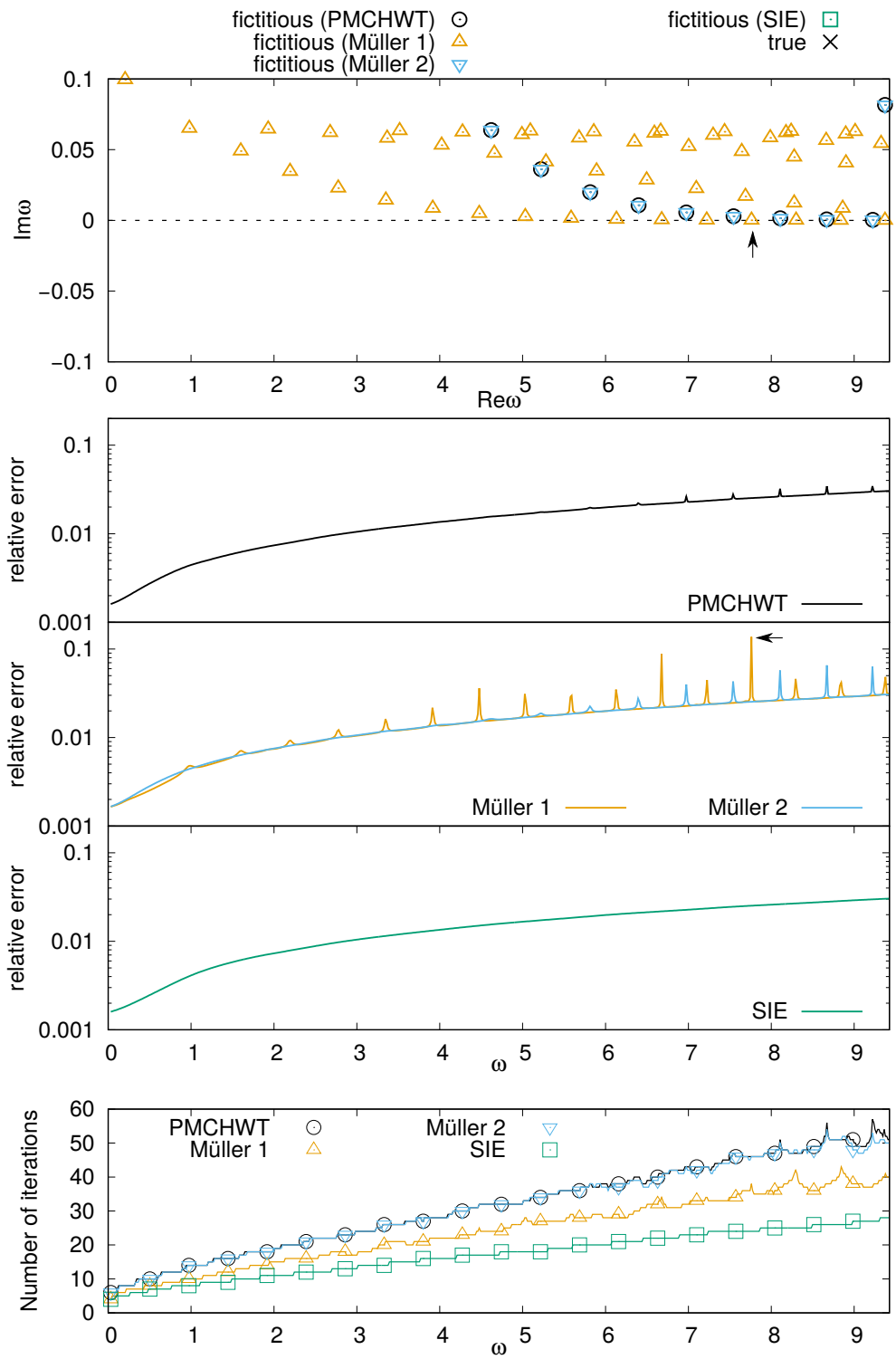

Figure 4.2: Eigenvalues with very small imaginary parts (top), relative errors of the BIEM solutions (middle 3 figures) and numbers of iterations (lower).

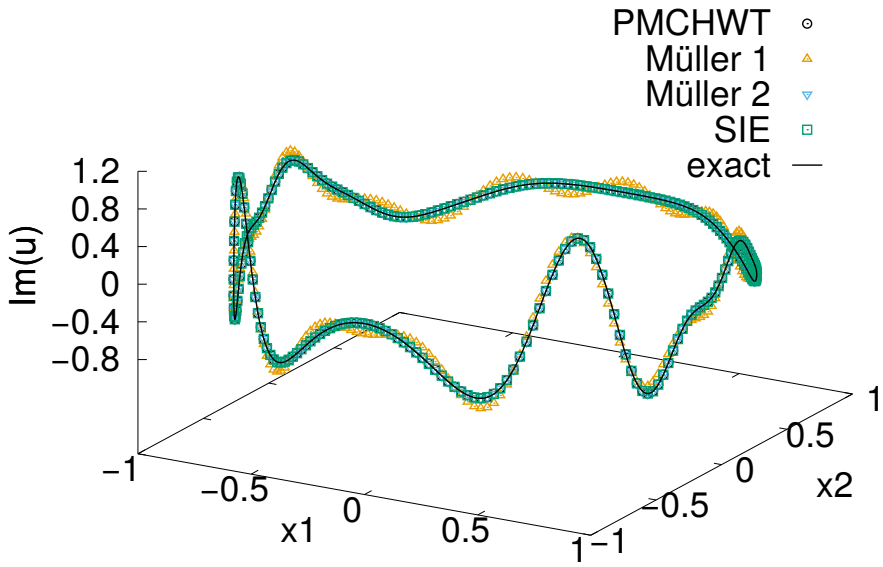

(a)

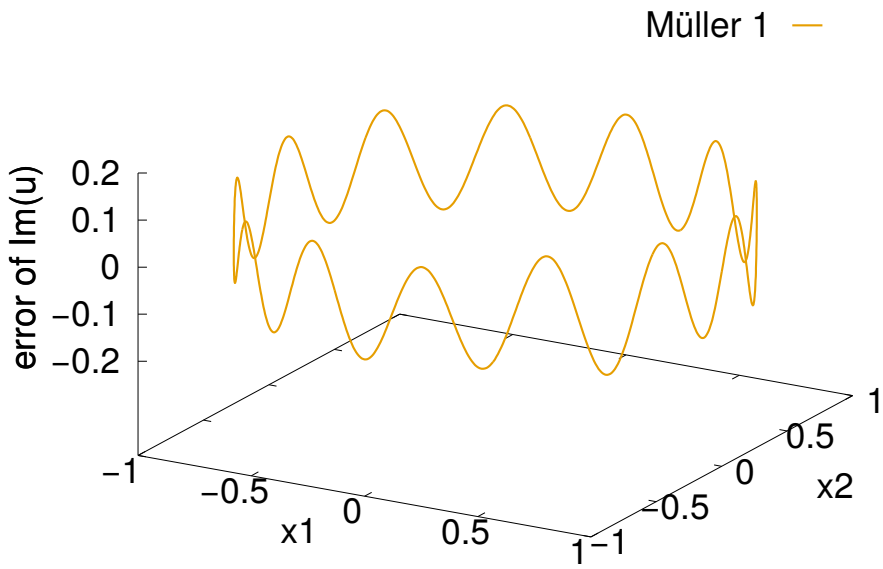

(b)

Figure 4.3: (a): Solutions obtained with BIEs on $\omega \approx 7.76$ (solution at the peak indicated by arrow in the middle figure of Fig. 4.2), (b): Error of the Müller 1 solution on the boundary defined by error $= \mathrm{Im}(u - u^{\mathrm{exa}})$

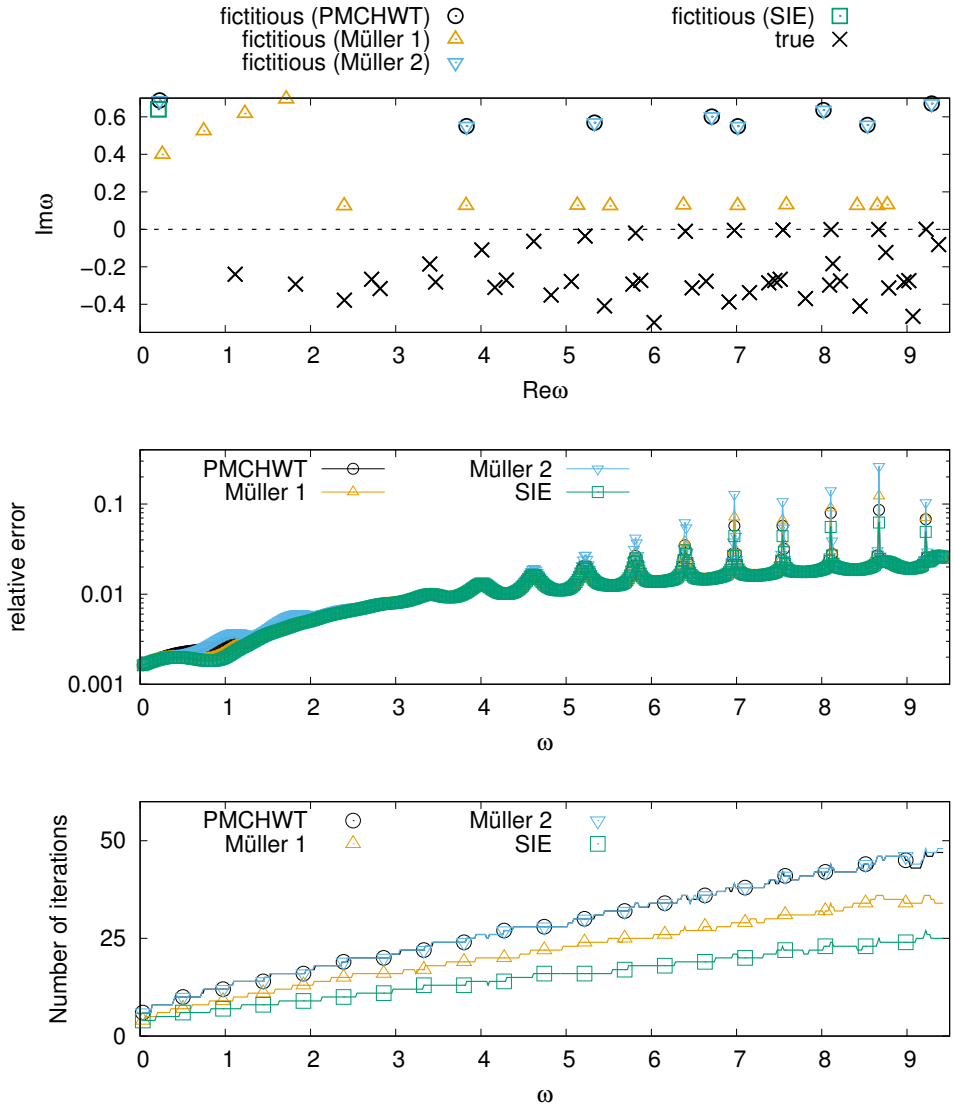

Figure 4.4: ($\epsilon_1 = 1, \epsilon_2 = 4$, circular scatterer) Eigenvalues (upper), relative errors of the BIEM solutions (middle), numbers of iterations (lower)

4.3.2 Smooth star shaped scatterer in the free space

We next consider the case where one cannot obtain exact solutions easily. Here, we set Ω_2 to be a smooth star shaped scatterer shown in Fig. 4.5 given by $(x_1, x_2) = ((1 + 0.3\cos 5\theta)\cos\theta/1.3, (1 + 0.3\cos 5\theta)\sin\theta/1.3)$ [54]. Fig. 4.6 shows the eigenvalues of the BIEs obtained with FMM accelerated BIEM and SSM (we discretized the star shape with 2000 piecewise constant elements. We used six paths to obtain Fig. 4.6 although only the periphery is shown for the visibility.). We see that all BIEs obtain true eigenvalues in the lower complex plane accurately (we have checked that the eigenvalue outside the contour is also close to true ones). We also see that fictitious eigenvalues of the SIE are more separated from real axis than those of the PMCHWT and Müller formulations in this case also. Fig. 4.7 shows the numbers of iterations needed in GMRES at the integration points ($\mathrm{Re}\,\omega$ v.s. number of iterations) for the SSM. We see that the SIE converges faster than the PMCHWT and Müller 2 formulations, and as fast as the Müller 1 formulation on the whole. We thus see that the SIE converges with small number of iterations in this case also.

4.3.3 Computational cost

We first note that double integrals in (4.6) are calculated in $O(N)$ cost since we use FMM. We next consider the computational cost of one matrix vector multiplication. In the PMCHWT and Müller formulations, small sized matrix vector multiplications such as $\mathcal{S}_i q$ and $\mathcal{D}_i u$ are needed 8 times for single scatterer (see (4.11)). In SIE, on the other hand, the small matrix vector multiplications are needed 6 times (4 times for $\mathcal{L}_i\psi, \mathcal{M}_i\psi$, 2 times for (4.5)). We thus see that the computational cost of one matrix vector multiplication for the SIE is smaller than those of the PMCHWT and Müller formulations. In fact, we checked that the average computational times of one matrix vector multiplications for the SIE and the PMCHWT and Müller formulations are 0.036s (0.156s) and 0.038s (0.173s), respectively, in the case of the smooth star shape with 2000 (10000) piecewise constant elements. We used FX10 Supercomputer System (with SPARC64^{TM}IXfx cores) at the Information Technology Center of the University of Tokyo for the computation. The code is parallelized with OpenMP and the number of CPU is 16.

4.4 Conclusions

In this chapter, we investigated the behavior of fictitious eigenvalues of the SIE numerically. Our results suggest that the fictitious eigenvalues of the SIE are more separated from real axis than those of the PMCHWT and Müller formulations, and the SIE can avoid the inaccuracies caused by the fictitious eigenvalues with very small imaginary parts in the analysis with real frequencies. Our results also suggest that one has to take the presence of fictitious eigenvalues close to real axis into account in order to obtain highly accurate BIEs.

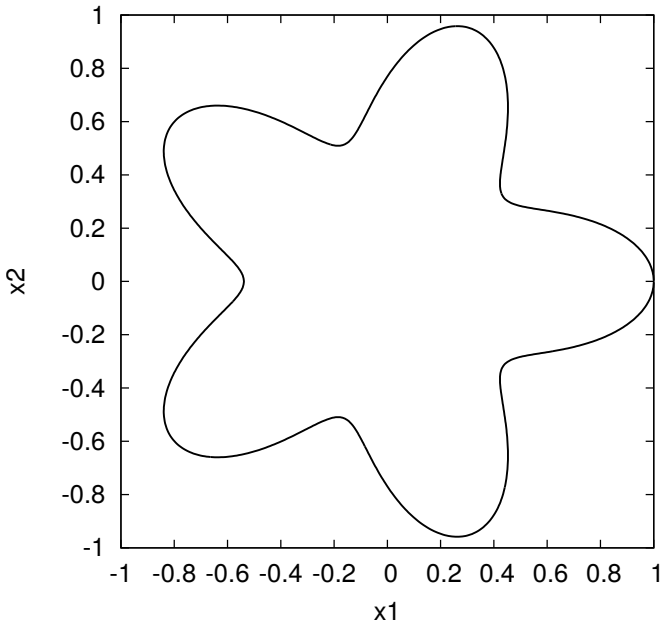

Figure 4.5: Smooth star shaped scatterer

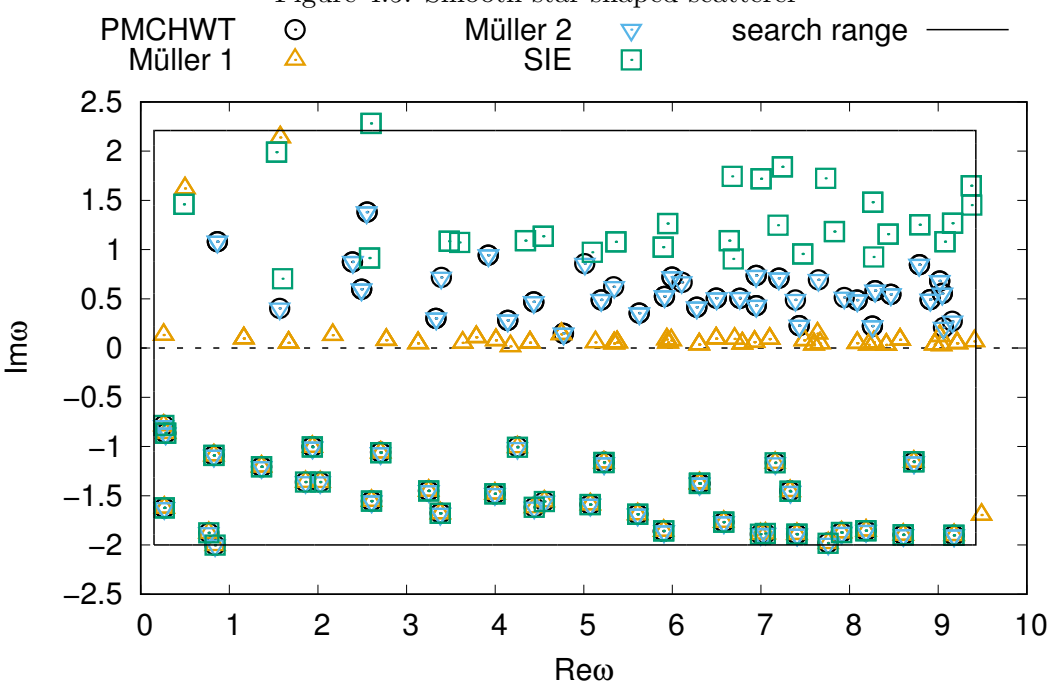

Figure 4.6: Eigenvalues for the smooth star ($\epsilon_1 = 4,\ \epsilon_2 = 1$)

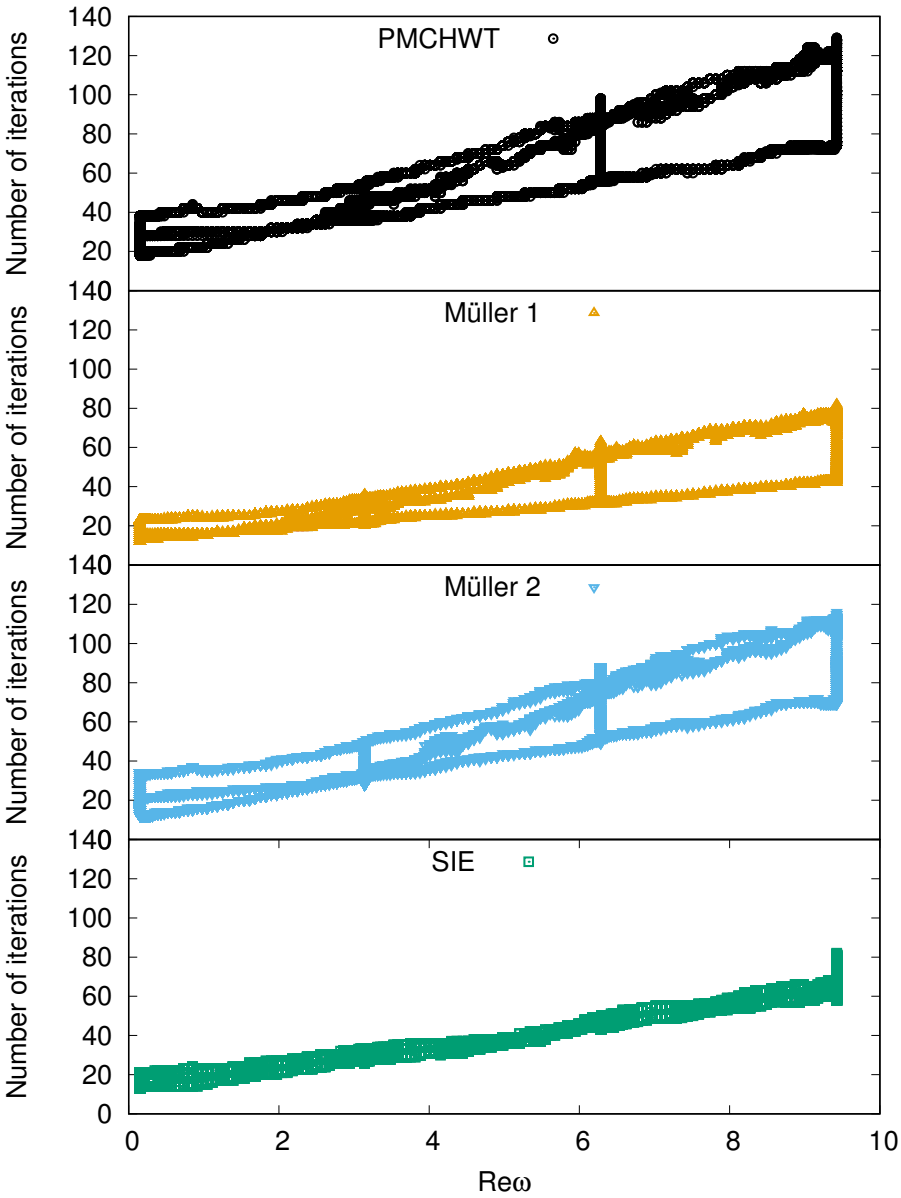

Figure 4.7: $\mathrm{Re}\,\omega$ v.s. Numbers of iterations needed at integration points on the contours for SSM.

Chapter 5

Conclusions

In this thesis, we discussed the calculation of complex eigenvalues for boundary value problems in open spaces such as waveguides and the free space. We obtained the following results:

- In chapter 2, we have developed an FMM which efficiently calculates potentials related to Green's function for 2-D Helmholtz' equation in waveguides with the homogeneous Neumann boundary condition on the sides. We then applied the FMM to find resonance frequencies (eigenvalues) in conjunction with Sakurai-Sugiura projection method after considering the analytic continuation of the FMM-BIEM to complex frequencies, which has branch cuts extending from cut-off frequencies. The numerical method was validated with some numerical examples. In particular, we could verify that our method is quite reliable even near branch cuts. We have also presented some numerical examples which show the relevance between complex resonance frequencies and physical phenomena such as stopbands.

- In chapter 3, we have shown that one can distinguish true and fictitious eigenvalues of BIEs for transmission problems just by using incoming fundamental solutions for integral representations for finite sized scatterers in boundary integral equations. We have also shown the equivalence of eigenvalues of the PMCHWT and Müller formulations for Maxwell's equations. We have verified the usefulness of the proposed method through some numerical examples. We have also shown that even boundary integral equations without real fictitious eigenvalues may have complex fictitious ones with very small imaginary parts, and these eigenvalues cause inaccuracies of the BIEM solutions in real frequency.

- In chapter 4, we have verified numerically that the single integral equation (SIE) proposed in [37] can resolve the inaccuracies with real frequencies seen in the PMCHWT and Müller formulations. We have explained this improvement by showing that the fictitious eigenvalues of the SIE are more separated from real axis than those of the PMCHWT and Müller formulations. This result is quite plausible because the fictitious eigenvalues of the SIE are not eigenvalues of transmission problems, which may have small imaginary parts, while this is the case in PMCHWT and Müller formulations.

We comment on some extensions of the results in this thesis and on issues which should be further studied in future works:

- The extension of the proposed FMM to three dimensional rectangular waveguides is straightforward and can be done with similar method of images because the relevant Green's function can be written as lattice sums. However, extension of the proposed FMM to three dimensional cylindrical waveguides is not easy and is left as a future subject. Extension of the FMM to impedance boundary conditions is another future subject. Although a method similar to ours for impedance half plane was developed in [20], its extension to the infinite strip case has not been considered yet. Another challenging future subject is the extension of the present approach to elasticity. In these cases, a new methodology will be required since the related Green's functions cannot be written as lattice sums and the problem cannot be solved only with the method of images shown in this thesis.

- Although we have considered electromagnetic and elastic waves, the FMM-BIEM presented in chapter 2 could be applied to other physical problems such as acoustics or water-waves which are governed by linear BVPs. However, applications of the proposed method to non-linear eigenvalue problems may not be very easy if the wavenumber k and frequency ω are related in a complicated manner (e.g., materials which follow the Drude model, etc.). Extension of the work presented in chapter 3 to these cases remains as a future work.

- The use of fast direct solvers [13, 14] in conjunction with the proposed BIE in chapter 3 and SSM is also worth studying because one may sometimes have to take L large, thus having to invert the same matrix repeatedly with many different RHSs. The fast direct solvers may also resolve the problem of increased iteration numbers for small $|\operatorname{Im}\omega|$ mentioned in 3.3.4.

- Error estimate of the BIEM solutions in relation to the distance of a target frequency and eigenvalues close to the frequency is also a challenging future work.

Bibliography

[1] C. M. Linton and P. McIver, *Embedded trapped modes in water waves and acoustics*, Wave Motion, 45 (2007), pp. 16–29.

[2] D. V. Evans, M. Levitin, and D. Vassiliev, *Existence theorems for trapped modes*, J. Fluid Mech., 261 (1994), pp. 21–31.

[3] D. V. Evans and R. Porter, *Trapped modes embedded in the continuous spectrum*, Quart. J. Mech. Appl. Math., 51 (1998), pp. 263–274.

[4] A. Aslanyan, L. Parnovski, and D. Vassiliev, *Complex resonances in acoustic waveguides*, Quart. J. Mech. Appl. Math., 53 (2000), pp. 429–447.

[5] C. M. Linton, M. McIver, P. McIver, K. Ratcliffe, and J. Zhang, *Trapped modes for off-centre structures in guides*, Wave Motion, 36 (2002), pp. 67–85.

[6] C. M. Linton and D. V. Evans, *Integral equations for a class of problems concerning obstacles in waveguides*, J. Fluid Mech., 245 (1992), pp. 349–365.

[7] S. Hein, T. Hohage, and W. Koch, *On resonances in open systems*, J. Fluid Mech., 506 (2004), pp. 255–284.

[8] S. Hein, W. Koch, and L. Nannen, *Fano resonances in acoustics*, J. Fluid Mech., 664 (2010), pp. 238–264.

[9] Y. Duan, W. Koch, C. M. Linton, and M. McIver, *Complex resonances and trapped modes in ducted domains*, J. Fluid Mech., 571 (2007), pp. 119–147.

[10] L. Nannen and A. Schädle, *Hardy space infinite elements for Helmholtz-type problems with unbounded inhomogeneities*, Wave Motion, 48 (2011), pp. 116–129.

[11] L. Greengard and V. Rokhlin, *A fast algorithm for particle simulations*, J. Comput. Phys., 73 (1987), pp. 325–348.

[12] E. Bleszynski, M. Bleszynski, and T. Jaroszewicz, *AIM: Adaptive integral method for solving large-scale electromagnetic scattering and radiation problems*, Radio Sci., 31 (1996), pp. 1225–1251.

[13] P. G. Martinsson and V. Rokhlin, *A fast direct solver for boundary integral equations in two dimensions*, J. Comput. Phys., 205 (2005), pp. 1–23.

[14] M. Bebendorf, *Hierarchical Matrices*, Springer, Berlin, Heidelberg, 2008.

[15] K. V. Horoshenkov and S. N. Chandler-Wilde, *Efficient calculation of two-dimensional periodic and waveguide acoustic Green's functions*, J. Acoust. Soc. Am., 111 (2002), pp. 1610–1622.

[16] S. Venakides, M. A. Haider, and V. Papanicolaou, *Boundary integral calculations of two-dimensional electromagnetic scattering by photonic crystal Fabry-Perot structures*, SIAM J. Appl. Math., 60 (2000), pp. 1686–1706.

[17] C. M. Linton, *Lattice sums for the Helmholtz equation*, SIAM Rev., 52 (2010), pp. 630–674.

[18] Y. Otani and N. Nishimura, *An FMM for periodic boundary value problems for cracks for Helmholtz' equation in 2D*, Internat. J. Numer. Methods Engrg., 73 (2008), pp. 381–406.

[19] T. Fukui and M. Kozuka, *Analysis of sound reflection and diffraction in half space by fast multipole boundary element method*, Proc. of "17th Japan National Symposium on Boundary Element Methods", 17 (2000), pp. 49–54, `http://gspsun1.gee.kyoto-u.ac.jp/JASCOME/paper/files/bem2000/1710.pdf`. (in Japanese).

[20] M. O'Neil, L. Greengard, and A. Pataki, *On the efficient representation of the half-space impedance Green's function for the Helmholtz equation*, Wave Motion, 51 (2014), pp. 1—13.

[21] S. P. Shipman and S. Venakides, *Resonance and bound states in photonic crystal slabs*, SIAM J. Appl. Math., 64 (2003), pp. 322–342.

[22] H. Cheng, W. Y. Crutchfield, M. Doery, and L. Greengard, *Fast, accurate integral equation methods for the analysis of photonic crystal fibers I: Theory*, Opt. Express, 12 (2004), pp. 3791–3805.

[23] T. Sakurai and H. Sugiura, *A projection method for generalized eigenvalue problems using numerical integration*, J. Comput. Appl. Math., 159 (2003), pp. 119–128.

[24] T. Ikegami, T. Sakurai, and U. Nagashima, *A filter diagonalization for generalized eigenvalue problems based on the Sakurai-Sugiura projection method*, J. Comput. Appl. Math., 233 (2010), pp. 1927–1936.

[25] J. Asakura, T. Sakurai, H. Tadano, T. Ikegami, and K. Kimura, *A numerical method for nonlinear eigenvalue problems using contour integrals*, JSIAM Lett., 1 (2009), pp. 52–55.

[26] H. Gao, T. Takahashi, H. Isakari, and T. Matsumoto, *A study on eigensolutions of 2D elastic problem by using BEM and FEM*, Trans. Jpn. Soc. Comput. Methods Eng., 13 (2013), pp. 49–54, `http://gspsun1.gee.kyoto-u.ac.jp/JASCOME/denshi-journal/13/JA139.pdf`.

[27] A. Kleefeld, *A numerical method to compute interior transmission eigenvalues*, Inverse Problems, 29 (2013), p. 104012.

[28] W.-J. Beyn, *An integral method for solving nonlinear eigenvalue problems*, Linear Algebra Appl., 436 (2012), pp. 3839–3863.

[29] T. Nose and N. Nishimura, *Calculation of eigenvalues related to 2 dimensional periodic boundary value problems for the Helmholtz equation using the Sakurai-Sugiura method and periodic fast multipole method*, Trans. Jpn. Soc. Ind. Appl. Math., 24 (2014), pp. 185–201, `http://ci.nii.ac.jp/naid/110009863510`. (in Japanese).

[30] C.-J. Zheng, H.-F. Gao, L. Du, H.-B. Chen, and C. Zhang, *An accurate and efficient acoustic eigensolver based on a fast multipole BEM and a contour integral method*, J. Comput. Phys., 305 (2016), pp. 677–699.

[31] D. Colton and R. Kress, *Integral Equation Methods in Scattering Theory*, John Wiley & Sons, New York, 1983.

[32] A. J. Burton and G. F. Miller, *The application of integral equation methods to the numerical solution of some exterior boundary-value problems*, Proc. Roy. Soc. Lond. Ser. A, 323 (1971), pp. 201–210.

[33] W. C. Chew, J.-M. Jin, E. Michielssen, and J. Song, eds., *Fast and Efficient Algorithms in Computational Electromagnetics*, Artech House, Boston, 2001.

[34] C. Müller, *Foundations of the Mathematical Theory of Electromagnetic Waves*, Springer, Berlin, Heidelberg, 1969.

[35] O. Steinbach and G. Unger, *Combined boundary integral equations for acoustic scattering-resonance problems*, Math. Methods Appl. Sci., (2016), doi:10.1002/mma.4075. (in press).

[36] R. Misawa and N. Nishimura, *Boundary integral formulations for one-periodic transmission problems for Helmholtz' equation in 2-D*, Trans. Jpn. Soc. Comput. Methods Eng., 12 (2012), pp. 109–114, `http://gspsun1.gee.kyoto-u.ac.jp/JASCOME/denshi-journal/12/JA1219.pdf`. (in Japanese).

[37] R. E. Kleinman and P. A. Martin, *On single integral equations for the transmission problem of acoustics*, SIAM J. Appl. Math., 48 (1988), pp. 307–325.

[38] R. Misawa, K. Niino, and N. Nishimura, *An FMM for waveguide problems of 2-D Helmholtz' equation and its application to eigenvalue problems*, Wave Motion, 63 (2016), pp. 1–17.

[39] R.Misawa, K.Niino, and N.Nishimura, *Boundary integral equations for calculating complex eigenvalues of transmission problems*, arXiv:1608.00500[math.NA], (2016), `https://arxiv.org/abs/1608.00500`. (preprint, accepted for publication in SIAM. J. Appl. Math.).

[40] R. Misawa and N. Nishimura, *A study on the single boundary integral equation method for transmission problems for Helmholtz' equation in 2D based on the distribution of fictitious complex eigenvalues*, Trans. Jpn. Soc. Comput. Methods Eng., 16 (2016), pp. 73–78, `http://gspsun1.gee.kyoto-u.ac.jp/JASCOME/denshi-journal/16/JA1618.pdf`. (in Japanese).

[41] A. Barnett and L. Greengard, *A new integral representation for quasi-periodic scattering problems in two dimensions*, BIT, 51 (2011), pp. 67–90.

[42] Y. Saad, *Iterative Methods for Sparse Linear Systems*, Society for Industrial and Applied Mathematics, Philadelphia, PA, 2003.

[43] K. Niino and N. Nishimura, *Preconditioners based on Calderon's formulae for 1 periodic boundary value problems for Helmholtz' equation in 2D*, Trans. Jpn. Soc. Comput. Methods Eng., 9 (2009), pp. 1–6, `http://gspsun1.gee.kyoto-u.ac.jp/JASCOME/denshi-journal/9/JA091.pdf`. (in Japanese).

[44] K. Niino and N. Nishimura, *Preconditioning based on Calderon's formulae for periodic fast multipole methods for Helmholtz' equation*, J. Comput. Phys., 231 (2012), pp. 66–81.

[45] V. Rokhlin, *Rapid solution of integral equations of scattering theory in two dimensions*, J. Comput. Phys., 86 (1990), pp. 414–439.

[46] A.-S. Bonnet-Bendhia and F. Starling, *Guided waves by electromagnetic gratings and non-uniqueness examples for the diffraction problem*, Math. Methods Appl. Sci., 17 (1994), pp. 305–338.

[47] S. Kim and J. E. Pasciak, *The computation of resonances in open systems using a perfectly matched layer*, Math. Comp., 78 (2009), pp. 1375–1398.

[48] R. Kress and G. F. Roach, *Transmission problems for the Helmholtz equation*, J. Math. Phys., 19 (1978), pp. 1433–1437.

[49] K. Niino and N. Nishimura, *On the boundary element methods with Müller's formulation for electromagnetic scattering problems in periodic domains*, in Proc. of "2013 International Symposium on Electromagnetic Theory", 2013, pp. 139–142.

[50] P. Monk, *Finite Element Methods for Maxwell's Equations*, Oxford University Press, New York, 2003.

[51] Y. Boubendir, C. Turc, and V. Domínguez, *High-order Nyström discretizations for the solution of integral equation formulations of two-dimensional Helmholtz transmission problems*, IMA J. Numer. Anal., 36 (2016), pp. 463–492.

[52] S. Amini, *On the choice of the coupling parameter in boundary integral formulations of the exterior acoustic problem*, Appl. Anal., 35 (1990), pp. 75–92.

[53] R. Kress, *Minimizing the condition number of boundary integral operators in acoustic and electromagnetic scattering*, Quart. J. Mech. Appl. Math., 38 (1985), pp. 323–341.

[54] A. Barnett, *Boundary integral equations for BVPs, and their high-order Nyström quadratures: a tutorial.* Lecture materials for "2014 CBMS-NSF Conference: Fast Direct Solvers for Elliptic PDEs", `https://math.dartmouth.edu/~fastdirect/notes/quadr.pdf`.